UNIVERSITY OF KWAZULU-NATAL ™

INYUVESI YAKWAZULU-NATALI

Monsonia burkeana induces caspase-dependent apoptosis in Caco-2 cells and nitrosative stress-induced necroptosis in HepG2 cells.

Mayanka Naicker (215025490)

Dr Rene Khan

Dr Hezekiel Kumalo

BSc LES (Biochemistry and Genetics), BMedSc (Hons in Medical Biochemistry) (UKZN)

Submitted in fulfilment of the requirements for the degree of

Master of Medical Science

in the Discipline of Medical Biochemistry and Chemical Pathology

School of Laboratory Medicine and Medical Sciences

College of Health Sciences

University of KwaZulu-Natal

Durban

2023

DECLARATION

I, Mayanka Naicker, declare as follows:

That the work described in this thesis has not been submitted to UKZN or other tertiary institution for purposes of obtaining an academic qualification, whether by myself or any other party. The use of work conducted by others has been acknowledged in the text. The research described in this study was carried out in the Department of Medical Biochemistry and Chemical Pathology, School of Laboratory Medicine and Medical Science, Faculty of Health Sciences, University of KwaZulu-Natal, Durban, under the supervision of Dr RB Khan.

Signed: [redacted] Date: 15 January 2024
Mayanka Naicker

Signed: [redacted] Date: 15 January 2024
Rene Khan

Signed: [redacted] Date: 15 January 2024
Hezekiel Kumalo

ACKNOWLEDGEMENTS

GOD

All glory and thanks to God.

MY FAMILY

Words can't describe my gratitude for your endless motivation and support throughout my journey. Your love and guidance have shaped me into the person I am today.

DR KHAN

It is an absolute honour to be one of your students. Thank you for all the learning opportunities that you have provided me with. You have taught me that hard work and dedication always pays off. Thank you for all the motivation and inspiration throughout my academic years.

DR KUMALO

Thank you for all your support and encouragement over the last two years.

FRIENDS IN MEDICAL BIOCHEMISTRY

Your friendship, laughter and assistance have made the last two years some of my favourite. I could not have done it without you.

NATIONAL RESEARCH FOUNDATION,

Thank you for the academic financial support as a postgraduate student.

TABLE OF CONTENTS

LIST OF FIGURES

CHAPTER 2

LIST OF ABBREVIATIONS

αKGDH	α-Ketoglutarate dehydrogenase
µg	Microgram
ΔΨm	Mitochondrial membrane potential
4-HNE	4 - Hydroxy - 2 – nonenal
5-FU	5- Fluorouracil
8-oxo-dG	8-oxo-7,8-dihydroguanine
AP-1	Activator protein - 1
APAF-1	Apoptotic protease activating factor 1
APC	Adenomatous polyposis coli
ATP	Adenosine triphosphate
BAK	B-cell lymphoma 2 (BCL-2) antagonist/killer
BAX	B-cell lymphoma 2 (BCL-2) associated X-protein
BCA	Bicinchoninic acid
BCLC	Barcelona clinic liver cancer
BHT	Butylated hydroxytoluene
BSA	Bovine serum albumin
Caco-2	Colorectal adenocarcinoma
CAP	Capecitabine
CARD	Caspase activation and recruitment domain
CAT	Catalase
CCM	Complete culture medium
cDNA	Complementary DNA
c-FLIP	Cellular FADD-like-IL-1β-converting enzyme) inhibitory protein
ClO^-	Hypochlorite
Cox	Cyclooxygenase
CRC	Colorectal cancer

CST	Cell Signalling Technology
Cu-SOD	Copper superoxide dismutase
CXCR4	C-X-C motif chemokine receptor type 4
CYP3A4	Cytochrome P450 3A4
DAMPs	Damage associated molecular patterns
dATP	Deoxyadenosine triphosphate
DCC	Deleted in colorectal cancer
DISC	Death-inducing signalling complex
DED	Death effector domain
DMSO	Dimethyl sulfoxide
DNA	Deoxyribonucleic acid
EC	Epicatechin
EC-SOD	Extracellular superoxide dismutase
ECG	Epicatechin gallate
EGC	Epigallocatechin
EGCG	Epigallocatechin gallate
FADD	Fas-associated death domain
FCC	Familial colorectal cancer
GAPDH	Glyceraldehyde 3-phosphate dehydrogenase
GIST	Gastrointestinal stromal tumours
Gpx-1	Glutathione peroxidase 1
GSH	Reduced glutathione
GSSG	Oxidised glutathione
GST	Glutathione S-transferase
LDH	Lactate dehydrogenase
Lox	Lipoxygenase
H_2O_2	Hydrogen peroxide
H_3PO_4	Phosphoric acid
HBV	Hepatitis B virus

HCC	Hepatocellular carcinoma
HCL	Hydrochloric acid
HCV	Hepatitis C virus
Hek293	Human embryonic kidney cells
HeLa	Human cervical cancer cells
HepG2	Human hepatocellular carcinoma
HIF-1α	Hypoxia-inducible factor-1α
HRP	Horseradish peroxidase
IARC	International Agency for Research on Cancer
IC_{20}	Inhibitory concentration causing 20% cell death
IC_{50}	Half maximal inhibitory concentration
IL	Interleukin
iNOS	Nitric oxide synthase
INT	Iodonitrotetrazolium
IRI	Irinotecan
KRAS	Kirsten rat sarcoma
LDH	Lactate dehydrogenase
M. burkeana	*Monsonia burkeana* Planch. ex Harv
MDA	Malondialdehyde
miRNA	Micro ribonucleic acid
MLKL	Mixed lineage kinase domain-like protein
Mn-SOD	Manganese superoxide dismutase
MOMP	Mitochondrial outer membrane permeability
MTT	3-(4,5-dimethylthiazol-2-yl)-2,5-diphenyl-2H-tetrazolium bromide
NaCl	Sodium chloride
NADPH	Nicotinamide adenine dinucleotide phosphate
NAFLD	Non-alcoholic fatty liver disease
$NaNO_3$	Sodium nitrate
NASH	Non-alcoholic steatohepatitis

NEDD	N-1-(naphthyl)ethylenediamine
NF-κB	Nuclear factor kappa B
NOS	Nitric oxide synthase
$NO^{\bullet}$	Nitric oxide radical
NO_2^-	Nitrite
NO_3^-	Nitrate
NRF2	Nuclear factor erythroid 2-related factor 2
O_2	Oxygen singlet
$O_2^{\bullet -}$	Superoxide anion radical
OD	Optical density
$OH^{\bullet}$	Hydroxyl radical
OGG1	8-Oxoguanine glycosylase
$ONOO^-$	Peroxynitrite
OX	Oxaliplatin
p53	Tumour protein p53
PBS	Phosphate-buffered saline
PCR	Polymerase chain reaction
PS	Phosphatidylserine
PJS	Peutz-Jeghers syndrome
PRDX/PRXs	Peroxiredoxins
PRRs	Pattern recognition receptors
PUFAs	Polyunsaturated fatty acids
$Q^{\bullet}$	Ubisemiquinone radical
RBI	Relative band intensity
RIPK1	Receptor interacting protein kinase 1
RIPK3	Receptor interacting protein kinase 3
RLU	Relative light units
ROS	Reactive oxygen species
RNS	Reactive nitrogen species
RT	Room temperature
RT-PCR	Reverse transcription polymerase chain reaction

SDS-PAGE	Sodium dodecyl-sulfate polyacrylamide gel electrophoresis
STAT 3	Signal transducer and activator of transcription 3
Stats SA	Statistics South Africa
SULF	Sulfanilamide
TBA	Thiobarbituric acid
TBARS	Thiobarbituric acid reactive substances
TNF	Tumour necrosis factor
TNFR1	Tumour necrosis factor receptor 1
TRADD	TNF receptor-associated death domain
TRAIL	Tumour necrosis factor-related apoptosis inducing ligand
TRIS	Tris(hydroxymethyl)aminomethane
VCl_3	Vanadium chloride
WHO	World Health Organisation
XEL	XELODA
Zn-SOD	Zinc superoxide dismutase

ABSTRACT

Introduction: Cancer is one of the leading causes of death globally. Increased incidence and mortality rates of colorectal and liver cancer have been reported in South Africa and worldwide. Cytotoxic side effects associated with current treatments have sparked interest in using plant phytochemicals as a potential alternate, cost-effective cancer therapeutic. *Monsonia burkeana* Planch. Ex Harv, also known as "special tea", is a medicinal plant native to southern Africa that treats various ailments. It has also shown potential application in anticancer therapy. This study investigated the anticancer effects of *M. burkeana* crude aqueous extract in the Caco-2 and HepG2 cell lines.

Methods: The target cells were reconstituted in CCM and treated with 0 - 5000µg/ml of *M. burkeana* plant extract for 48 hours during the MTT assay to obtain the 20% and 50% inhibitory concentration (IC_{20} and IC_{50}), which was used for experiments that followed. The cytotoxic effects were further evaluated using the LDH and CYP3A4 activity assay to determine oxidative breakdown and assess the ATP and JC-10 levels to measure mitochondrial integrity. The antioxidant response of *M. burkeana* involved conducting the TBARS/NOS assay to extrapolate reactive oxygen and nitrogen species, GSH quantification, and western blotting to detect (SOD, NRF2, iNOS) protein expression. The mRNA gene expression of *Gpx* and *OGG1* was evaluated using qPCR. To assess cell death, the Annexin-V assay distinguished apoptotic and necrotic cells, caspase activation assays were conducted as a marker of apoptosis, and western blotting determined the expression of the following proteins: p53, p-p53, BAX, NFκB, cIAP2, cleaved caspase 3 and BCL-2. Gene expression of *MLKL, RIP1, RIP3, NFκB*, and *TNF-α* was also assessed to evaluate its role in cell death. Lastly, data analysis was conducted using statistical tests in GraphPad Prism.

Results: Cytochrome P450 3A4 activity increased for both cell lines, causing a dose-dependent decrease in cell viability in Caco-2 cells and HepG2 cells, with an IC_{50} value of 293.8 µg/ml and an IC_{20} value of 169.8 µg/ml in Caco-2 cells. In HepG2 cells, the IC_{50} value was 335.4 µg/ml of *M. burkeana* extract, and the IC_{20} value was 154.9 µg/ml. The decreased ATP concentration in Caco-2 and HepG2 cells for both treatments was consistent with the increased $\Delta\Psi m$, confirming a reduced metabolic activity. Decreased MDA levels indicating lipid peroxidation occurred for both cell lines, while increased *OGG1* for the Caco-2 IC_{20} treatment suggests DNA oxidation for this treatment

only. Nitrite levels decreased for both treatments in Caco-2 cells but increased in HepG2 cells. There was also a decrease in iNOS protein expression for both cell lines. Membrane disruption was validated by increased LDH for both cell lines and HepG2 cells were associated with RNS-induced membrane disruption. Oxidative stress is implied due to decreased GSH concentration and upregulation of SOD2 protein expression at both treatment concentrations for Caco-2 and HepG2 cells. However, *Gpx-1* decreased for Caco-2 cells and the IC_{20} treatment in HepG2 cells. There was an associated upregulation of NRF-2 protein expression for both cell lines at the IC_{50} treatment concentrations to regulate antioxidant proteins. Initiator caspase 8 activity increased for both treatment concentrations in Caco-2 cells, implying that in Caco-2 cells, apoptosis was stimulated via the extrinsic pathway. In addition, intrinsic apoptosis was initiated in the IC_{20}-treated Caco-2 cells as caspase 9 activity increased. Caspase 8 and caspase 9 activity decreased for both treatment concentrations in HepG2 cells. The p-p53/p53 ratio decreased for both treatments in Caco-2 cells. Thus, p53 did not mediate the transcription of pro-apoptotic BCL-2 family genes such as BAX, which dropped in both treatment concentrations. Anti-apoptotic BCL-2 was also reduced in Caco-2 cells. In HepG2 cells, the protein expression of p-p53/p53 remained relatively unchanged for IC_{20}-treated cells and increased for IC_{50}-treated, but the BAX decreased for $IC_{20,}$ and BCL-2 protein expression increased for the IC_{50} treatment concentration. *M. burkeana* facilitated the execution of apoptosis in both cell lines, as caspase 3/7 was increased and phosphatidylserine was externalised, but necrosis was also increased. There was downregulation of *TNF*α in Caco-2 cells, and decreased *RIPK1, RIPK3* and *MLKL* for both treatment concentrations corresponding with increased cIAP2. In HepG2 cells, there was an increase in *RIPK1* gene expression for both the IC_{20} and IC_{50} treatment concentrations, decreased cIAP2 protein expression, increased *RIPK3* and *MLKL* gene expression.

Conclusion: According to the results, *M. burkeana* crude aqueous extract caused caspase-dependent apoptosis in Caco-2 cells and nitrosative stress-induced necroptosis in HepG2 cells, which validates that *M. burkeana* can be further explored as an anticancer therapeutic.

KEYWORDS: *Monsonia burkeana* Planch. ex Harv, Caco-2 cells, HepG2 cells, cytotoxicity, free radicals, apoptosis, necroptosis.

CHAPTER 1: INTRODUCTION

1.1 BACKGROUND

Cancer occurs when healthy cells are transformed into tumour cells through various changes that lead to disease in different body organs (National Cancer Institute, 2021). Cancer is one of the leading causes of death globally, accounting for nearly 10 million deaths in 2020 (World Health Organisation, 2020). There are many types of cancer classified according to the organ affected; some forms are more common, and others have higher mortality rates. Colorectal cancer (CRC) is a disease whereby cells divide uncontrollably in the rectum or colon. In 2020, it was estimated to be the third most common cancer in men and the second most common cancer in women, after breast cancer, as described by the International Agency for Research on Cancer (IARC) (Ferlay *et al.*, 2020). Colorectal cancer is the second most common cause of death globally, with almost 1 million deaths reported and nearly 2 million new cases, representing an incidence rate of 10% and a mortality rate of 9.4% for all cancers, respectively (World Health Organisation International Agency for Research on Cancer (IARC), 2021). Studies have estimated that rectal and colon cancer-related deaths would increase by 60% and 71%, respectively, by 2035 and 63% and 73% by 2040 (Morgan *et al.*, 2023, Douaiher *et al.*, 2017). Numerous studies have also drawn attention to the fact that colorectal cancer survival varies depending on the stage at which it is identified, with worse survival rates for late-stage diagnoses (Andrew *et al.*, 2018, Rawla *et al.*, 2019). For localised CRC (35.5% of cases), the 5-year relative survival is 90.9%, regional CRC (36% of cases) has a survival rate of 76.4%, distant (23% of cases) accounts for 15.6% 5-year relative survival rate and unstaged cancer (6% of cases) accounts for 48.6% survival (National Cancer Institute, 2023). In 2020, primary liver cancer accounted for over 906,000 new cases and 830,000 cancer deaths worldwide, making it the sixth most prevalent disease diagnosed and the third leading cause of cancer-related death (Sung *et al.*, 2021). Hepatocellular carcinoma (HCC) is the second most significant cause of cancer-related death among men after lung cancer, with a 5-year survival rate of 18%, which is second to pancreatic cancer (Sung *et al.*, 2021, Jemal *et al.*, 2017). Research suggests that underlying Hepatitis B Virus (HBV) has the greatest effect on overall survival, followed by Hepatitis C Virus (HCV), metabolic diseases and alcoholic liver disease

to a lesser extent. According to a study conducted in 2020 using the American Cancer Society which uses information from the Surveillance, Epidemiology, and End Results (SEER) program, the median survival periods after diagnosis of HCC in patients with the aforementioned etiologies were 10.3, 8.3, 7.6 and 6.1 months (Brar *et al.*, 2020). If diagnosed early, cancer is more likely to be treated effectively.

Current cancer treatment involves aggressive therapies such as surgical removal and radiation on affected areas, followed by chemotherapy for maintenance. This may occur as a single treatment or can be combined (Debela *et al.*, 2021). Although effective, chemotherapy has disadvantages such as nonspecificity, reoccurrence, and toxic effects on untargeted cells, decreasing quality of life through side effects like nausea, fatigue, and infections. Drug resistance, long-term health risks, emotional strain, and high costs further complicate treatment, underscoring the need for more targeted cancer therapies (Nurgali *et al.*, 2018). The search for potentially less harmful anticancer agents to combat the adverse side effects of current cancer treatment is ongoing, offering hope for more effective, targeted therapies with fewer side effects, improved patient quality of life, and reduced long-term health risks. Additionally, these advancements could lead to lower treatment costs, decreased emotional strain, and increased overall survival rates for cancer patients. Phytochemicals and their derivatives are biologically active compounds that occur in plants. They have promising potential in cancer treatment due to their antitumour properties (Choudhari *et al.*, 2019). Medicinal plants have been used for centuries to treat infections and ailments and have recently become increasingly popular (El Orfi *et al.*, 2022). They provide nutritional value, and secondary metabolites such as phenols, flavonoids, tannins, proanthocyanidins, carotenoids, alkaloids, and saponins confer various biological and pharmacological properties (Roy *et al.*, 2022). Medicinal plants are usually prepared as decoctions, infusions, and tonics, commonly known as herbal teas, containing phenolic compounds that significantly contribute to their antioxidant capacity (Qasim *et al.*, 2017).

Monsonia burkeana Planch. Ex Harv*,* also known as "special tea," is a medicinal plant utilised to treat various ailments (Malongane *et al.*, 2022). It is a dicotyledon that is part of the

Geraniaceae family. This plant is native to southern African countries and is found in the Eastern Cape, Free State, Gauteng, and Limpopo (Nnzeru *et al.*, 2016). *M. burkeana* is combined with other herbs as a blood cleanser, a cure for sexually transmitted diseases, restores erectile dysfunction disorders, and enhances male libido (Malongane *et al.*, 2022). In addition to indigenous knowledge obtained over decades, studies have reported various health benefits regarding its antidiabetic and anticancer effects. These benefits are attributed mainly to this medicinal plant's high concentration of phenolic constituents (Tshivhandekano *et al.*, 2014). Phenolic compounds have antioxidant capabilities *in vivo* that have been reported to assist in maintaining the balance between oxidants and antioxidants, thus reducing oxidative stress in cells (Mathivha *et al.*, 2019).

Oxidative stress is described as a relative excess of free radicals compared to the antioxidant levels in cells (Hayes *et al.*, 2020). Uncontrolled levels of oxidative stress may lead to neurodegenerative diseases, cardiovascular disease, diabetes mellitus, cancer, and other pathologies (Jomova *et al.*, 2023). Reactive oxygen species (ROS) and reactive nitrogen species (RNS) are unavoidable free radical products of metabolism that are used for intracellular signalling processes (Mandal *et al.*, 2022). However, they are potentially harmful when produced in excess. Antioxidant systems ensure that ROS/RNS levels are controlled for cellular signalling and that oxidative stress is minimised. A central component in the defence against oxidative stress is nuclear factor erythroid 2-related factor 2 (NRF-2), which controls the expression of antioxidant and detoxification genes such as glutathione-S-transferases (GSTs), reduced glutathione (GSH), superoxide dismutases (SODs) and catalase. This is essential is maintaining redox homeostasis (Ghareghomi *et al.*, 2022). These antioxidant systems detoxify harmful metabolites produced from ROS/RNSor limit the amount produced (Hayes *et al.*, 2020). The superoxide anion radical ($O_2^{\bullet-}$) is a ROS produced in the cytosol and mitochondria. The $O_2^{\bullet-}$ is also a source of RNS when it reacts with nitric oxide ($NO^{\bullet}$) to produce the peroxynitrite anion ($ONOO^-$) (Jie *et al.*, 2023). The $O_2^{\bullet-}$ is detoxified by superoxide dismutase (SOD) to the less reactive hydrogen peroxide (H_2O_2) by catalase or glutathione peroxidase, which requires GSH as a cofactor (Rosa *et al.*, 2021). Alternatively, H_2O_2 forms the hydroxyl radical ($^{\bullet}OH$) in the Fenton reaction (Abe *et al.*, 2022). The reactive species have different half-lives and physiochemical properties. The most oxidising ROS is

$^{\bullet}OH$, followed by $O_2^{\bullet-}$, and H_2O_2 is a weak oxidant (Kıran *et al.*, 2023). The H_2O_2 and $NO^{\bullet}$ are essential in signalling, and $O_2^{\bullet-}$ and $ONOO^-$ are very reactive and can damage intracellular macromolecules such as polyunsaturated fatty acids (PUFAs) and nucleic acids. The oxidation of PUFAs by ROS causes lipid peroxidation, where the peroxidised PUFAs and their byproducts, such as 4-hydroxy-2-nonenal (4-HNE), may serve as signalling molecules for inflammation, apoptosis, necroptosis or ferroptosis (Breitzig *et al.*, 2016).

Apoptosis is programmed cell death, crucial for development, homeostasis, and eliminating unwanted cells. Apoptosis may occur via the intrinsic or extrinsic pathway, depending on whether an intracellular or extracellular signal is received. Intracellular signals include DNA damage, growth factor deprivation, and cytokine deprivation. The most common extracellular signals are death-inducing signals produced by cytotoxic T cells. These pathways converge at the executioner caspases (Kashyap *et al.*, 2021). The intrinsic pathway is mainly inhibited in cancer; thus, DNA damage or uncontrolled cellular proliferation does not activate apoptotic pathways (Pfeffer and Singh, 2018). Cancer cells that lack the tumour suppressor protein p53 are implicated, which suggests disruption in the regulation of apoptosis. Furthermore, the non-sequestration of the anti-apoptotic protein B-cell lymphoma 2 (Bcl-2) by Puma/Noxa and the inability of B-cell lymphoma 2-associated X protein (BAX) to form pores for cytochrome c release results in the disruption of apoptosome formation and subsequent activation of caspase 9, pivotal steps in the apoptotic cascade (Obeng, 2021). Dysregulation of apoptosis results in causing cancer cells to survive, proliferate, and accumulate mutations (Hassan *et al.*, 2014).

The Fas/Tumour necrosis factor (TNF) pathway plays an essential role in apoptosis triggered by the binding of Fas ligand (FasL) or TNF-α ligands to their respective receptors. In turn, this activates caspase 8, initiating the extrinsic apoptotic pathway leading to the execution of programmed cell death (Bertheloot *et al.*, 2021). In extrinsic apoptosis, the FasL binds to the Fas receptor (FasR), which initiates programmed cell death. This binding causes the recruitment of the Fas-associated death domain (FADD), and the formation of a death-inducing signalling complex (DISC) results when pro-caspase 8 binds. Pro-caspase 8 gets cleaved once activated into caspase 8 and can thereafter activate downstream molecules to execute cell death (Jan and Chaudhry, 2019). The second extrinsic apoptosis pathway includes

the pro-inflammatory cytokine TNF, which binds to the TNFR receptor, thus initiating a signalling cascade that promotes cell survival or can lead to cell death. In the case of apoptosis, the binding of TNF to TNFR causes the recruitment of TNF receptor-associated death domain (TRADD), TNFR-associated factors 2/5 (TRAF 2/5), rip kinase 1 and inhibitor of apoptosis proteins (cIAP1/2) which forms complex 1 (Seo *et al.*, 2021). If RIPK1 is polyubiquitinated by cIAP1/2, this induces the NF-κB pathway, resulting in cell survival. If internalisation of TNFR occurs, there may be alterations in the proteins of complex 1; for example, RIPK1 can be deubiquitinated by deubiquitinase cylindromatosis (CYLD); therefore, the NF-κB pathway will be limited. The death-inducing signalling complex called complex II (ripoptosome) is formed, consisting of RIPK1, TRADD, caspase 8 and FADD. Caspase 8 cleaves RIPK1 and RIPK3, leading to their inactivation and apoptosis results when caspase activation is initiated (Gong *et al.*, 2019). When caspase 8 is inhibited, the necrosome forms in which RIPK3 phosphorylates MLKL thus leading to its oligomerisation and translocation to the cell membrane for the execution of necroptosis (Zhao *et al.*, 2015).

Inhibitors of apoptosis proteins inhibit cell death by suppressing the activity of caspases by directly binding to them, ubiquitination of caspases for degradation, interacting with apoptosis-regulating proteins and the modulation of signalling pathways (Kumar *et al.*, 2020). Nuclear factor-kappa B (NF-κB) is a pivotal transcription factor in regulating cellular responses to various stimuli, including apoptosis and necrosis. In the regulation of apoptosis, NF-κB is associated with promoting cell survival by upregulating anti-apoptotic genes (IAPs, BCL-2 family) and suppressing transcription of pro-apoptotic components (Zinatizadeh *et al.*, 2021). Necroptosis is a type of programmed necrosis that is controlled by cytokines and pattern recognition receptors (PRRs). Cell death due to necroptosis results in cell swelling, membrane rupturing and the release of damage-associated molecular patterns (DAMPs), inflammatory cytokines and chemokines, which result in an inflammatory response (D'Arcy, 2019).

There is insufficient research on the antioxidant and antiproliferative properties of *M. burkeana* on Caco-2 and HepG2 cells. Consequently, this research focuses on the medicinal

plant *M. burkeana*, targeting the oxidative and apoptotic processes to close the knowledge gap about the potential anticancer effects of *M. burkeana*.

1.2 PROBLEM STATEMENT / RATIONALE

Cancer is a global threat, with an increasing number of deaths annually. According to statistics published in 2021, colorectal and liver cancer are on the rise as they are now among the most common cancers and a leading cause of death in most countries. Colorectal cancer was the second most common cause of death globally, and liver cancer was the third leading cause of death in 2021(Sung *et al.*, 2021). Five-year relative survival rates for colorectal cancer vary depending on the stage of metastasis. For example, a localised stage has a relative survival rate of 90.9%, compared to a 15,5% relative 5-year survival rate for the distant stage (National Cancer Institute, 2023). Early diagnosis of HCC is associated with more than 70% survival rates at 5 years, while advanced stages can have less than 20% survival rates in the same interval (Calderon-Martinez *et al.*, 2023). Although some drugs target these types of cancer, they have debilitating side effects (Anand *et al.*, 2023). Therefore, alternate treatments, such as using medicinal plant compounds with limited or no side effects, have gained interest in recent years and should be investigated to ensure optimal health and well-being of patients.

1.3 SIGNIFICANCE AND IMPLICATIONS

Both CRC and HCC have a poor prognosis if a patient is not screened in the early stages of cancer when it has not spread as significantly. Colorectal cancer treatment depends on the cancer stage, location, and other health concerns. Treatment usually involves surgery, radiation and chemotherapy. Surgery has risks and side effects that depend on the procedure's extent and the patient's general health. Issues during or after surgery can include bleeding, infection, and blood clots in the legs (American Cancer Society, 2020). For HCC patients, surgical resection and transplantation are only effective for patients diagnosed in the early stages. Rare and advanced forms of HCC in some patients make treating them with traditional methods like surgery impossible because liver transplants in people with impaired immune systems can be fatal (Tumen *et al.*, 2022). The outcomes of this study will help evaluate *M. burkeana* as a possible source for development of an anticancer regimen for the treatment of

CRC and HCC. The benefits of drinking the conventional African medicine, *M. burkeana* as a herbal tea, can be identified in this study's findings, which may benefit patients, the healthcare system and the economy.

1.4 RESEARCH QUESTION

Does *M. burkeana* alleviate oxidative stress and cause apoptosis within colorectal cancer (Caco-2) and hepatocellular carcinoma (HepG2) cells?

1.5 HYPOTHESIS

M. burkeana modulates oxidative stress to induce apoptosis in Caco-2 and HepG2 cells.

1.6 NULL HYPOTHESIS

There is no statistically significant relationship between *M. burkeana*, oxidative stress and apoptosis in Caco-2 and HepG2 cells.

1.7 AIM

This study aims to determine *M. burkeana* crude aqueous extract's antioxidant and antiproliferative mechanisms in Caco-2 and HepG2 cells.

1.8 OBJECTIVES

A crude aqueous extract of the *M. burkeana* leaves will be used to

- identify cytotoxic effects of *M. burkeana* on Caco-2 and HepG2 cancer cells by
  - using the MTT assay and derive the IC_{20} and IC_{50} concentrations for treatment.
  - measuring extracellular LDH levels as an indicator of cytotoxicity.
  - detecting CYP3A4 activity in oxidative breakdown.
  - evaluating mitochondrial viability and function by quantifying ATP levels

(luminometry) and determining mitochondrial membrane potential using the JC-10 assay.

- determine the role of *M. burkeana* antioxidant properties on the Caco-2 and HepG2 cell lines using the
  - thiobarbituric acid reactive (TBARS) and nitric oxide synthase (NOS) assays to extrapolate the production of reactive oxygen and nitrogen species, respectively.
  - glutathione (GSH) luminometric assay to quantify reduced glutathione concentration.
  - western blotting to detect protein expression (SOD, NRF-2 and iNOS).
  - qPCR to detect gene expression of Gpx and OGG1.
- verify the role of *M. burkeana* the Caco-2 and HepG2 cell lines on cell death by
  - distinguishing between apoptotic and necrotic cells using the luminometric Annexin V assay.
  - luminometrically assessing caspase activity as a measure of apoptosis.
  - detecting protein expression of p53, p-p53, BAX, NFκB, $cIAP_2$, cleaved caspase 3 and BCL-2 by western blotting.
  - using qPCR to detect gene expression of MLKL, RIPK1, RIPK3, NFκB, TNF-α)

CHAPTER 2: LITERATURE REVIEW

2.1 CANCER

Cancer has been identified as a global health threat in developed and developing countries.The world cancer incidence and mortality were estimated using GLOBOCAN 2020 data produced by the International Agency for Research on Cancer. There were an estimated 19.3 million new cancer cases globally and almost 10.0 million cancer deaths in 2020 (Sung *et al.*, 2021). The top 10 cancer types with estimated incidence and mortality rates for both men and women combined and separately are shown in Figure 2.1. These cancers accounted for >60% of new cancer cases and >70% of cancer deaths. The most commonly diagnosed cancer is female breast cancer (11.7% of total cases), lung cancer (11.4%), colorectal cancer (10%), prostate cancer (7.3%) and stomach cancer (5.6%). In terms of mortality worldwide, lung cancer contributes 18% of total cancer deaths, followed by colorectal cancer (9.4%), liver cancer (8.3%), stomach cancer (7.7%) and female breast cancer (6.9%) (Sung *et al.*, 2021).

In Africa, an estimated 1.1 million new cases and 711429 deaths occurred due to neoplasms. South Africa was ranked third in the country-specific cancer burden, with an expected incidence of 124815 and 108168 deaths (Sharma *et al.*, 2022). Information compiled in a report from the National Cancer Registry of the National Department of Health and the Health and Vital Statistics division within Stats-SA revealed the following information on cancer patients that were diagnosed and died in South Africa between 2008 and 2019: In males, the most diagnosed cancers were prostate, colorectal and lung cancer. These 3 cancer types accounted for one-third of all cancers diagnosed among males. Prostate cancer accounted for 25.3% of cancers, colorectal cancer for 5.6%, and lung cancer for 4.0%. Breast cancer was the most common type of cancer found in females, accounting for 23.2% of all cancers found in females. Cervical cancer came in second at 15.9%, while colorectal cancer came in fourth at 4.5%. An estimated 43.5% of female cancer diagnoses were for these top three malignancies (Statistics South Africa, 2023). A comparison of the cancer threat in 2020 and its predicted burden in 2040 is depicted in Figure 2.2 (Sharma *et al.*, 2022). It can be seen that colorectum and liver cancer are among the most common cancers with the highest incidence

and mortality rates, as well as their predicted values for 2040. By 2040, 5 major cancer groups, including breast, cervical, prostate, CRC, and liver cancer, are expected to double in incidence and mortality, as seen in Figure 2.2. In Africa, 12 neoplasms are anticipated to have more than 50,000 cases per annum and cancer deaths are predicted to be > 50,000 in nine neoplasms by 2040 (Sharma *et al.*, 2022).

Cancer risk factors include certain chemical exposure, age, family history, and lifestyle risk factors such as smoking and inadequate physical activity, amongst others. (National Cancer Institute, 2022). Cancer cells contain genetic alterations which impact the metabolic activity of these cells through the cell cycle process and apoptotic pathways. This, in turn, causes dysregulation of signalling pathways, leading to tumourigenesis. These oncogenic mutations, such as point mutations, truncations, and fusions, can cause genes to be over-expressed, amplifying genes or producing non-functional proteins (Sever and Brugge, 2015).

Current cancer treatment includes chemotherapy, immunotherapy, gene therapy and radiation therapy (Malik *et al.*, 2021). Chemotherapy utilises drugs that can kill cancer cells and, as a consequence, stop proliferation and metastasis. This therapy is most effective when multiple drugs are used and often used in combination with radiation and surgery. Neoadjuvant chemotherapy refers to chemotherapy given before radiation or surgery to reduce tumour size. Adjuvant chemotherapy is given post-radiation or surgery to destroy the remaining cancer cells (Akbari *et al.*, 2022). One of the limitations of chemotherapy is that both cancerous and healthy cells are killed (Anand *et al.*, 2023). Immunotherapy increases the body's natural immune system defence by making antibodies to kill cancer cells. Monoclonal antibodies are synthesised and injected into patients to block the activity of specific genes in cancer cells, a process known as targeted therapy (Riley *et al.*, 2019). Human gene transfer, also known as gene therapy, introduces genetic components into cancer cells to rectify the abnormal genes or to create functional proteins to replace mutated genes, thus restoring protein function (Cesur-Ergun and Demir-Dora, 2023). Radiation therapy includes the use of high doses of radiation to blast cancer cells, thus forming ions, in turn killing them. A significant drawback is ensuring that only cancerous cells are destroyed, not the healthy surrounding tissue (Baskar

et al., 2012).

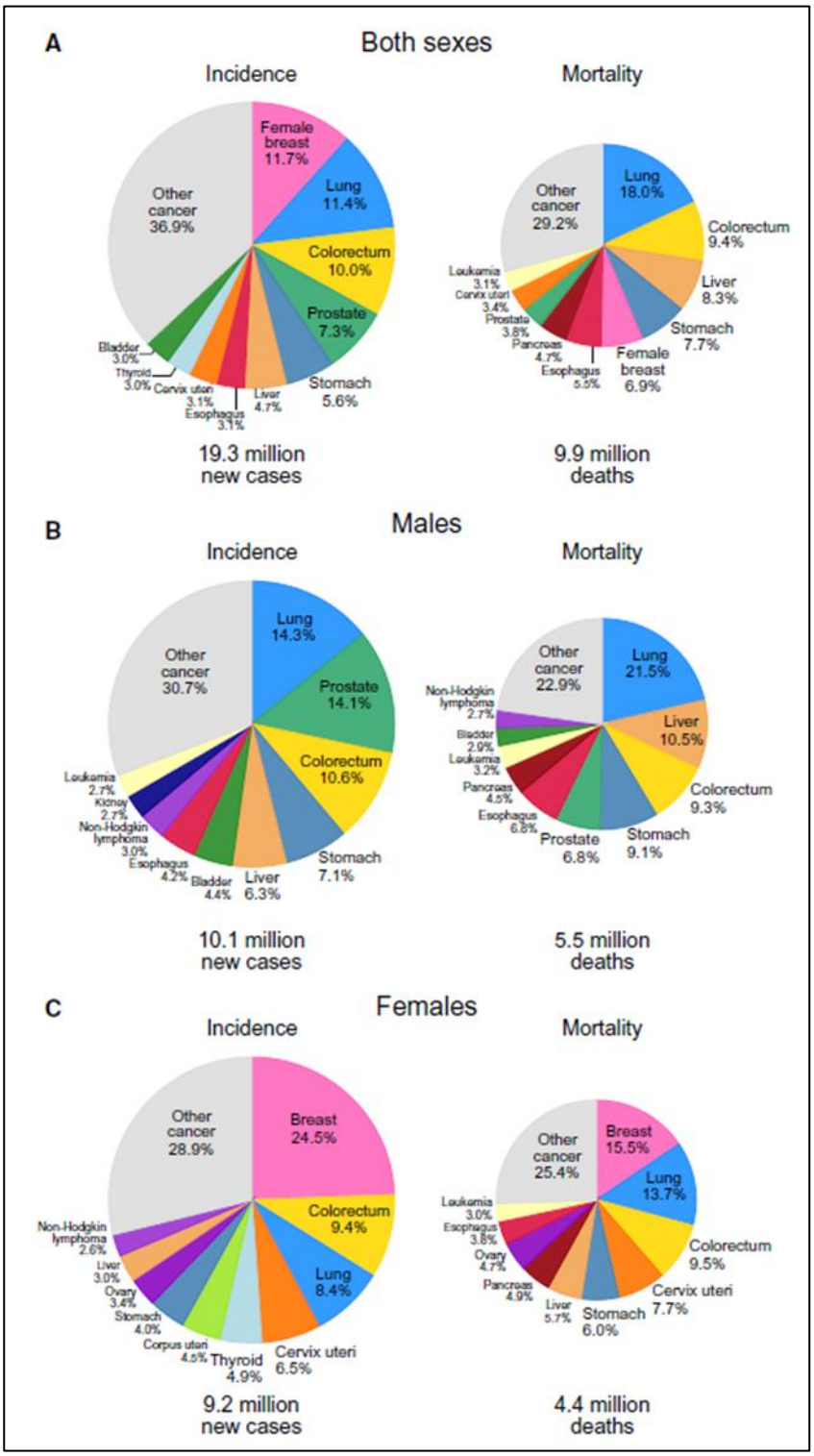

Figure 2.1: Cancer incidence and mortality rates in 2020 for the top 10 common cancers for both sexes (Sung *et al.*, 2021). **(A)** Of the 19.3 million incident cases in 2020**, (B)** 52% occurred in males and 48% in women **(C)**. Similarly, more men died of cancer-related diseases compared to women.

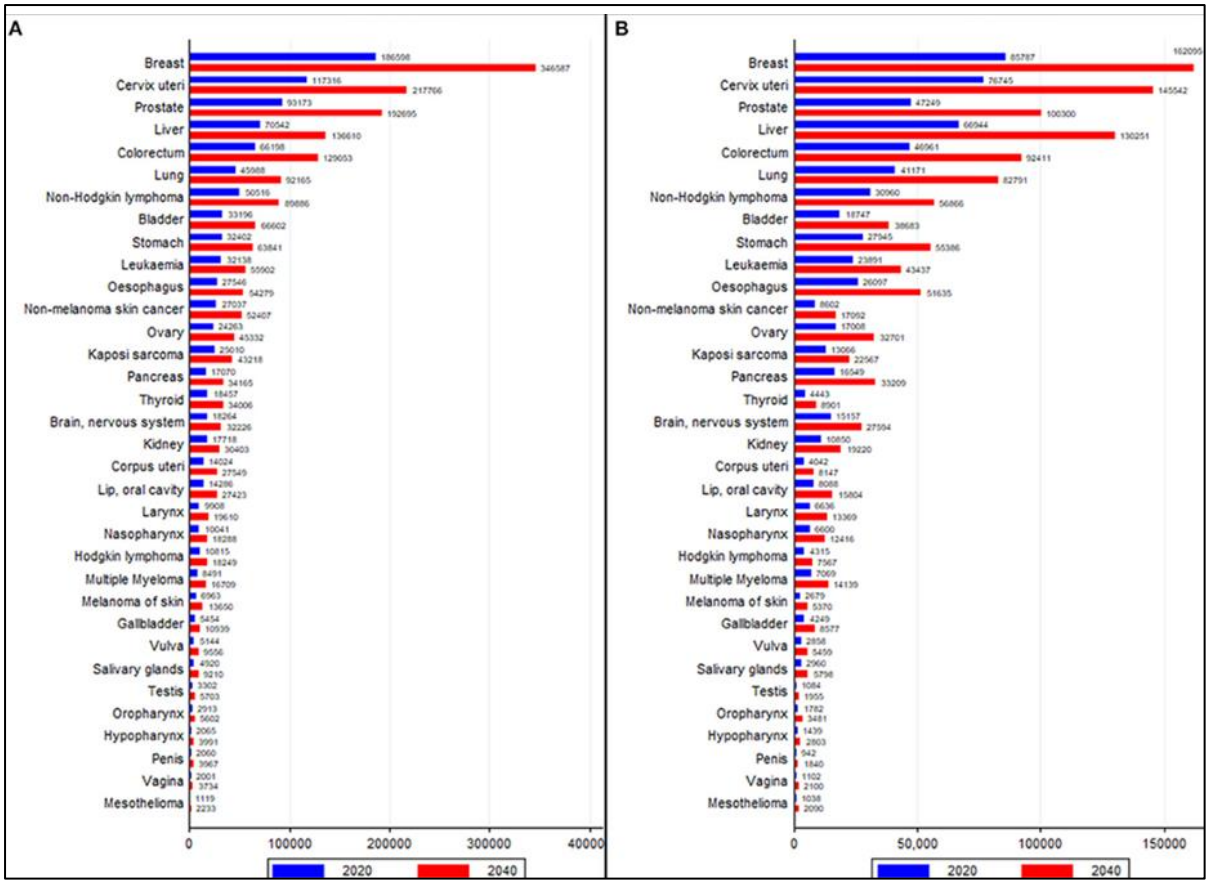

Figure 2.2: A comparison of cancer cases in Africa for 2020 and predicted values in 2040 for both genders. **(A)** Colorectal and liver cancer are among the top 5 incident cancers. **(B)** In terms of cancer-related deaths, liver cancer ranks 3rd and colorectal cancer 5th in Africa (Sharma *et al.*, 2022).

2.2 COLORECTAL ADENOCARCINOMA

Colorectal cancer (CRC) is a form of gastrointestinal cancer that occurs in the large intestine. Colorectal refers to the colon and rectum, which comprise the large intestine (Figure 2.3).

2.2.1 The colon and rectum

The colon is the most extended component of the large intestine. The colon receives food that is almost fully digestedfrom the cecum. It is involved in the absorption of water and nutrients and passes faeces to the rectum. The colon is made up of four parts: the ascending, transverse, descending and sigmoid colon (Figure 2.3). The proximal colon refers to the ascending and transverse colon, and the distal colon refers to the descending and sigmoidal colon (American

Cancer Society, 2022). The rectum is the large intestine's bottom part, which connects the sigmoidal colon (Figure 2.3). It is approximately 15cm in length and receives waste substances from the colon and stores them until it passes out of the body through the anus (American Cancer Society, 2022).

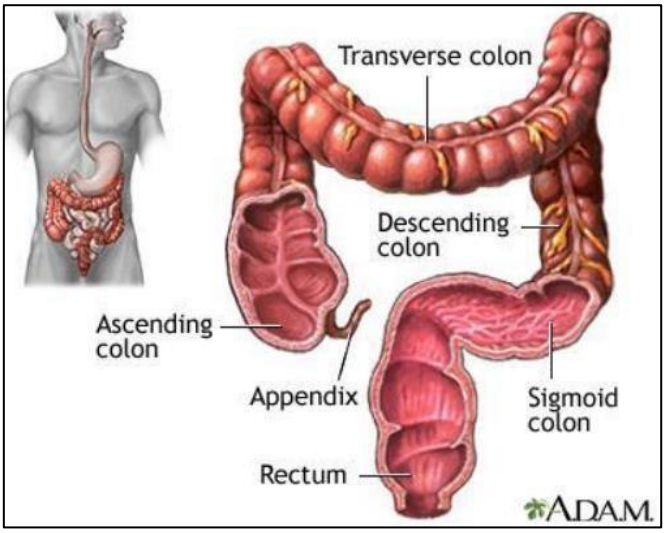

Figure 2.3: The colon and rectum are part of the gastrointestinal tract. The small intestine connects to the proximal colon, comprising the ascending and transverse colon, and the descending and sigmoid colon make up the distal colon. The rectum joins the sigmoid colon to the anus (Herbst, 2015).

2.2.2 Incidence of colorectal cancer

A reported 1.9 million new colorectal cancer cases and 935,000 deaths were estimated in 2020 (Sung *et al.*, 2021). This translates into approximately one in ten cancer cases and deaths (Figure 2.1A). Colorectal cancer is the third leading incident cancer and has the second-largest mortality rate globally. Among males, colorectal cancer ranks 3rd in global incidence and mortality (Figure 2.1B) and ranks 2nd for incidence and 3rd for mortality in females (Figure 2.1C) (Sung *et al.*, 2021). In Africa, CRC gained prominence with 66 198 cases and 42 875 deaths in 2020; it is among the top ten cancers in all 54 African countries, and 2040 projected increases continue to rank CRC amongst the top five cancers in Africa (Figure 2.2) (Sharma *et al.*, 2022). The age-standardised CRC incidence rate in South Africa per 100,000 males was 12.51 in 2019 (Figure 2.4A). The highest incidence was observed in White males (26.5), followed by Indian/Asian males (18.68), Coloured males (16.89) and Black African males (5.49). The age-standardised CRC incidence rate in South Africa per 100,000 females was

7.28 in 2019 (Figure 2.4B). The highest incidence was obtained for White females (18.48), followed by Indian/Asian females (10.92), Coloured females (10.47) and Black African females (3.39) (Statistics South Africa, 2023).

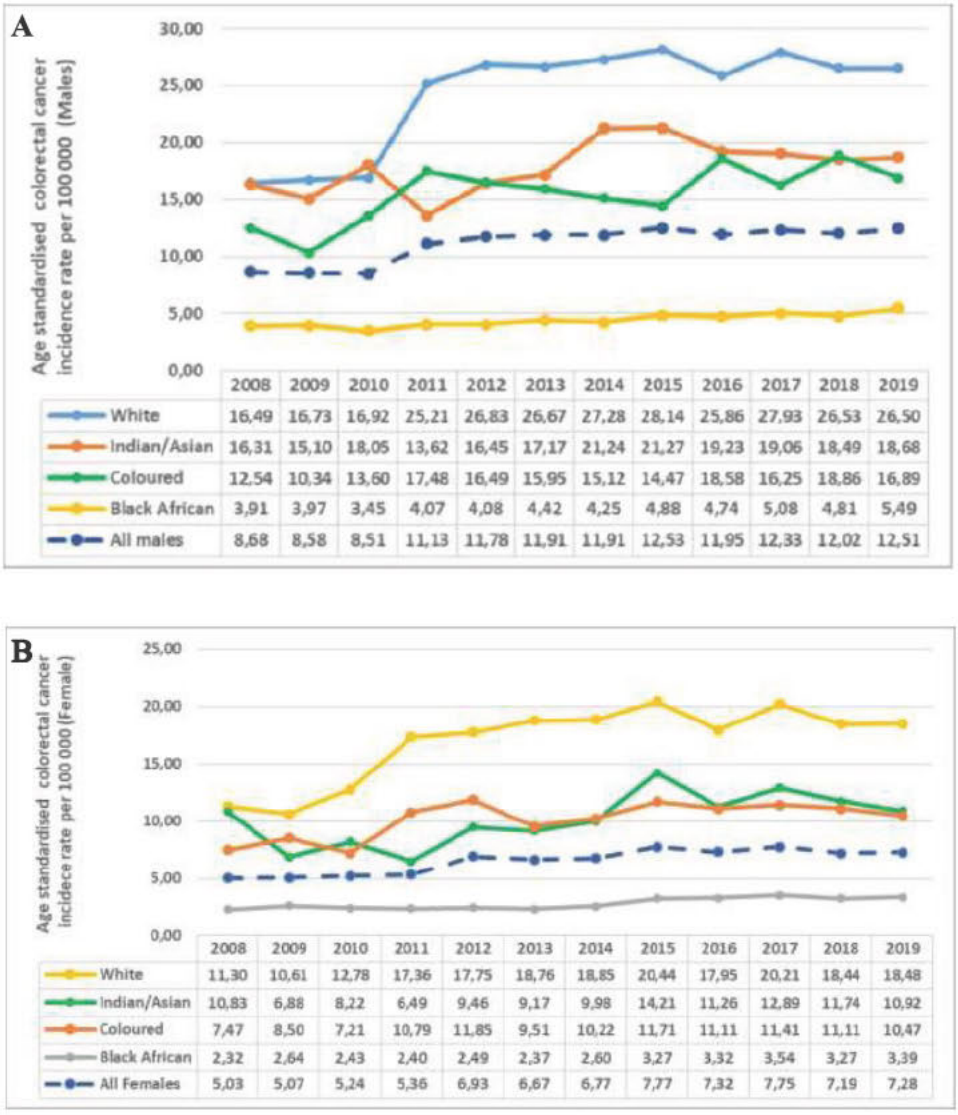

	2008	2009	2010	2011	2012	2013	2014	2015	2016	2017	2018	2019
White	16,49	16,73	16,92	25,21	26,83	26,67	27,28	28,14	25,86	27,93	26,53	26,50
Indian/Asian	16,31	15,10	18,05	13,62	16,45	17,17	21,24	21,27	19,23	19,06	18,49	18,68
Coloured	12,54	10,34	13,60	17,48	16,49	15,95	15,12	14,47	18,58	16,25	18,86	16,89
Black African	3,91	3,97	3,45	4,07	4,08	4,42	4,25	4,88	4,74	5,08	4,81	5,49
All males	8,68	8,58	8,51	11,13	11,78	11,91	11,91	12,53	11,95	12,33	12,02	12,51

	2008	2009	2010	2011	2012	2013	2014	2015	2016	2017	2018	2019
White	11,30	10,61	12,78	17,36	17,75	18,76	18,85	20,44	17,95	20,21	18,44	18,48
Indian/Asian	10,83	6,88	8,22	6,49	9,46	9,17	9,98	14,21	11,26	12,89	11,74	10,92
Coloured	7,47	8,50	7,21	10,79	11,85	9,51	10,22	11,71	11,11	11,41	11,11	10,47
Black African	2,32	2,64	2,43	2,40	2,49	2,37	2,60	3,27	3,32	3,54	3,27	3,39
All Females	5,03	5,07	5,24	5,36	6,93	6,67	6,77	7,77	7,32	7,75	7,19	7,28

Figure 2.4: Colorectal cancer incidence rates of male **(A)** and female **(B)** South Africans (Statistics South Africa, 2023). In both males and females, colorectal cancer is most prevalent in White South Africans, followed by Indian, Coloured and Black Africans.

2.2.3 Types of colorectal cancer and carcinogenesis

There are different types of CRC, with the most common being adenocarcinoma. Other types

of CRC include carcinoid tumours, gastrointestinal stromal tumours (GIST), colorectal lymphoma, carcinoids, Turcot Syndrome, Peutz-Jeghers Syndrome (PJS), Familial Colorectal Cancer (FCC) and Juvenile Polyposis Coli (Stanford Healthcare, 2022). Colorectal cancer carcinogenesis models include three global genetic and epigenetic aberrations, which include chromosomal instability (CIN), methylation of CpG island methylator phenotype (CIMP) and instability of microsatellite DNA regions (MSI). The CIN pathway follows a pattern of the progression of an adenoma. This is present in 85% of sporadic colorectal cancer instances and occurs due to structural alterations in chromosomal segments. The CIMP pathway consists of alterations in the methylation frequency of CpG islands in promoter regions of tumour suppressor genes, causing decreased expression or complete silencing (Ahmed *et al.*, 2021). Microsatellite instability is a mutator phenotype due to a deficient mismatch repair system (MMR) utilised to repair replication errors. A significant characteristic of MSI is polymorphisms of microsatellite sequences due to DNA polymerase slippage (De' Angelis *et al.*, 2018).

In most instances, CRC begins as a polyp in the intestinal mucosa; however, it can also exist as an adenoma initially and, after that, has the potential to transform into a malignant lesion. This depends on the location and size of the malignant lesion. Most CRC cases are carcinomas, and >90% are adenocarcinomas (Lotfollahzadeh *et al.*, 2023). The staging system for CRC is classified according to the Astler-coller-Dukes system. This system is also referred to as "TNM" as described by the American Joint Committee on Cancer, where T represents the spread of propagation through colonic or rectal wall layers, N denotes the presence of malignant tumours in lymph nodes, and M signifies metastasis to distant organs (Silva *et al.*, 2005). When adenocarcinomas become metastatic, they can spread via blood and lymphatic arteries. However, it may take up to 5-15 years between the development of a polyp and invasive cancer (Huck and Bohl, 2016).

Colorectal cancer is classified by stage 0 through stage IV (Figure 2.5). Typically, a non-cancerous development causes the production of dysplastic tissue (tumour), which results in the development of CRC after the cells have experienced multiple aberrant DNA mutations

(Hossain *et al.*, 2022). A growth that does not invade different body regions is referred to as a non-cancerous (benign) soft tissue tumour. A benign polyp or adenoma forms due to hyperproliferation and is referred to as stage 0 (Pai *et al.*, 2019). Stage I refers to 10% of adenomatous polyps that can become malignant and form adenocarcinomas that invade muscularis propria (Aarons *et al.*, 2014). In stages II and III, the tumour increases in size and infiltrates the visceral peritoneum and serosa. Stage IV results from lymphatic or blood metastases (Hossain *et al.*, 2022).

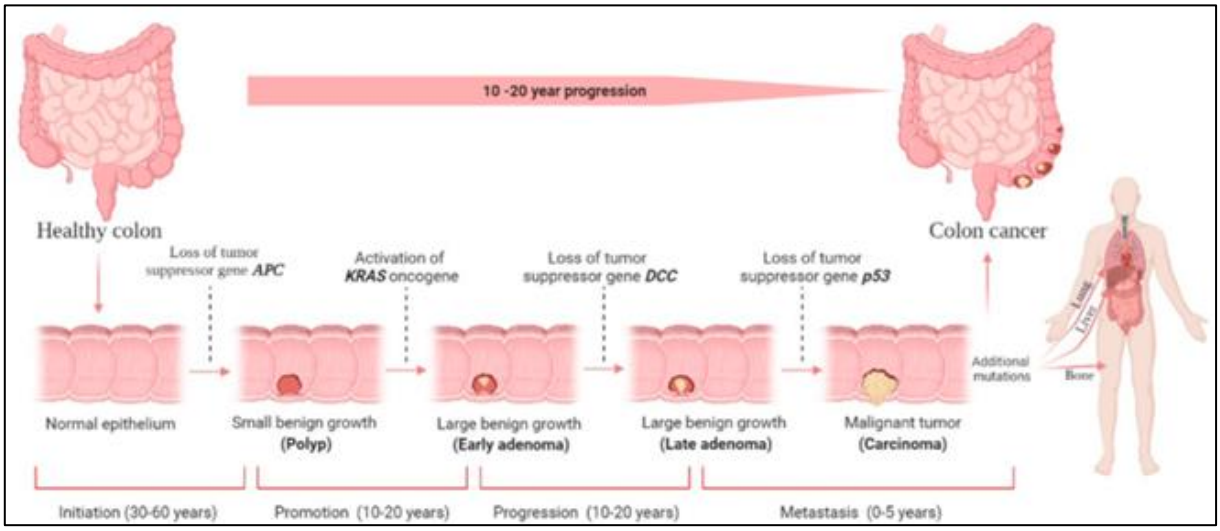

Figure 2.5: The stages and development of CRC from the benign polyp in stage 0 to the adenoma in stage 1. The tumour size increases in stages II and III and becomes a malignant carcinoma in stage IV (Hossain *et al*., 2022).

2.2.4 Risk factors

Some risk factors associated with developing colorectal cancer include a family history of cancer, a history of polyps, inflammatory bowel disease, diabetes mellitus, or cholecystectomy (Lewandowska *et al.*, 2022). Lifestyle factors such as overweight and obese individuals, physical inactivity levels, smoking,consuming alcohol, and an unhealthy diet (low in fibre, fruit, vegetables, calcium, and high consumption of red and processed meat) increase an individual's risk of CRC. An individual's gut microbiome, age, gender, race, and socioeconomic status can also influence CRC risk (Sawicki *et al.*, 2021). This disease can be viewed as a marker of the country's socio-economic development (Bray *et al.*, 2018). It has been established that nations with medium to high human development indices (HDIs)

embracing a "western" way of life see the most significant increases in CRC incidence and mortality. The risk of colon cancer is more significant in developed nations. Obesity, sedentary behaviour, consumption of red meat, alcohol use, and cigarette use are thought to be the main contributors to the rise of CRC (World Health Organisation, 2020).

2.2.5 Treatment options for colorectal cancer

Treatment depends on the location of the cancer, its stage, and the patient's general health. After that, treatment usually involves surgery to remove the tumour or other therapies such as radiation and chemotherapy (Malik *et al.*, 2021). For early stages of colon cancer, less invasive surgeries may be recommended, such as removing polyps during colonoscopy (polypectomy), endoscopic mucosal resection and laparoscopic surgery for polyps that cannot be removed using a colonoscopy (Cruz *et al.*, 2011). For more advanced colon cancer, a partial colectomy, surgery to create a path for waste to exit the body or lymph node removal may be recommended. In certain instances where the cancer has spread only to the liver or lung but a patient's general health is otherwise good, a physician may recommend surgery or other localised treatments to remove the cancer (Chakrabarti *et al.*, 2020). Chemotherapy may be used before or after this type of procedure. This approach allows the patient to be cancer-free over the long term (Mayo Foundation for Medical Education and Research, 2022). Chemotherapy is used as an addition to surgery to prevent cancer reoccurrence and can be palliative, adjuvant or neoadjuvant (Akbari *et al.*, 2022). When cancer has spread to other bodily parts and surgical removal is not an option, palliative care is performed. Palliative chemotherapy aims to lessen the symptoms, decrease the tumour size, and extend life. Following surgery, adjuvant chemotherapy eradicates any cancer cells that may have survived. Neoadjuvant chemotherapy is administered before surgery to reduce tumour size, which aids in its removal during surgery. Chemotherapy currently used consists of both a single-agent therapy that is mostly fluoropyrimidine-based (5-FU based) as well as multiple agent regimens which include one or several drugs such as oxaliplatin (OX), irinotecan (IRI) and capecitabine (CAP or XELODA or XEL) (Xie *et al.*, 2020).

2.3 LIVER CANCER

Liver cancer is a form of cancer that begins in the cells of the liver. Since hepatocytes are the main cells affected, hepatocellular carcinoma (HCC) is the most common type of liver cancer (Chidambaranathan-Reghupaty *et al.*, 2021).

2.3.1 The liver

The liver is a vital organ making up about 2% of an adult's body weight. It is involved in various processes that support immunity, digestion, detoxification, metabolism, and vitamin storage (Kalra *et al.*, 2022). The hepatic lobule of the liver (Figure 2.6A) appears hexagonal, and the portal triad area, which consists of the hepatic artery, portal vein and bile duct, is shown by the vertices. Blood flows through the sinusoid (Figure 2.6B), which results in many gradients along its length that influence the metabolic processes in the liver (Trefts *et al.*, 2017). The organisation of the liver comprises many types of cells (Figure 2.6B), such as hepatocytes, biliary epithelial cells (cholangiocytes), stellate cells, Kupffer cells, and liver sinusoidal endothelial cells (Bonnardel *et al.*, 2019). Hepatocytes make up most of the liver and perform many of its functions. Cholangiocytes are the second most prevalent cell type, and they line the lumen of bile ducts. Stellate cells can exist in a quiescent state where they store vitamin A in lipid droplets or in an activated state, which occurs through damage to the liver (Yin *et al.*, 2013).

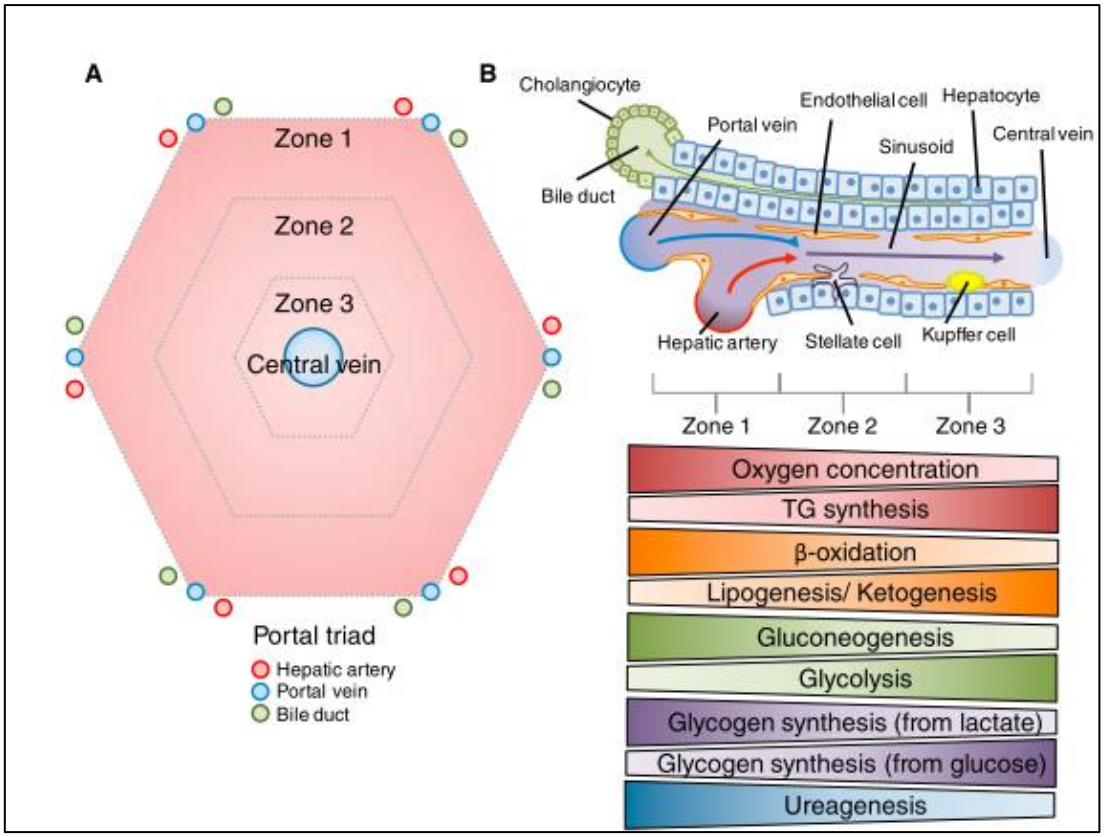

Figure 2.6: (A) The hepatic lobule of the liver showing the gross organisation of the liver. **(B)** The sinusoid with the various cells resident in the liver and zonation influences metabolic processes within the liver (Trefts *et al*., 2017).

2.3.2 Incidence of liver cancer

Primary liver cancer was the sixth leading cause of cancer and the third leading cause of cancer death worldwide in 2020. On estimate, there were 906,000 new cases and 830,000 deaths globally, corresponding to an incidence of 4.7% and mortality of 8.3% (Figure 2.1A). Among males, incidence and mortality rates are 2 to 3 times higher than females in most regions, and liver cancer ranks 5th in global incidence and 2nd in mortality (Figure 2.1B). Among females, liver cancer ranks 6th in incidence and 3rd in mortality (Figure 2.1C) (Sung *et al.*, 2021). Liver cancer is also one of the deadliest cancers in Africa, with more than 70,000 new cases and 67,000 deaths reported in 2020. South Africa is ranked third (Figure 2.2) in terms of cancer incidence, with 124,815 new cases and 108,168 deaths (Sharma *et al.*, 2022).

2.3.3 Types of liver cancer

Liver tumours may be classified as benign (non-cancerous) or malignant (cancerous) growths (Figure 2.7). With over 90% of cases, HCC is the most prevalent type of malignant liver cancer. Intrahepatic cholangiocarcinoma (bile duct cancer) is another common malignant liver cancer, accounting for approximately 10% of primary liver cancer cases, with hepatoblastoma being the least common (Sung *et al.*, 2021). Focal nodular hyperplasia and hepatocellular adenomas are benign liver lesions that are less common (Mills, 2015).

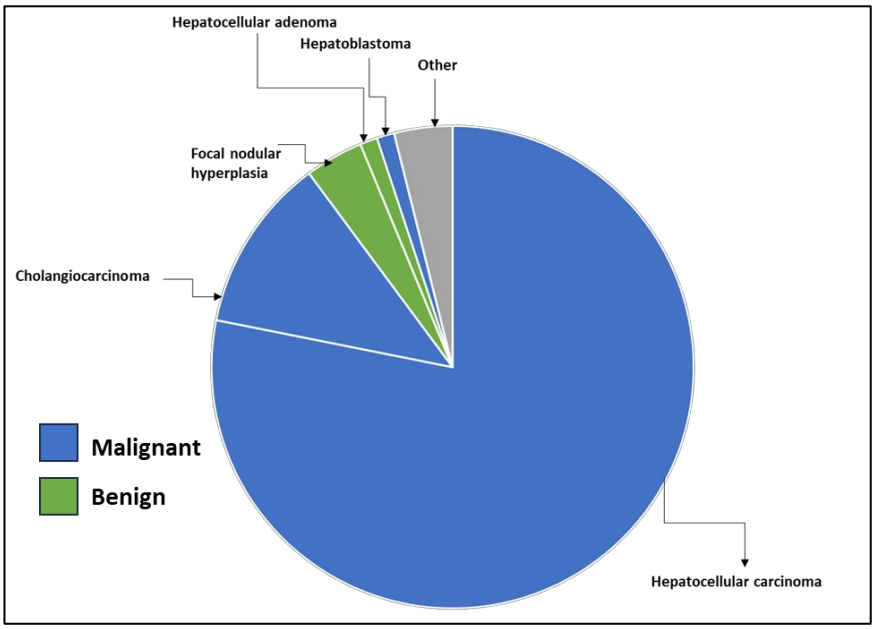

Figure 2.7: Liver tumour types by incidence rates, hepatocellular carcinoma being the most common malignant liver cancer [Prepared by author and adapted from (Mills, 2015)].

2.3.4 Risk factors

The development of HCC is frequently linked to liver cirrhosis brought on by long-term liver conditions like chronic hepatitis, hepatitis B virus (HBV) or hepatitis C virus (HCV) infection, and autoimmune hepatitis (Figure 2.8) (Dhanasekaran *et al.*, 2016). People with multiple risk factors have a higher risk of developing liver cancer. Risk factors include drinking too much alcohol, developing non-alcoholic fatty liver disease (NAFLD) or non-alcoholic steatohepatitis (NASH), smoking, having diabetes mellitus, being exposed to or ingesting aflatoxin, and having sporadic genetic conditions such alpha-1 antitrypsin deficiency,

hemochromatosis, tyrosinaemia, porphyria, and Wilson's disease (Mittal and El-Serag, 2013). Hepatocyte injury or cell death results following exposure to any of the risk factors. These damaged and dead cells are replaced by proliferative regeneration. Continuous exposure results in a destructive–regenerative process that contributes to chronic inflammation and culminates in cirrhosis (Di-Iacovo *et al.*, 2023). Collagen deposition and scarring of the liver that ensues characterises hemangioma formation, followed by hyperplastic and dysplastic nodules that progress to HCC (Chartampilas *et al.*, 2022).

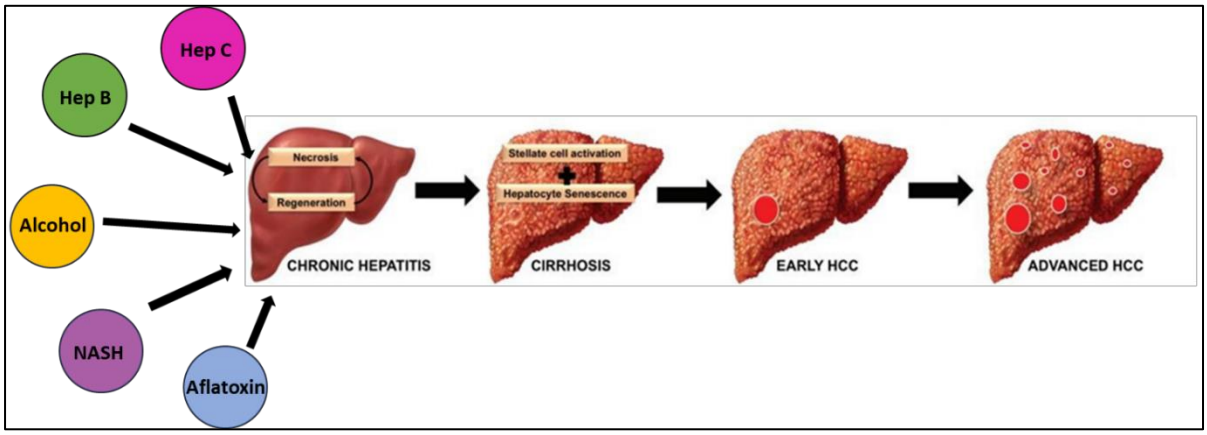

Figure 2.8: The pathogenesis of hepatocellular carcinoma. When hepatocytes are exposed to various risk factors, it initiates a sequence of molecular events that progresses to chronic liver disease such as cirrhosis and culminates in the development of HCC [Prepared by author and adapted from (Dhanasekaran *et al.*, 2016)].

2.3.5 Treatment options for liver cancer

Both curative and/or palliative treatments are available for HCC patients, and this is determined based on the stage of cancer, the individual's age, available resources, and the patient's comorbidities (Maida *et al.*, 2014). The Barcelona Clinic Liver Cancer (BCLC) staging system categorises patients into very early, early, moderate, advanced, and terminal stages by considering the pertinent HCC criteria. For patients in the early stages (BCLC stage 0 and BCLC stage A), resection, ablation, and transplantation are thought to be possible curative alternatives. For BCLC stage B, three groups of patients are classified according to the state of the tumour and the function of the liver (Golfieri *et al.*, 2019). The first stage consists of well-defined HCC nodules that are still candidates for liver transplantation, the second subgroup consists of patients that are clear candidates for TACE without the option of having

a liver transplant, and the third stage consists of systemic therapy. Stage C is an advanced stage which consists of portal invasion and extrahepatic spread, which requires systemic therapy. Current options for systemic treatment for HCC include a first-line therapy with Atezolizumab/ Bevacizumab. Sorafenib is approved for HCC therapy irrespective of any other or previous treatment. Cabozantinib, ramucirumab and regorafenib are approved if a patient has been previously treated with sorafenib (Regorafenib for patients that have previously responded to sorafenib and Ramucirumab in patients with AFP-overexpressing tumours (AFP > 400 ng/mL)). Finally, Stage D is a terminal stage, and palliative care is provided to patients nearing the end of their lives to improve their quality of life (Tumen *et al.*, 2022).

2.4 *MONSONIA BURKEANA*

Medicinal plants have been used routinely in traditional or ayurvedic medicine to treat a range of ailments (Kumar *et al.*, 2017). Herbal teas are especially renowned for their medicinal benefits. Several herbal tea shrubs are native to South Africa and are celebrated for their unique flavours and medicinal properties. *Aspalathus linearis* that is used to make rooibos tea has a high flavonoid content that confers antidiabetic and anti-cancer properties (Huang *et al.*, 2020). 'Bush tea' is made from the leaves of *Athrixia phylicoides*; its abundant flavonoids and tannins are potent antioxidants that exert anti-inflammatory and anticancer activity (Tungmunnithum *et al.*, 2018). Similarly, *M. burkeana* 'special tea' has potential anti-diabetic and anti-cancer properties, but its molecular mechanisms have not been fully explored (Mathivha *et al.*, 2019).

2.4.1 Geographical occurrence

M. burkeana Planch. ex Harv is part of the family Geraniaceae and is native to Southern African countries such as Botswana, Lesotho, Mozambique, Namibia, and Swaziland, where it is typically found in open wooded grassland (Figure 2.9) (Tshivhandekano *et al.*, 2014, Ngoepe *et al.*, 2018). In South Africa, this 'special tea' may be found in Limpopo and Gauteng region; Chuenespoort and Zebediela are Limpopo villages where the plant has been harvested, and Rietondale is located in Gauteng (Nnzeru, 2019).

2.4.2 Description

This shrubby, upright perennial plant can grow up to 60cm tall. *M. burkeana* annual shoots grow from the rootstock. Most of the plant contains short, gland-tipped and long scattered hairs. The plant leaves are narrow and elliptic (1.5-4 cm long), and the leaf margins are serrated (Figure 2.9A). The petiole is 5-14 mm long, and stipules are 3-6mm in length and are needle-like. Pale blue or pinkish flowers can grow in isolation or clusters of up to 3 (Figure 2.9B). Petals are 18-24mm long and have atruncated apex; fruit are 6-9cm long (Hyde *et al.*, 2022).

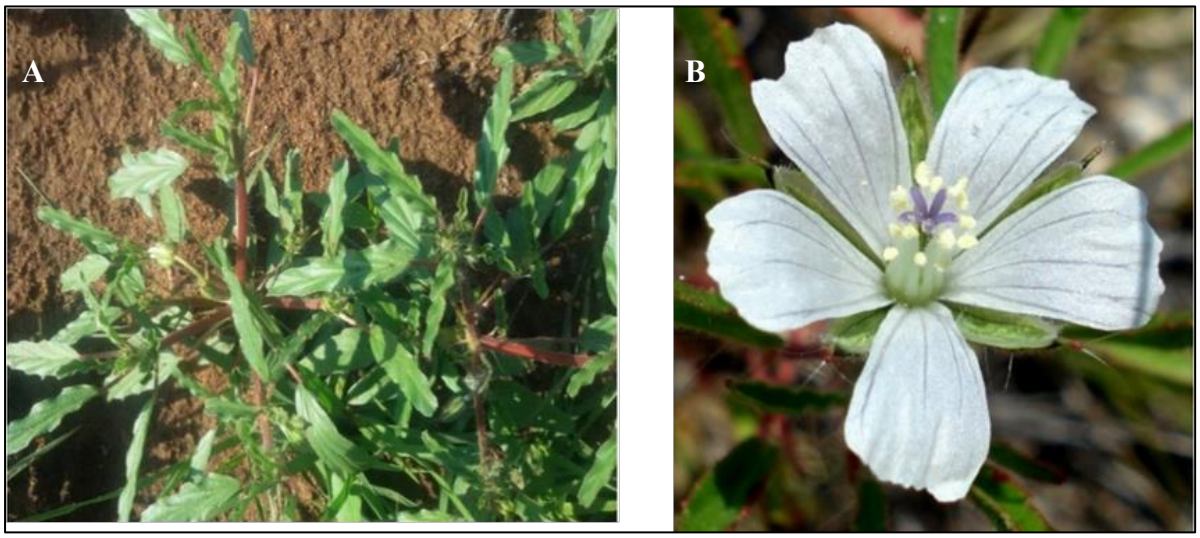

Figure 2.9: *M. burkeana* Planch. ex Harv plant growing in Rietondale, Gauteng province, South Africa (Nnzeru, 2019, Wells *et al.*, 1986) **(A)** The narrow elliptical leaves have serrated margins. **(B)** An isolated white flower comprising five petals with a truncated apex.

2.4.3 Preparation and uses

Preparing the tea for use and its medicinal properties involves boiling the plant. Nzeru and colleagues (2016) revealed that 45% of respondents to the questionnaire boiled the whole plant, 42% boiled the leaves, and 9% prepared it like regular tea. Most individuals (91%) specify that boiling the tea took less than 30 minutes. According to 97% of individuals, the tea prepared was black (Nnzeru *et al.*, 2016). Many communities frequently use this plant's decoctions for their numerous health benefits. Consumers believe it offers health benefits, including improving libido, treating erectile dysfunction, purifying the blood, and having antidiabetic and anticancer properties (Nnzeru *et al.*, 2016).

2.4.4 Phytochemical content

Numerous substances, including polysaccharides, volatile oils, vitamins, minerals, purines, alkaloids (such as caffeine), and polyphenols (catechins and flavonoids) are found in tea leaves (Mamphiswana *et al.*, 2010a). A study conducted by Mathiva and his team in 2019 investigated the antidiabetic and antiproliferative activities of herbal teas *Athrixia phyllodes* and *M. burkeana* Planch. Ex Harv on human cervical cancel (HeLa) cells (Mathivha *et al.*, 2019). Polyphenols such as gallic acid, chlorogenic acid, quercetin and catechins (Figure 2.10) were present in significant quantities (Nnzeru, 2019, Mathivha *et al.*, 2019). These compounds have been investigated and shown to have anti-cancer properties (Lerotholi *et al.*, 2017, Mamphiswana *et al.*, 2010b). Both 'bush tea' and 'special tea' displayed significant phenolic content and high antioxidant activity (Mathivha *et al.*, 2019). Tshivhandekano *et al.* (2014) showed that *M. burkeana* contained a significantly higher content of total polyphenols (8.34 mg/100g) and total antioxidants (0.83 mg/100 g) than *A. phyllodes* and that the leaves and fruits contained significantly more total phenols and antioxidants compared to the stem with moderate levels, and the roots with the lowest content (Tshivhandekano *et al.*, 2014).

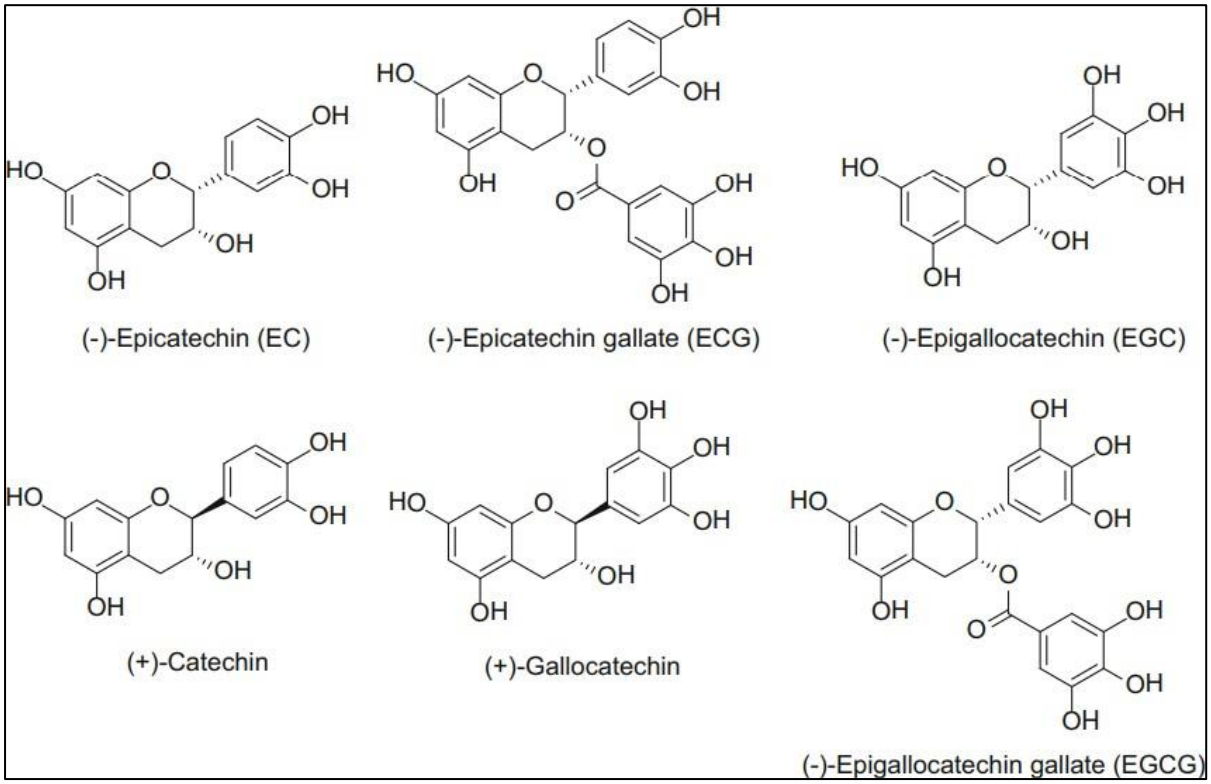

Figure 2.10: Chemical structures of major polyphenolic catechins found in herbal teas (Bansal *et al.*, 2011).

2.5 OXIDATIVE STRESS

When the amount of free radical production, referred to as reactive oxygen species (ROS), exceeds the antioxidants present in the body, this leads to oxidative stress (Figure 2.11). When exogenous and endogenous ROS are produced for an extended period in cells under excessive stress, the resulting oxidative stress may lead to cell structural and functional damage, which may induce somatic mutations and neoplastic transformations (Sies, 2020).

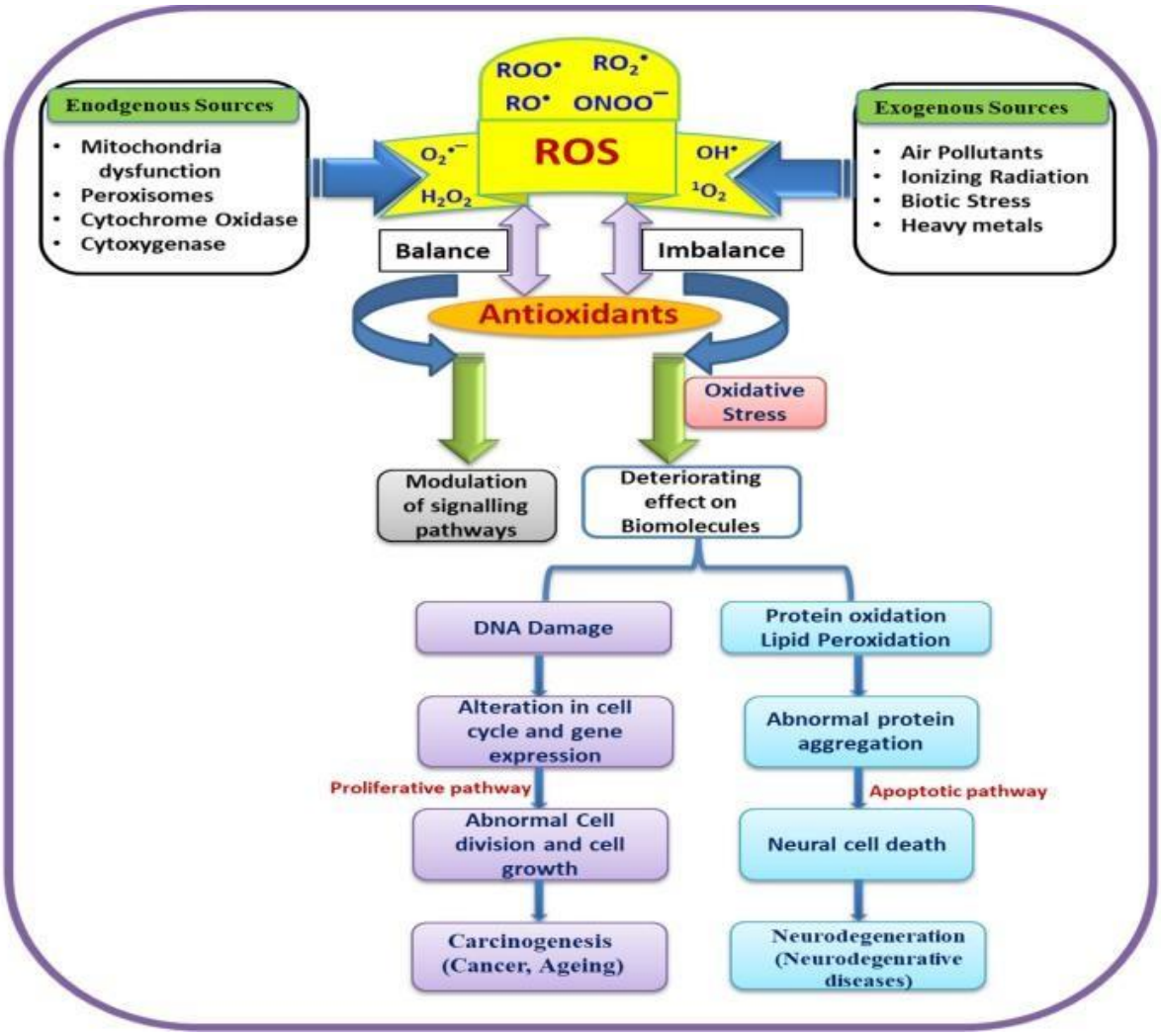

Figure 2.11: A summarised depiction of endogenous and exogenous sources of ROS and their role in oxidative DNA damage, involved in carcinogenesis and ageing, along with alteration of gene expression (Singh *et al.*, 2019).

2.5.1 Free radicals

Free radicals are molecules that exist independently and possess an unpaired electron. This causes specific common properties shared among radicals, such as instability and high reactivity. They behave as oxidants or reductants by donating or accepting electrons (Chaudhary *et al.*, 2023). The most significant free radicals that are involved in causing diseases include ROS such as the hydroxyl radical ($HO^{\bullet}$), superoxide anion radical ($O_2^{\bullet-}$), hydrogen peroxide (H_2O_2), oxygen singlet ($^{\bullet}O_2$) and hypochlorite (ClO^-), as well as reactive nitrogen species (RNS) such as the nitric oxide radical ($NO^{\bullet}$) and peroxynitrite ($ONOO^-$) (Murphy *et al.*, 2022). These reactive species are products of aerobic cellular metabolism that play a part in activating signalling pathways (Juan *et al.*, 2021). Intracellular sources of ROS production include the reduction of oxygen within the mitochondrial respiratory chain. The leakage of electrons to O_2 in mitochondria by reverse electron transport at complex 1 produces ROS as well as the reaction between coenzyme Q (CoQ) with O_2 at complex III of the respiratory chain (Murphy, 2009). The major source of ROS is complex I (NADH–ubiquinone oxidoreductase) (Figure 2.12) with minor sources being the ubisemiquinone radicals ($Q^{\bullet}$) generated from complex III (ubiquinone–cytochrome c reductase) and as a by-product of α-ketoglutarate dehydrogenase (αKGDH) activity.

The $O_2^{\bullet-}$ that is generated within the mitochondrial matrix reacts with manganese superoxide dismutase (MnSOD), and that released into the intermembrane space reacts with copper/zinc superoxide dismutase (Cu/Zn-SOD) (Figure 2.13). Hydrogen peroxide formed by this dismutation reaction undergoes Fenton reactions involving transitional metal ions (iron, copper, or manganese) to form extremely harmful $HO^{\bullet}$ (Winterbourn, 2020)'. When NO reacts with the $O_2^{\bullet-}$, it forms $ONOO^-$ (Figure 2.13), which can react with carbon dioxide (CO_2) to produce nitrogen dioxide radicals ($NO_2^{\bullet}$) (Iovine *et al.*, 2008). The generation of ROS and RNS can further generate reactive aldehydes such as malondialdehyde (MDA) and 4-hydroxynonenal due to excessive lipid peroxidation (Juan *et al.*, 2021).

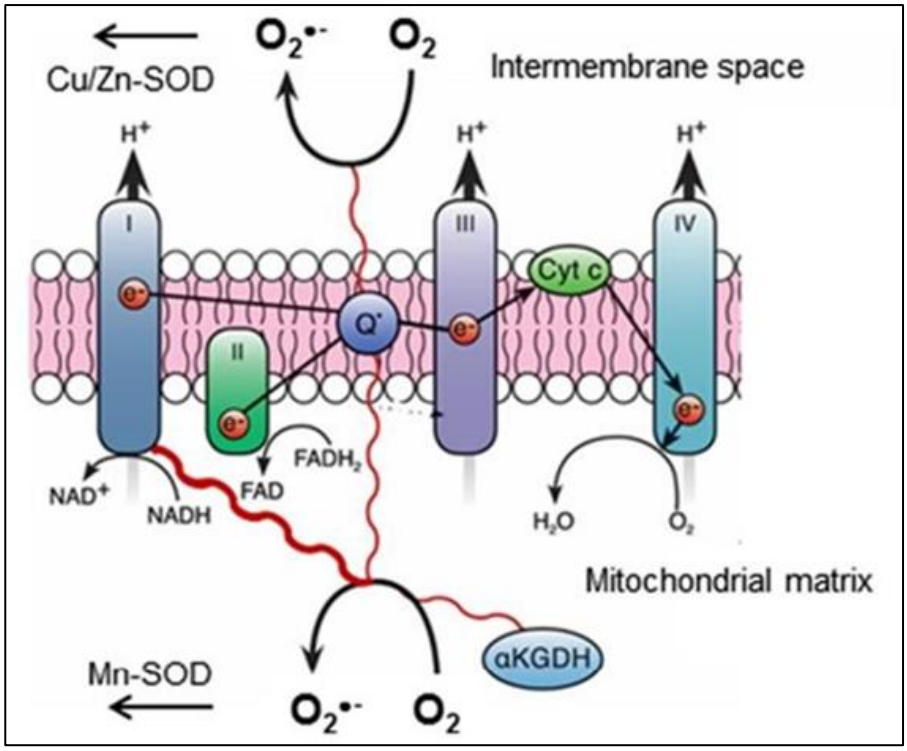

Figure 2.12: Sources of ROS from the electron transport chain, primarily at complexes I and III (Winterbourn, 2020).

2.5.2 Antioxidant response

Antioxidants are stable molecules that donate an electron to free radicals (radical scavenging), thus neutralising them and decreasing their ability to cause cellular damage (Vargas-Mendoza *et al.*, 2019). Cells contain various antioxidants to stop ROS and RNS accumulation in uncontrolled amounts (Figure 2.13). These are non-catalytic, endogenously produced molecules such as bilirubin, a-lipoicacid, melatonin, melanin, reduced glutathione (GSH), and uric acid, as well as exogenously derived vitamin E, vitamin C, β-carotene, and plant polyphenols that scavenge ROS and RNS (Halliwell and Gutteridge, 2015). There are also catalytic antioxidants that are scavengers of $O_2^{\bullet-}$ which include Cu/ZnSOD (SOD1), mitochondrial MnSOD (SOD2), and extracellular SOD (SOD3), which facilitate $O_2^{\bullet-}$ conversion to H_2O_2 and O_2 (Sheng *et al.*, 2014). The antioxidants SOD1 and SOD2 are called tumour suppressors because they protect against tumour formation; however, they may be upregulated during tumour formation (Gill *et al.*, 2016). Catalase is an antioxidant enzyme

that eliminates ROS by converting H_2O_2 to H_2O and O_2 (Figure 2.13). Peroxiredoxins (PRDX/PRXs) and glutathione peroxidases (Gpxs) reduce H_2O_2 to H_2O. Glutathione peroxidases utilise reduced glutathione (GSH) to detoxify molecules; oxidised glutathione (GSSG) is produced in the process (Figure 2.13) is reduced by glutathione reductase and NADPH to GSH (Hayes *et al.*, 2020). Nuclear factor erythroid 2-related factor 2 (NRF2) is a master regulator of the antioxidant and xenobiotic response (He *et al.*, 2020). This transcription factor is regulated by cycles of synthesis and degradation, whereby it is suppressed under normal cellular conditions through Keap1 (Kelch-like erythroid cell-derived protein with CNC homology-associated protein 1) ubiquitination, which causes degradation (Ma, 2013). Exposure to oxidants and electrophiles activates NRF2 by modifying cysteine thiols on Keap1 and NRF2. Once activated, NRF2 is translocated to the nucleus for binding with antioxidant response elements (AREs) of gene targets (Ngo and Duennwald, 2022). This results in the transcription of antioxidant enzymes as well as detoxifying enzymes such as SOD, catalase and Gpx.

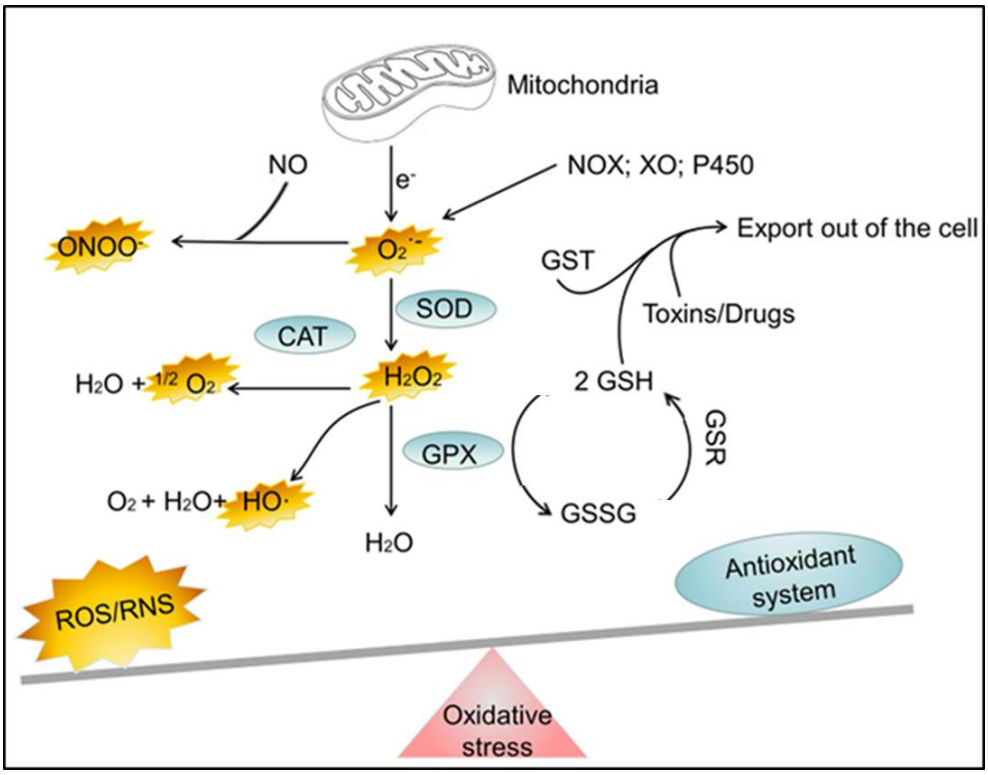

Figure 2.13: The major antioxidant response in cells involves NADPH oxidase (NOX), xanthine oxidase (XO), superoxide dismutase (SOD), catalase (CAT), glutathione peroxidase (Gpx), glutathione (GSH), reduced glutathione (GSSG), glutathione S-transferase (GST) [Prepared by (Liu *et al.*, 2023) and modified by author].

2.5.3 Oxidative damage to cellular macromolecules

Under oxidative stress, ROS and RNS reach toxic levels and attack essential cellular macromolecules such as lipids, proteins, and nucleic acids (Figure 2.11). Cell membranes have a high contentof polyunsaturated fatty acids (PUFAs), which are susceptible to ROS and RNS-induced damage called lipid peroxidation. This is a series of reactions where free radical compounds, e.g. oxyl, peroxyl, and hydroxyl radicals, remove electrons from lipids, producing reactive intermediate compounds that undergo further reactions. Phospholipids become damaged, and apoptosis may be signalled (Que *et al.*, 2018). Proteins can also be affected by ROS and RNS by the formation of carbonyls. Protein oxidation reactions due to ROS can oxidise arginine, lysine, threonine, proline, and other amino acid residues to form carbonyl groups through the catalysis of the transitional metal ion system. Reactive oxygen species can potentially remove hydrogen atoms from the α-carbon of a protein chain, which results in oxidative hydrolysis of the carbon atoms and carbonyl groups forming (Moller *et al.*, 2011). Nucleic acids can undergo ROS and RNS-induced damage by forming Guanine adducts. Oxidation of Guanine residues results in forming 8-oxo-7,8-dihydroguanine (8-oxo-dG). This oxidised DNA base is a marker of oxidation damage in diseases such as cardiovascular disease, neurodegenerative diseases, and cancer. The oxidised guanine can now pair with adenine via the Hoogsteen hydrogen bonding in place of cytosine, leading to the mutations arising (Singh *et al.*, 2019)

2.5.4 Polyphenols and oxidative stress

Polyphenols are secondary metabolites found in tea that have displayed antioxidant properties *in vivo* and *in vitro* due to their intrinsic reducing abilities. This will replenish antioxidant effects that have been slowed down by carcinogenesis and inhibit oxidative stress. Studies have revealed the chemopreventative capabilities of polyphenols toward organ-specific cancers, thus influencing the process of carcinogenesis by methods such as inhibition of DNA synthesis, modulating ROS produced, regulating cell cycle arrest and the control of proliferation pathways (Trisha *et al.*, 2022).

2.6 APOPTOSIS

Apoptosis was first described in 1972 by Kerr, Wylie, and Currie in an attempt to describe a type of cell death that was distinct in its shape, size, and structure (Kerr *et al.*, 1972). This process is called "programmed cell death" and is crucial for development and homeostasis (Obeng, 2021). During DNA damage or uncontrolled proliferation conditions, apoptosis may beactivated by either the intrinsic or extrinsic pathway, depending on the signal received (Pfeffer and Singh, 2018). Intracellular signals include damaged DNA as well as growth factor and cytokine deprivation. In contrast, extracellular signals include death-inducing signals produced from cytotoxic T cells as a response to damaged cells (Zaman *et al.*, 2014).

2.6.1 Intrinsic pathway

Internal cellular signals from cytotoxic stimuli initiate the intrinsic pathway (Figure 2.14). Intrinsic apoptosis is controlled by the B-cell lymphoma 2 (BCL2) family of proteins comprising pro-apoptotic and anti-apoptotic members. The anti-apoptotic BCL2 and BCL_{XL} prevent apoptosis by binding to and sequestering pro-apoptotic members such as BCL2-associated X protein (BAX) and BCL-2 antagonist/killer (BAK) (Hatok and Racay, 2016). For apoptosis to proceed, transcription of BH3-only PUMA and NOXA is stimulated by p53; these pro-apoptotic proteins bind BCL2 and BCL_{XL}, thus freeing BAX and BAK to undergo homodimerisation or heterodimerisation to activate them (Roufayel *et al.*, 2022). Activation allows these proteins to insert into the mitochondrial membrane, thus introducing pores which causes mitochondrial outer membrane permeability (MOMP) and leakage of intermembrane proteins into the cytosol (Green. *et al.*, 2000). Cytochrome C is one of the proteins released that initiates the formation of an apoptosome by binding to apoptotic protease activating factor 1 (Apaf-1) in the presence of adenosine triphosphate (ATP). Oligomerization of Apaf-1 causes a conformational change that exposes a caspase activation and recruitment domain (CARD) (Bratton and Salvesen, 2010). The apoptosome forms when Apaf-1 CARD domains bind to procaspase-9 CARDs. Procaspase-9 then dimerises and auto-activates caspase 9. Thereafter, caspase 9 causes activation of executioner caspase 3 and 7, which leads to apoptosis (Obeng, 2021). It is important to note that intrinsic apoptosis may be circumvented by the binding of inhibitor of apoptosis protein (IAP). Binding of IAP to activated caspase 9

and/or caspase 3/7 prevents apoptosis. However, the IAP may be sequestered by a second mitochondrial activator of caspases (Smac) and direct IAP-Binding Protein with Low pI (DIABLO), thus ensuring that apoptosis is executed by ensuring caspase activation. The Smac and DIABLO are released from the mitochondria as a result of cellular stressors. Another protein that assists in cell death within the intrinsic pathway is the mitochondrial nuclease, endonuclease G. This protein plays a part in mitochondrial DNA replication under normal cellular conditions; however, upon certain stimuli, it is translocated to the nucleus to cleave chromatin DNA into nucleosomal fragments in a caspase-independent manner (Benitez-Guzman *et al.*, 2018).

2.6.2 Extrinsic pathway

The extrinsic pathway induces apoptosis through death ligands interacting with death receptors (Figure 2.14). The death ligands and death receptors are part of the tumour necrosis factor (TNF) family and include the first apoptosis signal (Fas) and TNFα (Annibaldi and Walczak, 2020). The Fas ligand (FasL) or TNFα bind to their cognate death receptors, Fas receptor (FasR) and TNF receptor (TNFR), respectively. Receptor trimerisation initiates the recruitment of Fas-associated death domain (FADD) and TNF receptor-associated death domain (TRADD). Subsequent binding of the death effector domain (DED) of FADD to the DED of pro-caspase 8 forms an activated death-inducing signalling complex (DISC) (Tummers and Green, 2017). The proximity of numerous pro-caspases causes cleavage and activation of the initiator caspase 8 or 10. Activated caspase 8 cleaves and activates downstream molecules such as caspase 3 and 7 to execute cell death (Obeng, 2021). In addition, BID is cleaved to activate intrinsic apoptosis. This process is terminated by the cellular Fas-associated death domain protein (FADD) interleukin-1β-converting enzyme (FLICE) inhibitory protein (c-FLIP) that binds to the death domains (Obeng, 2021).

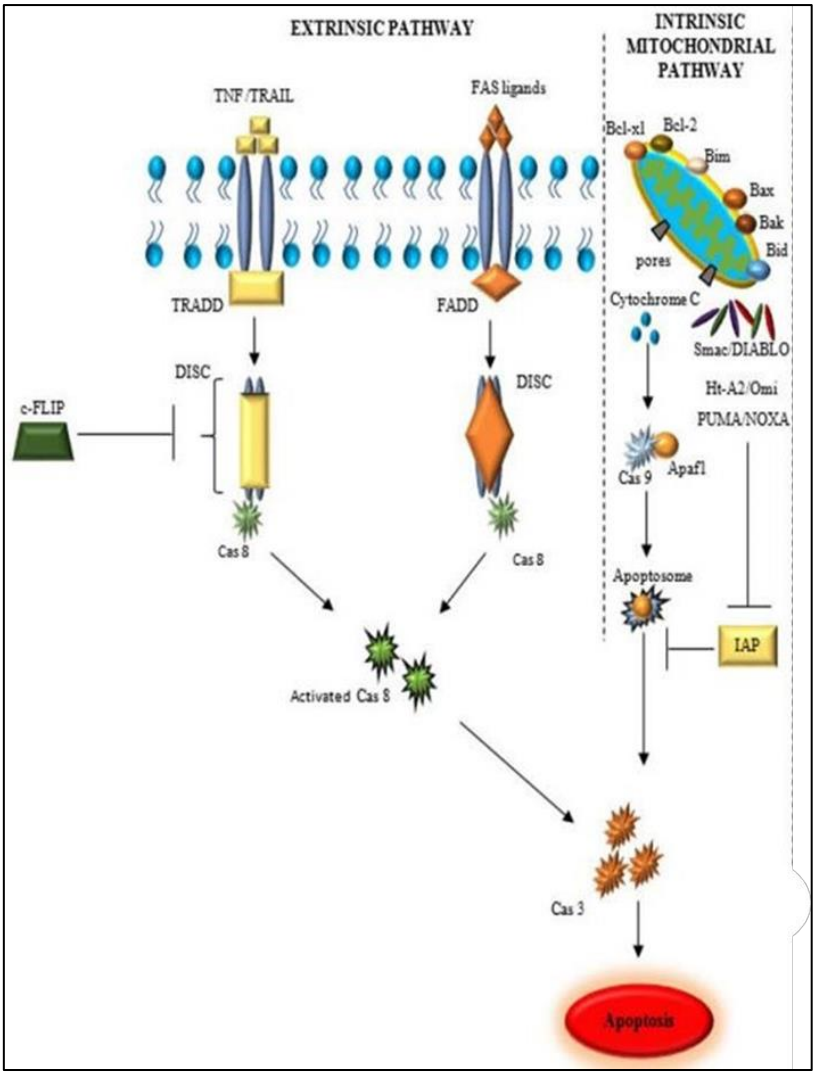

Figure 2.14: Extrinsic and intrinsic pathways leading to apoptosis (Obeng, 2021).

2.6.3 Execution of apoptosis

The last stage of apoptosis, known as the execution phase, is marked by cell shrinkage, chromosomal condensation, DNA breakage, and blebbing of the cell membrane (Kashyap *et al.*, 2021). A key player in the execution pathway, caspase-3 cleaves cytoskeleton proteins and DNAase inhibitors, leading to cellular fragmentation (Singh *et al.*, 2022). Microtubule disassembly is a crucial step in the execution process, leading to the extrusion of cells and occurs through the depolymerisation of actomyosin filaments (Villars *et al.*, 2022). This process plays a crucial role in dispersing cellular fragments, preserving the integrity of the plasma membrane to contain hazardous components within the cell, and providing defence

against inflammatory events. Ultimately, phagocytosis eliminates apoptotic bodies, thereby preventing any adverse effects from inflammation (Battistelli and Falcieri, 2020). Phosphatidyl serine (PS), a phospholipid in eukaryotic cell membranes, is kept inside the cell by an enzyme flippase. Processes such as apoptosis and platelet activation lead to the exposure of PS on the cell surface by the enzyme scramblase (Nagata *et al.*, 2016). This facilitates the action of phagocytes, which are attracted towards dying cells (Naeini *et al.*, 2020).

2.6.4 Polyphenols and apoptosis

Polyphenols can influence points in the apoptotic pathway as well as expression of regulatory proteins such as the release of cytochrome c and, therefore, activation of caspase 9, 3, and 8, increase in tBid levels, downregulation of BCL-2 and BCL_{XL} expression, increased BAX and BAK expression and modulation of nuclear factor kappa B (NF-κB) (D'Archivio *et al.*, 2008). Caffeic acid is a hydroxycinnamic acid present in many types of fruit and tea and found in high concentrations in coffee, which induces apoptosis in human breast cancer cells. Activating proapoptotic factors, including Fas, BAX, and caspases, increases caspase 3 activity in stomach, colon, andpre-myelocytic leukaemia cells (Watabe *et al.*, 1999). Further studies must investigate polyphenols' underlying mechanisms resulting in apoptosis and its efficacy as a potential chemotherapeutic treatment.

2.7 NECROSIS AND NECROPTOSIS

Necrosis is a form of uncontrolled cell death brought on by external cell injury such as hypoxia, inflammation, radiation and chemical exposure, amongst others, thus leading to a loss of cell membrane integrity (Tonnus *et al.*, 2019). Pro-inflammatory proteins such as NF-κB are upregulated, resulting in the cell membrane bursting and cellular components' spillage into surrounding tissue. This causes inflammation and tissue damage. During inflammatory conditions, TNFα is released in excess. Necrosis, unlike apoptosis, is energy-independent cell death, which occurs when the cells cannot function due to severe damage caused by sudden shock. The cells undergo a process of swelling called oncosis (Park *et al.*, 2023). Unlike necrosis, necroptosis is tightly regulated. However, certain morphological features are similar.

Necroptosis (Figure 2.15) is controlled by receptor-interacting proteins (RIPKs). Death receptors, mainly TNFR, mediate the most widely accepted activation of necroptosis. However, the tumour necrosis factor-related apoptosis-inducing ligand (TRAIL), and Fas receptors can also induce necroptosis (Tang *et al.*, 2019). Upon binding of TNFα to TNFR, a membrane-associated complex called complex I forms and recruits TRADD and RIPK1 through homotypic and death domain interactions (Kang *et al.*, 2022). Other factors such as tumour necrosis factor receptor-associated factors (TRAF2 and 5), receptor-interacting protein kinase-1 (RIPK1), cellular inhibitor of apoptosis proteins (cIAP1/2), several ubiquitin E3 ligases are also recruited to complex I (Figure 2.15a).

Upon polyubiquitination of RIPK1 (see Figure 2.15b), TNFR signalling triggers NF-κB activation, resulting in the expression of proinflammatory cytokines. Deubiquitination of RIPK1 by deubiquitinase cylindromatosis (CYLD) leads to complex II forming. The activation of caspase-8 in complex IIa prevents necroptosis by blocking the activation of RIP and stopping the induction of necroptosis, resulting in apoptosis (Figure 2.15c). When caspase 8 is inhibited, complex IIb activates necroptosis (Figure 2.15d) (Ye *et al.*, 2023). To initiate necroptosis via complex IIb, RIPK1 recruits RIPK3 and induces auto and transphosphorylation with oligomerisation of phosphorylated RIPK3. This results in the assembly of the necrosome (D'Arcy, 2019). Mixed lineage kinase domain–like pseudokinase (MLKL), RIPK1 and RIPK3 are involved in necroptosis. Phosphorylation occurs at MLKL Threonine 357/Serine 358 when recruited by RIPK3. After phosphorylation, MLKL oligomerises and moves to the cell membrane of the cell (Martinez-Osorio *et al.*, 2023). Membrane permeabilisation results, possibly by MLKL binding to phosphatidylinositol lipids and cardiolipin (Wang *et al.*, 2014). Necroptotic cell death thus occurs.

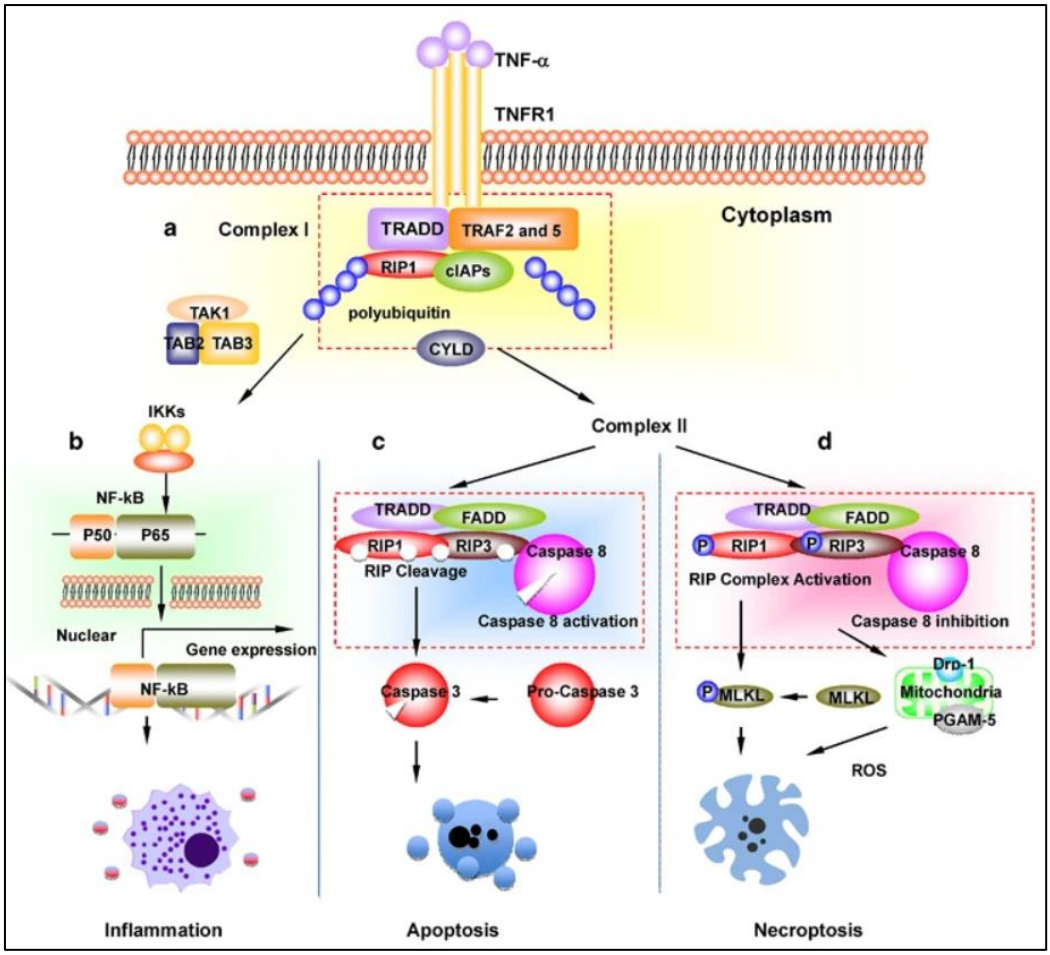

Figure 2.15: Summary of steps in inflammation, apoptosis and necroptosis signalling pathways after the activation of TNFR1 (Zhao *et al.*, 2015).

CHAPTER 3: MATERIALS AND METHODS

3.1 MATERIALS

The Caco2, HepG2 and Hek293 cells were obtained from Cellonex (Johannesburg, South Africa (SA)). Cell culture reagents and plasticware were procured from Whitehead Scientific (Johannesburg, SA). Promega luminometry reagents and Cell Signalling Technology (CST) antibodies were purchased from Anatech (Johannesburg, SA). The western blot reagents, iScript cDNA synthesis kit and iTaq Universal SYBR® Green supermix, were bought from Bio-Rad (Hercules, California, USA). Primers were procured from Inqaba Biotech (Pretoria, SA). Unless stated otherwise, all other reagents were procured from Merck (Darmstadt, Germany) or Lasec® Group (Johannesburg, SA).

3.2 OVERVIEW OF THE STUDY

Colorectal adenocarcinoma (Caco-2), human liver (HepG2) and human embryonic kidney (Hek293) cells were reconstituted in 25cm^2 flasks in complete culture medium (CCM). Once confluent, the cells were dislodged from the flask using trypsin and counted using trypan blue. After that, the cells were subcultured in a 96-well plate and underwent treatment with the plant extract for 48 hours. The MTT assay was conducted to obtain the half maximum inhibitory concentration (IC_{50}) and IC_{20}. Confluent flasks were treated with the IC_{20} and IC_{50} for 48 hours, and control cells were untreated (CCM only). Cells were collected and counted for luminometric assays that monitored oxidative stress and cell death parameters. The treatment medium was used for spectrophotometric assays for free radical production and cell death. Isolated proteins from treated cells were used to conduct western blot and qPCR. Data analysis was performed using statistical tests.

3.3 CELL CULTURE

3.3.1 Principle

Immortalised cell lines obtained from multicellular organisms proliferate continuously. They

are utilised inplace of primary cells for research as they have many benefits. Utilising cell lines is cost- effective, easy to use, and reduces ethical concerns as animal or human tissue is not used and a pure population of cells can be studied (Kaur and Dufour, 2012). In addition, drug metabolism and cytotoxicity can be tested using a variety of cell lines. Some of the cell lines utilised in this study are Caco-2, HepG2, and Hek293 cells. In the 1970s, the Caco-2 cell line was derived from a human colorectal adenocarcinoma by Jogen Fogh at the Sloan-Kettering Cancer Research Institute (Lea, 2015). When colorectal adenocarcinoma cells are cultured, they will differentiate into a mixture of intestinal epithelial cells (Lea, 2015). Human hepatocellular carcinoma cells are non-tumourigenic human liver cancer cells isolated from the liver tissue of a 15-year-old white male (Arzumanian *et al.*, 2021). They are most commonly utilised in the metabolism of drugs and hepatotoxicity studies (Donato *et al.*, 2015). The Hek293 cell line was created by immortalising human embryonic kidney cells with sheared adenovirus type 5 (Ad5) DNA fragments (Abaandou *et al.*, 2021). This cell line is commonly used in cancer research.

3.3.2 Protocol

3.3.2.1 Reconstitution and cell maintenance

The Caco-2, HepG2 and Hek293 cells were thawed and centrifuged (400xg, 10 minutes). The pelleted cells were reconstituted in 5ml of CCM comprising of Dulbecco's essential medium supplemented with 1% L-glutamine, 1% antibiotic-antimycotic and 10% foetal bovine serum. The cell suspensions were transferred to 25cm^2 flasks and incubated for 24 hours (37°C, 5% CO_2). The cell lines were monitored for confluence, and CCM was replaced when needed. When cells reached 80% confluence, they were washed thrice with 0.1M phosphate-buffered saline (PBS). Cells were then trypsinised with 1ml trypsin and counted using the trypan blue exclusion method for storage or sub-culture.

3.3.2.2 Trypsinisation

Flasks were cultured until 80% confluent and thereafter underwent trypsinisation using aseptic techniques. Into each flask, 5ml of 1 M PBS was added to rinse the cells and then

discarded. This was repeated 3 times to remove media and cell debris as FCS deactivates trypsin. For a 25cm^2 flask 1ml of trypsin was used and for a 75cm^2 flask 2ml of trypsin was used. Cells were viewed under the microscope to see trypsinisation, which consisted of cells starting to dislodge and rounding. The trypsin was discarded and the vessels were hit against the palm of one's hand to dislodge cells. Complete culture media was then added to the flasks and cells were either stored for future use or counted to be used in assays.

3.3.2.3 Cell counting

Cell counting was conducted for each cell line and involved 150µl CCM, 50µl of cell suspension and 50µl trypan blue into an Eppendorf tube. The tubes were vortexed for 5 seconds to ensure mixing. Using a hematocytometer, 10µl of the mixture in the Eppendorf tube was added between the coverslip and hematocytometer. After viewing, cells were counted and the cells per ml was evaluated using the following equation. Cell number was adjusted as needed for different assays:

$$\frac{counted\ cells}{5} \times dilution\ factor\ \times\ 10^4 = cells\ per\ ml$$

3.4 PREPARATION OF *M. BURKEANA* CRUDE AQUEOUS EXTRACT

A commercial blender was used to grind dried *M. burkeana* leaves (voucher specimen for *M. burkeana* (3925000) at the South African National Biodiversity Institute, National Herbarium) into a fine powder, which was used to prepare a traditional tea by combining 15g of the leaves with 300ml boiling distilled water and steeping the mixture for 30 minutes with constant stirring. The boiled solution was cooled and centrifuged (Eppendorf Centrifuge 5804 R, Hamburg, Germany) at 400xg for 10 minutes. The supernatant was stored in the freezer (20ºC) overnight. The frozen product was then lyophilised for 48 hours using the VirTis lyophiliser (Sentry 2.0 from SP Scientific) and stored at 4ºC until needed. A stock solution (5mg/ml) was prepared by dissolving 25mg of the lyophilised aqueous extract in 5 ml CCM, and was diluted to obtain the concentrations for the various experiments.

3.5 3-(4,5-DIMETHYLTHIAZOL-2-YL)-2,5 - DIPHENYLTETRAZOLIUM BROMIDE (MTT) ASSAY

3.5.1 Principle

The MTT technique is a calorimetric measure of the metabolic activity of cells (Ghasemi *et al.*, 2021). It is widely utilised in the assessment of cytotoxic drug therapies. This assay involves the reduction of yellow, water-soluble tetrazolium salts by viable cells into insoluble purple formazan crystals (Figure 3.1) (Winikoff, 2005). When the positively charged MTT salt enters the cell, it is reduced by mitochondrial succinate dehydrogenase, an NADPH-dependent oxidoreductase enzyme. This results in an intracellular formazan product and the reducing by-products NAD^+/$NADP^+$/ FAD^+. An organic solvent such as dimethylsulfoxide (DMSO) solubilises the formazan crystals. The optical density (OD) is determined using a plate reader equipped with wavelengths of 570 and 690 nm to quantify the intensity of the formazan product, and thus cell viability. Some advantages of utilising the MTT assay are that it is low in cost, easy to implement, has increased sensitivity and can be used on various cell types (Carreño *et al.*, 2021). Drawbacks of using this study include some technical complexities, such as using excess MTT salt concentration may lead to non-specific cell death depending on the cell type, and some photosensitising compounds can directly reduce MTT to formazan which may interfere with the accuracy of results (Stepanenko and Dmitrenko, 2015).

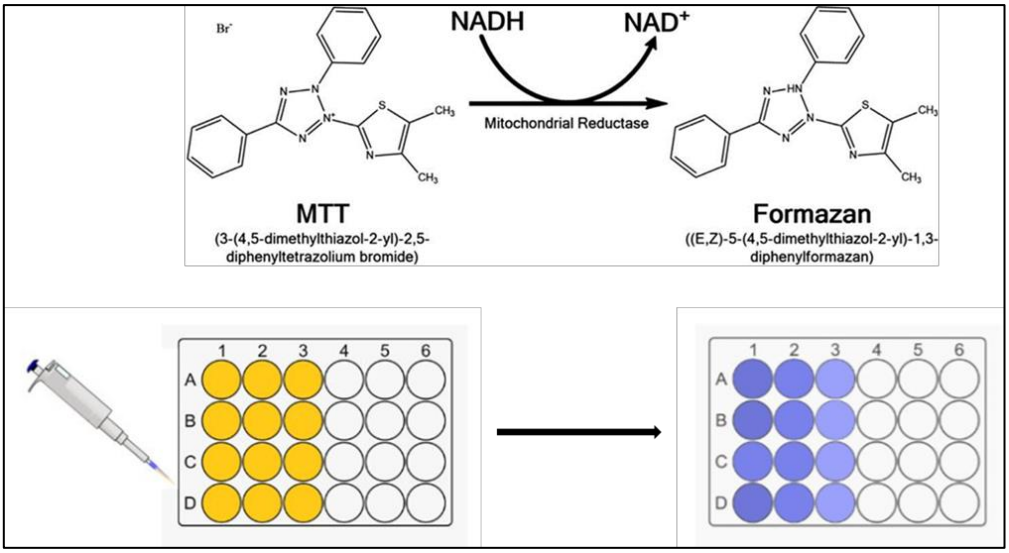

Figure 3.1: The reduction of yellow MTT to purple formazan measured at 570nm by mitochondrial oxidoreductases using NAD(P)H as a source of reducing equivalents [Prepared by author and adapted from (Kamiloglu *et al.*, 2020)].

3.5.2 Protocol

The 3 cell lines were seeded in a 96-well microtitre plate at a concentration of 20,000 cells/well (150µl CCM/well) and allowed to attach overnight (37°C, 5% CO_2). Cells were treated with *M. burkeana* plant extract at various concentrations (0, 50, 125, 250, 500, 1000, 2500 and 5000 µg/ml) in triplicate (200µl/well). Following 48 hours of incubation, the treatment medium was removed and the cells were incubated (37°C, 3 hours) with 120µl/well MTT solution (7.5mg MTT salt in 1.5ml of 0.1M PBS and 7.5ml CCM). After that, the MTT solution was aspirated, and cells were incubated for 1 hour with 100µl/well DMSO. The OD of the formazan product was measured at 570nm, with a reference wavelength of 690nm by a SPECTROstar® Nano microplate reader (BMG LABTECH, Ortenberg, Germany). The percentage of cell viability was calculated (Appendix 1):

$$\% \text{ Cell Viability} = \frac{\text{Absorbance of treated cells}}{\text{Absorbance of Control Cells}} \times 100$$

The log concentration-response curves were plotted using GraphPad Prism v5.0 software (La Jolla, California, USA). Non-linear regression analysis was used to extrapolate the half maximum inhibitory concentration (IC_{50}) and concentration that produced 20% inhibition of cell viability (IC_{20}). For subsequent assays, the cells were treated at 80% confluency with the

compound's IC_{50} and IC_{20} concentrations for 48 hours.

3.6 LACTATE DEHYDROGENASE (LDH) ASSAY

3.6.1 Principle

As reported by Warburg in 1956, cancer cells undergo glycolysis at an enhanced rate due to accelerated metabolism in cancerous versus normal cells (Tran *et al.*, 2020). Lactate dehydrogenase (LDH) is an oxidoreductase that is mainly located in the cell cytoplasm. It facilitates the conversion of pyruvate to lactate and the transformation of NADH to NAD^+ during glycolysis (Kolappan *et al.*, 2015). When cell membranes experience damage, LDH gets released into the extracellular surroundings. This extracellular LDH can be quantified and serves as a measure of cellular toxicity. Quantification occurs by a coupled enzymatic reaction whereby LDH facilitates the conversion of pyruvate to lactate and the reduction of NADH to NAD^+during glycolysis (Kolappan *et al.*, 2015). Diaphorase, an oxidase enzyme, utilizes NADH to reduce 2-p-iodophenyl-3-pnitrophenyl-5-phenyl tetrazolium chloride (INT), a tetrazolium salt, into a formazan product (Figure 3.2). The formazan formed is measured at 490nm and is directly proportional to LDH released into the extracellular surroundings. (Thermo Fischer Scientific, 2022).

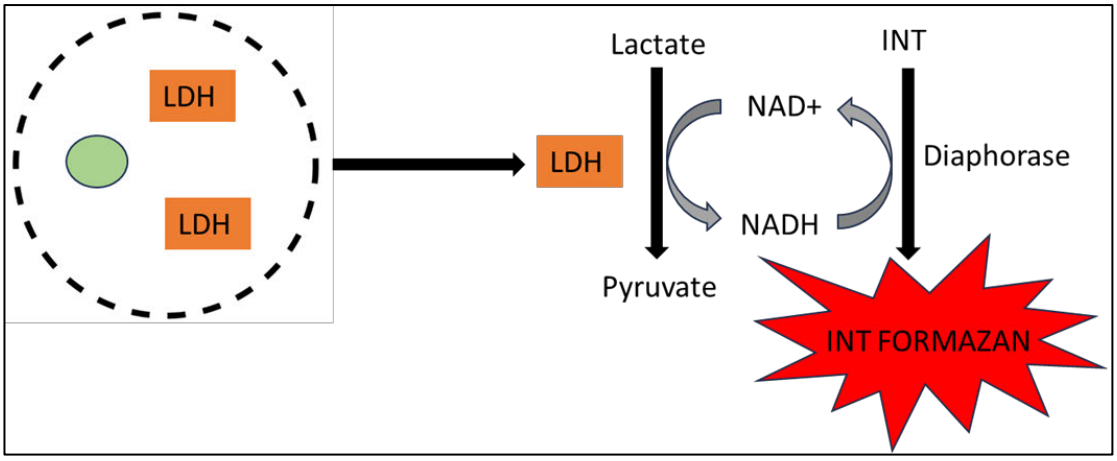

Figure 3.2: Schematic diagram showing the LDH assay mechanism whereby LDH is released from damaged cells and lactate is converted to pyruvate using lactate dehydrogenase enzymes. The NAD+/NADH ratio is essential in the conversion of INT to formazan [Prepared by author and adapted from (Thermo Fischer Scientific, 2014)].

3.6.2 Protocol

To measure extracellular LDH levels, a LDH cytotoxicity kit was used. The LDH reagent was prepared as per manufacturers' manual (#Roche, 04744926001). The cell culture medium was aspirated after the cells were treated with the compound of interest and was used to measure extracellular LDH activity. In triplicate, treated and untreated sample supernatants (50µl) were pipetted into a 96-well plate, then 25µl of the LDH reagent was pipetted into each well. After 30 minutes of incubation (dark) at room temperature (RT), 12.5µl/well of stop solution was added. An OD reading at 490nm with a reference wavelengthat 600nm was taken using a SPECTROstar® Nano microplate reader (BMG LABTECH, Ortenberg, Germany), and the LDH levels were expressed as mean OD.

3.7 THIOBARBITURIC ACID REACTIVE SUBSTANCES (TBARS) ASSAY

3.7.1 Principle

The TBARS assay is widely used to quantify oxidative damage caused by reactive oxygen species by measuring the end product of lipid peroxidation, malondialdehyde (MDA). Malondialdehyde is a reactive aldehyde that is produced as a by-product of lipid peroxidation of polyunsaturated fatty acids (Aguilar Diaz De Leon and Borges, 2020). A pink-coloured insoluble adduct forms between MDA and the methylene groups of two molecules of thiobarbituric acid (TBA-MDA) (Figure 3.3). The reaction is optimum at high temperatures and low pH, and butylated hydroxytoluene is added to the reaction mixture to prevent peroxidation from occurring in the reaction tube. The adduct is solubilized with a solvent, which absorbs light at 532-535nm. The concentration of MDA measured is proportional to the intensity of the colour viewed, measured using a spectrophotometer (Dasgupta. *et al.*, 2014). The TBARS assay was conducted using the molar extinction coefficient ($\varepsilon = 156{,}000\ M^{-1}cm^{-1}$) (Wozniak *et al.*, 2019).

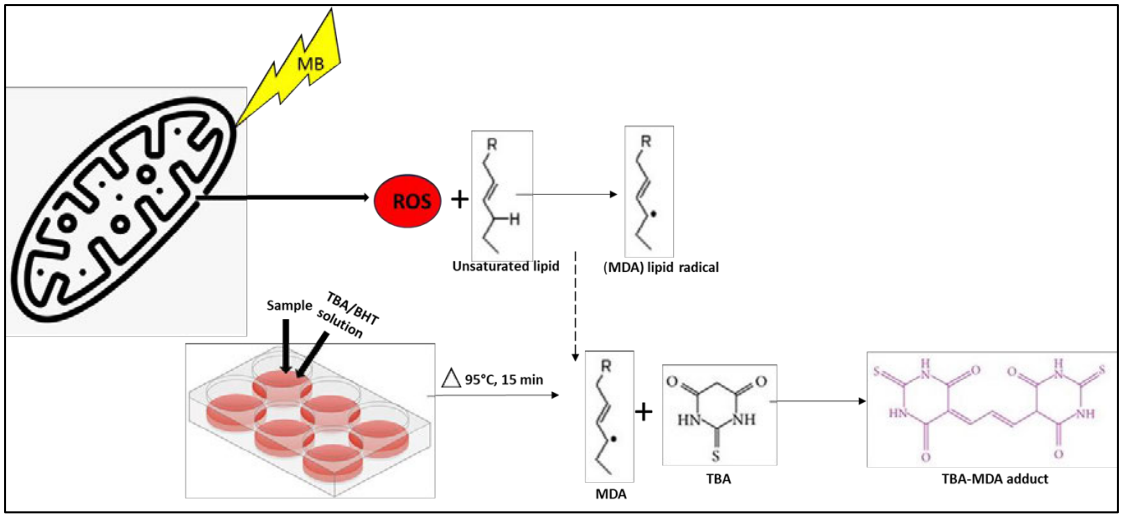

Figure 3.3: Reaction of MDA with two molecules of TBA to yield a pink chromogen that can be quantified at 532nm and is proportional to ROS production and lipid peroxidation (Prepared by author).

3.7.2 Protocol

The Caco-2 and HepG2 cell lines were treated with the IC_{20} and IC_{50} concentrations of *M. burkeana* plant extract. The control cells did not receive any treatment. The supernatants (200µl) were collected in correspondingly labelled test tubes (control, IC_{20}, and IC_{50}). These test tubes were assayed for MDA levels. To ensure the accuracy of the results, a positive control containing 1µl of MDA and 199µl CCM and a negative control containing 200µl CCM were prepared. To inactivate proteins or enzymes that may mislead results, 200µl of 2% phosphoric acid (H_3PO_4) and 200µl of 7% H_3PO_4 were added to each tube. Thereafter, 400µl thiobarbituric acid (TBA)/butylated hydroxytoluene (BHT) was added to each sample, excluding the negative control, which received 400µl of 3mM HCl. All test tubes were vortexed. After vortexing, 200µl of 1M HCL was added to each sample and the test tubes were placed in a water bath (100°C, 15 minutes). Thereafter, the test tubes were removed and cooled to RT in a dark environment. Into each test tube, 1500µl butanol was added followed by vortexing the tubes for 30 seconds. Once the samples settled, two distinct phases were visible. Approximately 500µl of the upper butanol phase was pipetted into a microcentrifuge tube and centrifuged at 1600×g for 10 minutes at 4°C. Thereafter, 100µl of each sample was transferred into a well of a 96-well microtiter plate in triplicates. The absorbance was then read at 532nm with a reference wavelength of 600nm using a SPECTROstar® Nano microplate

reader (BMG LABTECH, Ortenberg, Germany). The absorbance was used to determine the average concentration of MDA (µM).

$$[\text{MDA}] = \frac{\text{Sample absorbance}}{156\text{mM}^{-1}} \times 1000$$

3.8 NITRIC OXIDE (NOS) ASSAY

3.8.1 Principle

Both direct and indirect methods can measure nitric oxide. L-arginine and nitric oxide synthase generate endogenous nitric oxide (NO). However, the short half-life and low NO concentrations *in vivo* make this assay unfeasible. This can be resolved by measuring its stable metabolites, nitrite (NO_2^-) and nitrate (NO_3^-) (Liu *et al.*, 1998). With a sensitivity to 0.5 µM NO_3^-, the NOS assay can be conducted for numerous fluids such as cell culture media, serum, and plasma (Bryan and Grisham, 2007). This assay's principle is reducing nitrate by vanadium (III) chloride (VCl_3) to nitrite. The acidic Griess reaction facilitates the calorimetric detection of these anions as an azo dye product. The Griess reaction was first defined in 1879 and consists of two steps (Griess, 1879). First, the diazotization of sulfanilamide by NO_2^- forms a chromophore that couples with bicyclic amines such as N- 1-(naphthyl)ethylenediamine (NEDD) and is measured using a spectrophotometer (Figure 3.4).

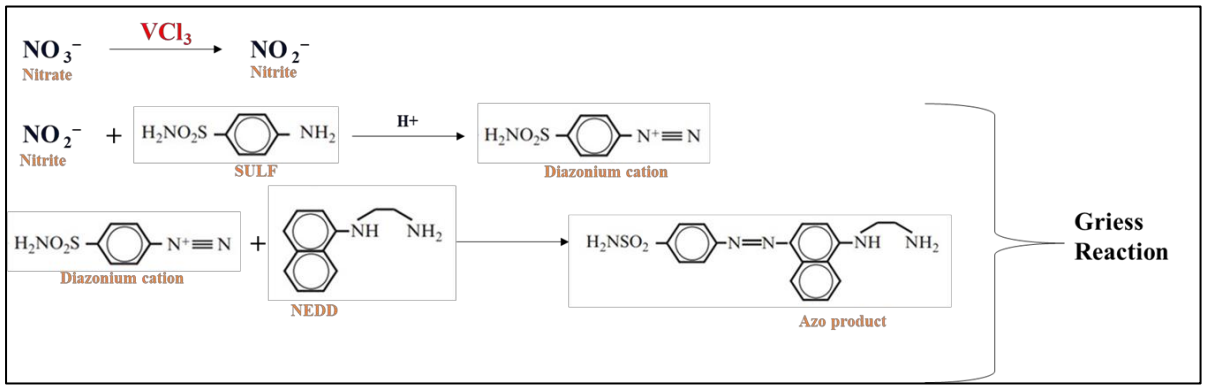

Figure 3.4: Formation of diazo compound by the Griess reaction [Prepared by the author and adapted from (Ghafourifar *et al.*, 2008)].

3.8.2 Protocol

Sodium nitrate ($NaNO_3$) standards were prepared (0 - 200µM) to assess the effects of the compound of interest on NO production in the two cell lines. First, the 2 cell lines were treated with the compound of interest at the IC_{20} and IC_{50} concentrations. The supernatants from the samples (50µl) were pipetted into a 96-well plate in triplicate. The $NaNO_3$ standards (50µl) were also pipetted into the 96-well plate in triplicate. Thereafter, 50µl VCl_3, 25µl sulfanilimide and 50µl NEDD were added to all sample wells. The plate was incubated in the dark at 37°C for 30 minutes. The OD was measured using a SPECTROstar® Nano microplate reader (BMG LABTECH, Ortenberg, Germany) at 540nm with a reference wavelength of 690nm. The standard mean values were used to plot a standard curve (Appendix 2), and extrapolation resulted in obtaining the nitrite levels (µM) produced by the cells.

3.9 LUMINOMETRY

Luminescence is the basic principle of luminometry and it involves the emission of light. Spontaneous emission from an electronically excited state through chemical reactions is referred to as chemiluminescence. The biochemical emission of light through enzymatic reactions is referred to as bioluminescence. Luminometry assays were utilised in this study to quantify various biomolecules. The emitted light is quantified as Relative Luminescence Units (RLU) (Tzani *et al.*, 2021).

Cultured cells with an 80% confluency were treated with the IC_{20} and IC_{50} concentrations of *M. burkeana* plant extract. Two flasks with Caco-2 and HepG2 cells were reconstituted. The flasks were incubated at 37ºC with 5% CO_2. Once confluent, the cells were trypsinised and counted using the trypan blue exclusion method, for the subsequent luminometric assays. The Caco-2 and HepG2 cells were seeded onto a 96-well luminometer plate (20000 cells/well, 150 µl/well) and incubated at (37ºC, 5% CO_2) overnight. After incubation, the medium was removed and cells were treated (300 µl/well) with the control, IC_{20}, and IC_{50} *M. burkeana* plant extract concentrations in triplicate for 48 hours (37ºC, 5% CO_2). The treatment medium was removed and 50µl PBS was added to each well. Thereafter, the luminometry assays for ATP, caspases (caspase 8, 9 and 3/7), CYP3A4, Annexin V, JC-10 and GSH (Appendix 3)

were performed as per the manufacturer's instruction.

3.9.1 Adenosine triphosphate (ATP) quantification assay

3.9.1.1 Principle

Living cells use ATP as their main source of energy, and it is used in numerous crucial metabolic processes. Adenosine triphosphate is produced through glycolysis, tricarboxylic acid cycle, and oxidative phosphorylation (electron transport chain) (Bonora *et al.*, 2012). When cells die, they stop producing ATP, which causes the amount of ATP that already exists to deplete quickly. As a result, ATP is frequently used as a sign of healthy cells. If more living cells are present, this is indicated by greater ATP levels. ATP assays are techniques that can gauge cell viabilityby measuring ATP levels. Numerous detection techniques can be used, including colorimetric, fluorescent, and bioluminescent. Due to their superior sensitivity, straightforward, homogenous procedures, and quick findings, bioluminescent ATP tests are the method of choice among researchers for determining cell viability (Promega Corporation, 2022a). During this enzymatic, bioluminescent reaction, luciferin is activated with ATP released from lysed cells to give luciferyl-adenylate and phosphate. The second step involves luciferyl-adenylate reacting with molecular oxygen to produce oxyluciferin in an electrically excited state and CO_2. When oxyluciferin returns to the ground state (550-570nm), a green-yellow luminescent signal is emitted. Luminescence is proportional to the intracellular ATP level (Figure 3.5).

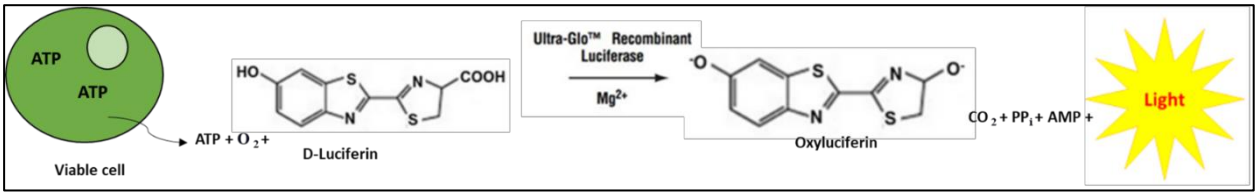

Figure 3.5: Intracellular ATP released from lysed cells provides the energy for the mono-oxygenation of luciferin to oxyluciferin by luciferase in the presence of Mg^{2+} and O_2 [Prepared by author and adapted from (Promega Corporation, 2022a)].

3.9.1.2 Protocol

The ATP levels were measured using the CellTiter-Glo® luminescent assay (Promega,

Madison, Wisconsin, USA, #G7570). The reagent was prepared as per the manufacturer's instructions. The CellTiter-Glo® reagent (25µl) was added to each well in row A selected for conducting this assay. After a 30 minute incubation in the dark at RT to allow for the luciferin-luciferase reaction to take place, luminescence was measured on a Modulus™ microplate luminometer (Turner BioSystems, Sunnyvale, California, USA). The data obtained was expressed as relative light units (RLU).

3.9.2 Caspase (8, 9 and 3/7) assays

3.9.2.1 Principle

Caspases are proteases that are made up of cysteine-aspartate residues. They play a role in apoptosis and inflammation. These two groups of caspases: initiator and effector caspases are inactive zymogens that require proteolytic processing to become active. Once activated by initiator caspases (e.g., caspase 2, 8, 9, 10), the effector caspases (e.g., caspase 3, 4, 7) will undergo cleavage and initiate apoptosis (Matsuura *et al.*, 2016). This assay depends on caspase cleavage of the substrate-conjugated proluciferin. Aminoluciferin is thereafter released and functions as a substrate for luciferase. In the presence of ATP, the luciferase reaction occurs, and light is produced (Figure 3.6). The luminescent signal is directly proportional to the level of caspase activity in the cells (Promega Corporation, 2023).

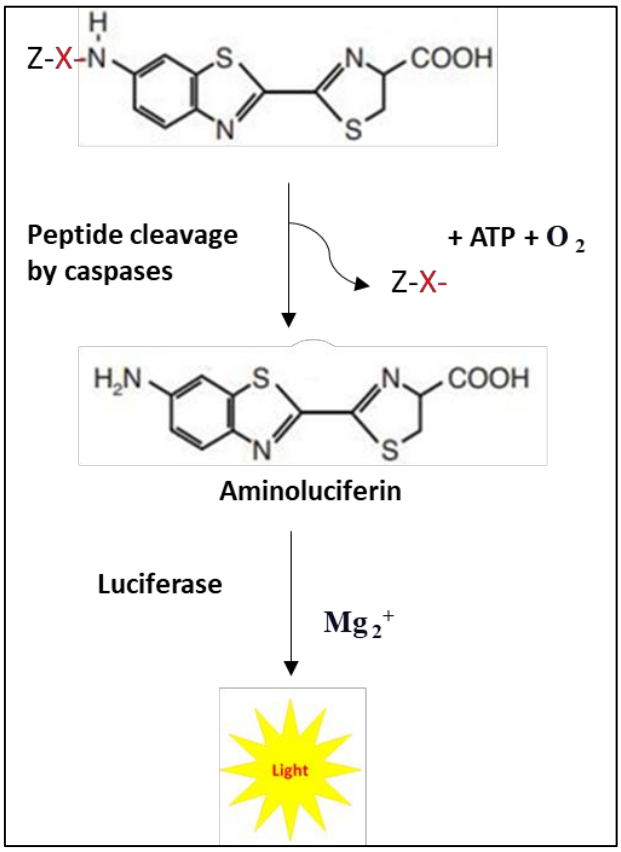

Figure 3.6: Schematic diagram of the bioluminescence quantification of caspase-Glo 8, 9, and 3/7 Assay. The peptide sequences are represented by X (Caspase 8-LETD, Caspase 9-LEHD and Caspase 3/7-DEVD). [Prepared by author and adapted from (Promega Corporation, 2023)].

3.9.2.2 Protocol

The Caspase-Glo® 8 (Cat. #G8200), Caspase-Glo® 9 (Cat. G8210) and Caspase-Glo® 3/7 (Cat. G8090) were used to assess caspase activity (Promega, Madison, USA). After preparing reagents according to the manufacturer's instructions, the caspase reagents (25µl) were added to each well in rows B, C, and D in the 96-well luminometer plate. The plate was incubated in the dark at RT for 30 minutes, then luminescence was measured on a Modulus™ microplate luminometer (Turner BioSystems, Sunnyvale, California, USA), and data was presented as RLU.

3.9.3 Cytochrome P450 oxygenase (CYP3A4)

3.9.3.1 Principle

Cytochrome P450 oxygenases (CYP) are the main enzymes that take part in the oxidative breakdown of xenobiotics. This assay provides a luminescent method to measure CYP activity. The P450-Glo™ substrates are CYP enzyme substrates which are proluciferins. The proluciferins are converted by CYP enzymes to luciferin products. The D-luciferin formed is detected in a second reaction with the luciferin detection reagent (Figure 3.7). The intensity of light produced in the second reaction is proportional to CYP activity (Promega Corporation, 2016).

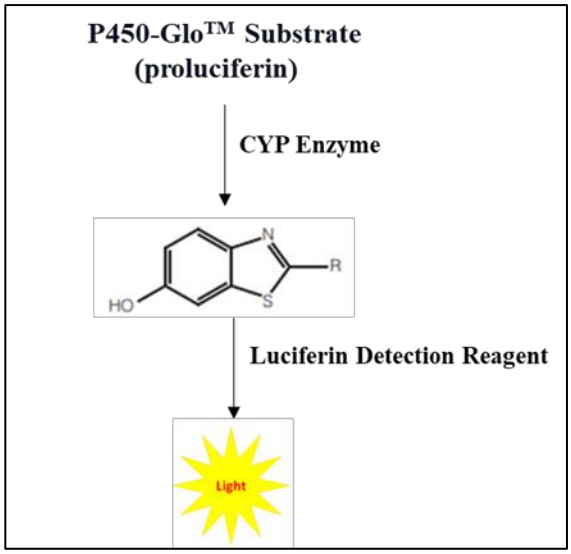

Figure 3.7: The conversion of P450-Glo™ substrate by cytochrome P450 to produce a luciferin product that generates light [Prepared by author and adapted from (Promega Corporation, 2016)].

3.9.3.2 Protocol

The P450-Glo™ assay kit (Promega, Madison, USA) was used to measure CYP3A4 activity. The CYP reagent was prepared according to the manufacturer's instructions, then 25µl was added to each well in row E in the 96-well luminometer plate. The plate was thereafter incubated in the dark at RT for 30 minutes. Following incubation, luminescence was measured on a Modulus™ microplate luminometer (Turner BioSystems, Sunnyvale, California, USA) and data was presented in RLU.

3.9.4 Annexin V

3.9.4.1 Principle

The Annexin V assay distinguishes between cells that are apoptotic and necrotic. A luminescence protocol detects apoptosis, and necrosis is detected using fluorescence. For apoptosis, this assay monitors the phosphatidylserine (PS) exposure on the cell membrane's outer leaflet during apoptosis. PS is an essential part of the cell membrane, which is used as a marker to detect early stages of apoptosis as it moves from the inside surface to the outer surface (Figure 3.8B). The assay reagent includes annexin V luciferase fusion proteins that bind to PS duringearly apoptosis and can be identified by a luminescence signal. The assay reagent also containsa DNA-binding dye that, when the integrity of the cell membrane is compromised, enters the cell and produces a fluorescent signal. This signal is proportional to PS exposure and is a marker of necrosis (Figure 3.8C) (Promega Corporation, 2022c). The Reagent used for detection in the RealTime-Glo™ Annexin V apoptosis assay is composed of annexin V fusion proteins that consist of complementary subunits of NanoBiT®luciferase (Annexin V-LgBiT and Annexin V-SmBiT) containing complementary subunits of NanoBiT® Luciferase. The two subunits form a functional unit luciferase when close together. Secondary necrosis occurring during late apoptosis is distinguished from necrosis brought on by other cytotoxic events by the combination and timing of luminescent (annexin V binding) and fluorescent (DNA release) signals. Necrotic cells are permeable and apoptotic cells are non-permeable. Multiple readings can be obtained from a single assay well using the RealTime-Glo^{TM} AnnexinV Apoptosis and Necrosis assay (Promega Corporation, 2022c).

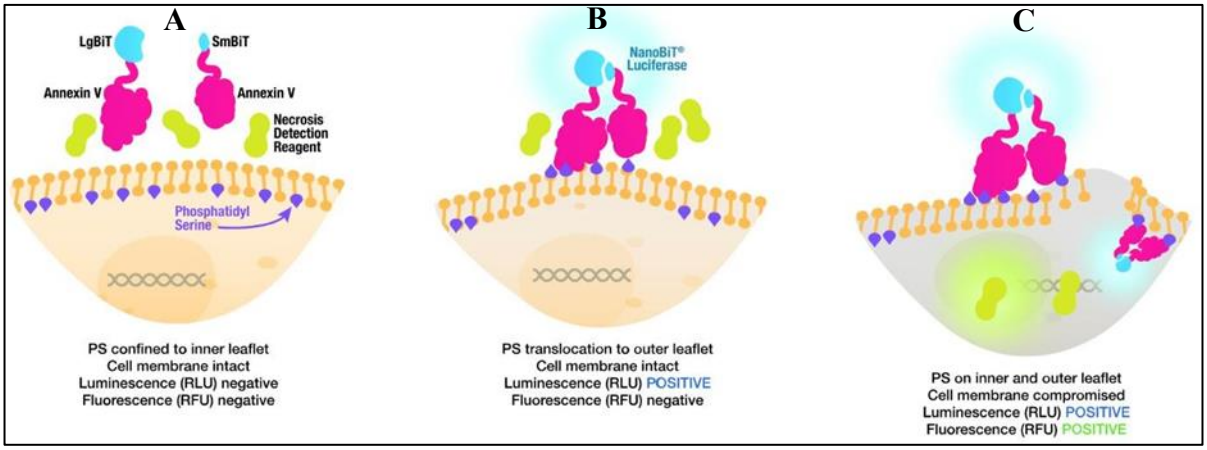

Figure 3.8: Schematic representation of a healthy cell **(A)**, early apoptosis **(B)** and secondary necrosis **(C)** using Annexin-V assay (Promega Corporation, 2022c).

3.9.4.2 Protocol

To evaluate apoptosis and necrosis the Real-Time-Glo™ annexin V apoptosis and necrosis kit was utilised (Promega, Madison, USA, Cat. JA1011). Reagents were prepared according to manufacturer'sinstructions, then the Annexin V reagent (25µl) was added to each well in row F in the 96-well luminometer plate. After a 30 minute incubation in the dark at RT, luminescence and fluorescence was measured using a Modulus™ microplate luminometer (Turner BioSystems, Sunnyvale, California, USA). Data was presented as RLU and relative fluorescence units (RFU) for apoptosis and necrosis respectively.

3.9.5 Mitochondrial membrane potential assay (JC-10)

3.9.5.1 Principle

The mitochondria, referred to as the "power house" of the cell, are crucial to cellular function. In eukaryotic cells, the mitochondria produce the majority of the cellular energy (ATP) by oxidative phosphorylation, through a series of redox processes, the mitochondrial electron transport chain generates an electrochemical gradient. This electrochemical gradient produces the mitochondrial membrane potential (ΔΨm), a measure for assessing mitochondrial activity, and stimulates the synthesis of ATP (Zorova *et al.*, 2018). Fluorescent dyes are used to monitor ΔΨm and evaluate mitochondrial viability and function. This assay is thus an

indicator of cell health. The fluorescent, lipophilic, cationic dye JC-1/JC-10 naturally emits green fluorescence. It enters the mitochondria, accumulating to form J-aggregates that display excitation and emission in the red spectrum (maximum at ~590 nm) instead of green (Figure 3.9).

In healthy cells with a normal ΔΨm, this dye enters and collects in the energised and negatively charged mitochondria and spontaneously forms red fluorescent J-aggregates. However, in unhealthy or apoptotic cells the dye enters the mitochondria at a lower rate as the inside of the mitochondria is less negative due to increased membrane permeability and therefore loss of electrochemical potential. The dye does not reach an adequate concentration to cause the formation of J aggregates, therefore, retaining its original green fluorescence (Sivandzade *et al.*, 2019). The absorption/emission of the aggregate green monomeric form is from 510/527nm, and the aggregate red form has absorption/emission from 585/590 nm (Smiley *et al.*, 1991).

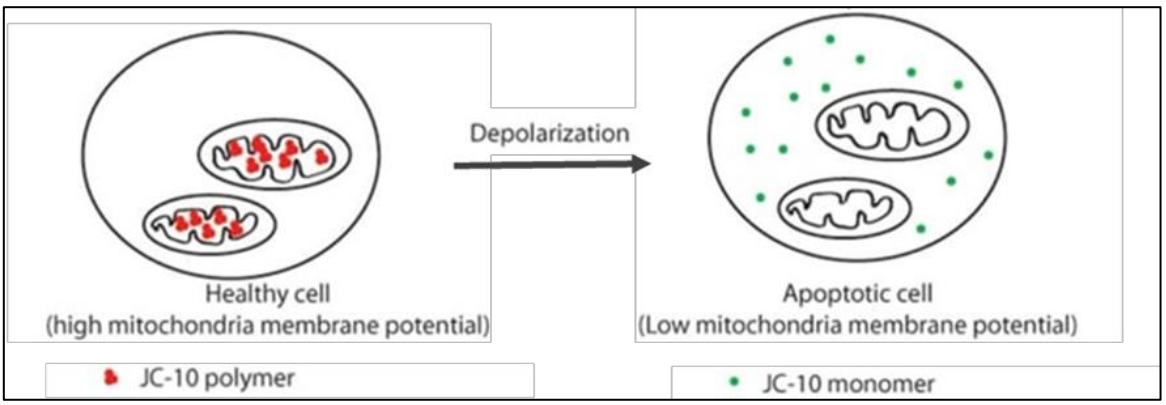

Figure 3.9: JC-10 Assay showing a healthy cell and an apoptotic cell (G-Biosciences, 2021).

3.9.5.2 Protocol

The ΔΨm, an indicator of mitochondrial function, was measured using the JC-10 dye (MAK159, Sigma, Johannesburg, South Africa). The JC-10 reagent was prepared a per the manufacturer's instruction, then 25µl was added to each well in row G in the 96-well luminometer plate, followed by incubation in the dark at RT. After 30 minutes of incubation, fluorescence was measured at 540/590 nm and 490/520nm using a Modulus™ microplate

luminometer (Turner BioSystems, Sunnyvale, California, USA). The RFU obtained was used to calculate the red/green ratio as an indicator of ΔΨm.

3.9.6 Glutathione (GSH)

3.10.6.1 Principle

The GSH-Glo™ Assay is a luminometric assay to detect and measure glutathione (GSH) levels in biological samples such as cells. When evaluating toxicological responses, a change in GSH levels is crucial because it is a sign of oxidative stress that could cause cell death or apoptosis (Pizzino *et al.*, 2017). A luciferin derivative is transformed into luciferin in the presence of GSH, which is the basis for the GSH detection assay. A glutathione S-transferase (GST) enzyme included in the kit catalyses the reaction. Utilising Ultra-Glo™ recombinant luciferase, the luciferin is detected in a linked reaction that results in glow-type luminescence proportional to the level of glutathione in the cells (Promega Corporation, 2022b).

This assay is performed in two steps (Figure 3.10). Firstly, cells are lysed in the presence of the luciferin-NT substrate and glutathione S-transferase. Luciferin-NT is converted to luciferin by GST; GSH is utilised and is the driving force of the reaction. ATP and CO_2 are produced as by-products. In the second step, luciferin is converted by luciferase to produce light, the luminescent light is directly proportional to the amount of GSH in the cells (Promega Corporation, 2022b).

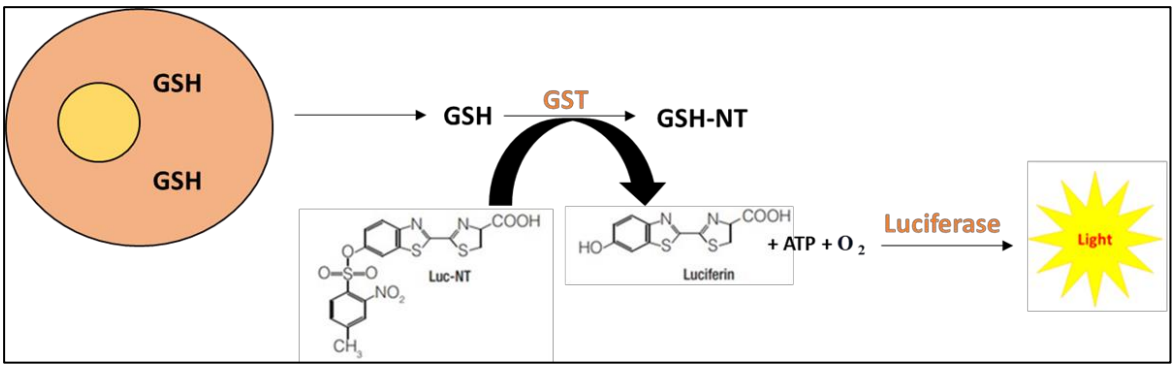

Figure 3.10: A diagram of the GSH-Glo™ glutathione assay involving the conversion of Luciferin-NT to Luciferin by glutathione S-transferase [Prepared by the author and adapted from (Promega Corporation, 2022b)].

3.9.6.2 Protocol

The Promega GSH-Glo™ reagent (Cat. V6911/2, Madison, USA) was used to quantify GSH in treated Caco-2 and HepG2 cells. The prepared reagent (25µl) was added to each well in row H in the 96-well luminometer plate, then the plate was incubated in the dark at RT for 30 minutes. Following incubation, 25µl of luciferin detection reagent was added to each well and the plate was incubated for 15 minutes in the dark at RT. Luminescence was measured using a Modulus™ microplate luminometer (Turner BioSystems, Sunnyvale, California, USA), and the result was presented in RLU.

3.10 WESTERN BLOT

3.10.1 Principle

This assay is utilised for the separation and identification of proteins. A protein mixture is prepared through cell lysis, and proteins are separated according to molecular weight through sodium dodecyl sulphate polyacrylamide gel electrophoresis (SDS-PAGE) (Figure 3.11). After that, the proteins are transferred electrophoretically to a membrane. The protein of interest in the membrane provides an antigenic band detected using primary and secondary antibodies (Figure 3.11) (Mahmood and Yang, 2012, Meftahi *et al.*, 2021).

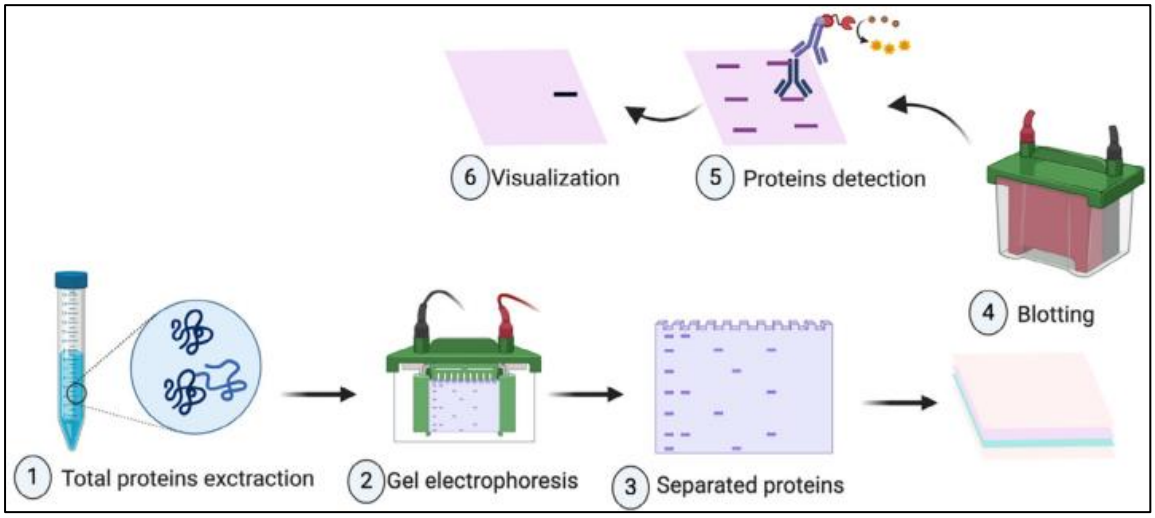

Figure 3.11: The workflow of conducting a western blot assay (Meftahi *et al.*, 2021).

3.11.2 Protocol

3.10.2.1 Preparation, isolation and standardisation of protein

This assay separated proteins using molecular weights and detected protein expression in a sample using gel electrophoresis. After treating Caco-2 and HepG2 cells for 48 hours with *M. burkeana* plant extract, the contents of the flasks were removed, and the flasks were rinsed 3x with PBS. Cytobuster reagent (500µl, Merck, Johannesburg, South Africa), supplemented with protease and phosphataseinhibitors (ThermoFisher, #A32963), was added to isolate crude proteins through lysis of the cells. Flasks were placed on ice for 15 minutes and thereafter scraped to dislodge the cells from the surface. The cell lysate was transferred to a microcentrifuge tube and placed on ice. The tubes were centrifuged (10 000xg, 4°C, 10 minutes). Supernatants were removed and used to conduct the bicinchoninic acid (BCA) assay to quantify and standardise proteins.

The bovine serum albumin (BSA) standards (0, 0.2 0.4 0.6 0.8 and 1mg/ml) and the crude protein were aliquoted into a 96-well microtitre plate (25µl per well in triplicate). The BCA solution was prepared (198µl BCA: 4µl $CuSO_4$ per reaction), and 200µl of the BCA reagent was added to each of the standard and sample well. The plate was incubated (37°C, 30 minutes) and the absorbance was measured at 562nm using a SPECTROstar^{Nano} microplate reader (BMG LABTECH, Ortenberg, Germany). A standard curve was constructed (Appendix 4) using the mean absorbances of the standards. The concentration of the crude protein within each sample was obtained by extrapolation. The crude protein samples were then standardised to 1mg/ml (200µl). Laemmli buffer [5x concentrate comprising dH_2O, 0.5M Tris-HCl (pH 6.8), glycerol, 10% SDS, 5% β-mercaptoethanol, 1% bromophenol blue] was added to the samples (50µl per sample), then samples were heated to 100ºC for 5 minutes to activate β- mercaptoethanol and SDS for the reduction and unfolding of proteins to take place. Once cooled, the samples were stored until ready to load onto prepared polyacrylamide gels.

3.10.2.2 Electrophoresis and protein transfer

The Mini-PROTEAN 3 SDS-PAGE gel casting apparatus was set up using 1.5mm spacer plates, then 7.5ml of the 10% resolving gel (1.5M Tris (pH 6.8), 10% SDS, Bis-Acrylamide,

10% ammonium persulphate (APS) and tetramethylethylenediamine (TEMED)) was added between the plates and overlayed with dH_2O. After 1 hour of polymerisation, an upper 4% stacking gel (0.5M Tris (pH 6.8), 10% SDS, Bis-Acrylamide, 10% APS and TEMED) was prepared and added, and a plastic comb was placed into the gel create loading wells. Once the gel was set, the comb was removed and the standardised samples (25µl) were loaded into the wells of prepared polyacrylamide gels. The gel cassette was placed into an electrophoresis tank with cold electrophoresis buffer (Tris; glycine; SDS; dissolved in dH_2O) and a voltage of 150 volts was applied for 90 minutes.

Once electrophoresis was completed, the gels were placed into a cold transfer buffer (Tris; glycine; SDS; dissolved in dH_2O) for 10 minutes. Thereafter, the proteins were electrotransferred onto a nitrocellulose membrane using the Trans-blot Turbo transfer system (Bio-Rad, California, USA). This transfer method consisted of assembling the sandwich using the electrophoresed polyacrylamide gel, nitrocellulose membrane, and fibre pads in a cassette submerged in transfer buffer. An electric current (25V, 2.5mA, 30 minutes) was applied to facilitate the transfer.

3.10.2.3 Immunoprobing and protein detection

After the transfer, the nitrocellulose membranes containing the transferred protein bands were blocked with 5% BSA in Tris- buffered saline [Tris-HCl (pH 7.4), NaCl, 0.05% Tween20; TTBS] for 2 hours at RT to prevent non-specific binding. The blocking solution was then removed and the membrane was probed for 1 hour on the shaker at RT with primary antibodies (1:1000 in 5% BSA) and thereafter incubated at 4°C overnight, to allow binding of the antibody to its specific target protein [SOD2 (#13141S), NRF-2 (#12721S), P53 (#48818S), p-P53 (#9286S), BAX (#27747S), NFκB (#8242S), $cIAP_2$ (#3130S), iNOS (#131205S), cleaved caspase 3 (#9661) and BCL-2 (#15071S)]. After the overnight incubation, membranes were equilibrated at RT for 1 hour, and washed 5 times (10 ml TTBS, 10 minutes per wash). Thereafter, the membranes were probed with 5ml horseradish peroxidase (HRP)-conjugated secondary antibody (anti-mouse IgG #7076 or anti-rabbit IgG #7074 diluted 1:2500 in 5% BSA/TTBS, at RT for 2 hours on a shaker. After removal of the secondary antibody, the

membranes were washed 5 times with TTBS (10ml TTBS, 10 minutes per wash).

Clarity western enhanced chemiluminescence (ECL) Substrate (Bio-Rad) and peroxide substrate solution was added to the nitrocellulose membranes. The images generated were captured using a gel documentation system Molecular imager® Chemidoc™ XRS+ and Bio-Rad imaging system. Protein expression was analysed with Image Lab™ Software (Bio-Rad, California, USA). Each membrane was then quenched with 5% hydrogen peroxide (H_2O_2) (5ml) and rinsed 3x with TTBS (10 minutes). The stripped membranes were thereafter blocked with 5% BSA (2 hours, RT). The blocking solution was discarded and the membranes were probed with β- actin (1 hour, RT), a house-keeping protein in a 1:5000 dilution with 5% BSA/TTBS for 30 minutes for protein normalisation. The results obtained was examined by analysing the intensity of each protein band and the bands were normalised against β-actin (A0bD12141, Sigma). The data acquired was expressed as mean relative band intensity (RBI).

3.11 REAL TIME QUANTITATIVE POLYMERASE CHAIN REACTION

3.11.1 Principle

Real time PCR also known as quantitative PCR or qPCR is widely used for gene expression research to amplify, isolate or identify RNA sequences (Kralik and Ricchi, 2017). It is sensitive and specific and a suitable method for detecting target RNA copies present in small quantities. During organic extraction of RNA, the sample is homogenized in a solution containing phenol and thereafter centrifuged. Three distinct phases can be viewed after centrifugation: the organic phase (lowest), a middle phase containing genomic deoxyribose nucleic acids (gDNA) and denatured proteins as well as the aqueous phase containing RNA (upper). The aqueous phase is collected and alcohol is used for the precipitation and rehydration of RNA (ThermoFisher Scientific, 2023). The RT-qPCR (reverse transcription polymerase chain reaction) procedure includes reverse transcription, denaturation, annealing and extension which is repeated in numerous cycles in order to exponentially amplify the target DNA. Single-stranded messenger RNA (mRNA) is used as a template in a reaction using reverse transcriptase to convert the mRNA into its complementary DNA (cDNA)

sequence. A second strand is thereafter synthesised with DNA polymerase and a double stranded cDNA molecule is generated. This cDNA can be amplified using PCR (Marmiroli and Maestri, 2007). The denaturation of the template DNA by heat (>90°C) causes the double stranded DNA to unwind and separates into single strands of cDNA which now becomes template strands (Green and Sambrook, 2019). The temperature of the reaction is thereafter lowered to allow for binding of primers to bind to the template DNA. The primers (20-25 nucleotides) have complementary bases to the bands on template DNA (Green and Sambrook, 2019). For extension to occur, the reaction temperature is increased (between 55˚C and 70˚C) and DNA polymerases synthesise a new DNA stand starting at the 3′ ends of the bound primers. A double stranded DNA molecule results (Obradovic *et al.*, 2013).

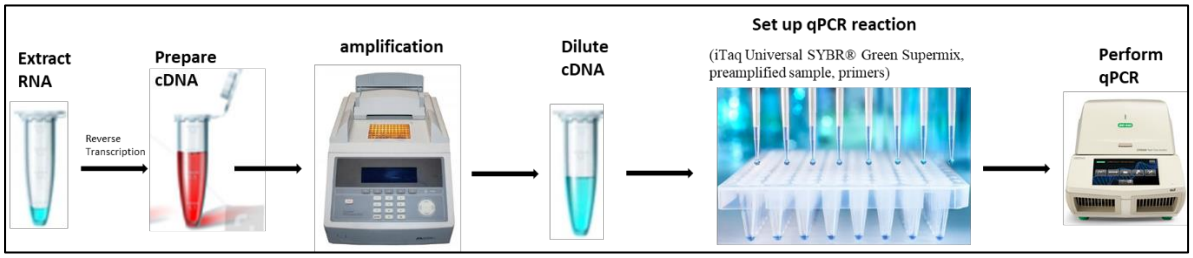

Figure 3.12: A standard qPCR procedure showing the steps involved from the extraction of RNA to the amplification of cDNA (Prepared by author).

3.11.2 Protocol

3.11.2.1 RNA isolation and standardization

After protein isolation, 250µl of Trizol and 250µl of PBS were added to each nuclear pellet in a 1.5ml RNAse/DNA-free microcentrifuge tube. Stored samples (-80ºC overnight) were thawed at RT, then 100µl chloroform was added and centrifuged (12,000 x g, 15 minutes, 4ºC). The supernatant was transferred to a new 1.5ml microcentrifuge tube and 250µl isopropanol was added. The samples were flicked to mix and stored overnight at -80ºC. Samples were thereafter thawed and centrifuged (12,000 x g, 20 minutes, 4ºC). The supernatants were removed and the RNA pellets were washed in 500µl ice-cold ethanol (75%) and centrifuged (7,400 x g, 15 minutes, 4 ºC). The ethanol was removed, and the samples were airdried for 1-1.5 hours. The RNA pellet was resuspended in 15µl nuclease-free water and incubated at RT for 2-3 minutes. The RNA was quantified using the Nanodrop2000 spectrophotometer (ThermoScientific, Waltham, Massachusetts, USA) and was standardised

to 1000ng/µl.

3.11.2.2 cDNA synthesis

The iScript cDNA Synthesis Kit (Cat. #1708891, Bio-Rad, Hercules, California, USA) was used for cDNA synthesis from template RNA. Each PCR tube contained a reaction volume of 4µl RNA template, 2µl 5x iScript reaction mix, 0.5µl iScript reverse transcriptase and 5.5µl nuclease free water. The samples were placed into the GeneAmp PCR 97000 instrument and the reaction conditions in the thermocycler were 25ºC for 5 minutes, 42ºC for 30 minutes, 85ºC for 5 minutes and a hold at 4ºC. When the reactions were complete, 80µl of nuclease free water was added to each tube and samples were stored at -80ºC until use.

3.11.2.3 qPCR

Gene expression of *MLKL, RIPK1, RIPK3, NF-κB, Gpx-1, OGG1*, *TNFα* and Glyceraldehyde 3- phosphate as a housekeeping gene was assessed using qPCR. The iTaq Universal SYBR® Green Supermix (Cat. #1725121), Bio-Rad, Hercules, California, USA was used. A master mix for each primer was prepared in RNAse and DNAse free microcentrifuge tubes using the following reagents per half-reaction for each well: 6.25µl Sybr green, 0.5µl of forward primer (Table 1), 0.5µl of reverse primer (Table 1) and 3.75µl nuclease free water. From the master mix, 11µl was added to each well in the plate followed by 1.5µl cDNA in triplicate for each sample. The plate was thereafter sealed with a plastic cover and placed in the centrifuge at 2000rpm for 1 minute at RT. The plate was then placed in the C1000 Touch Thermal Cycler CFX96 Real-Time System (Bio-Rad, Hercules, California, USA) for activation at 95 ºC for 4 minutes, denaturation at 95 ºC for 4 seconds, 40 seconds for annealing of the primers specific for the gene of interest, extension at 72 ºC for 30 seconds for 40 cycles. The melt curves (Appendix 5) and Cq values were obtained via the CFX Manager™ Software and gene expression was calculated using the $2^{-\Delta\Delta CT}$ method by Livak and Schmittgen (Willems *et al.*, 2008, Livak and Schmittgen, 2001).

Table 1: Primer sequences and their respective annealing temperatures

Gene	Primer sequence	Annealing temperature (°C)
MLKL	F (5'-CTGAGGGAACTGCTGGATAGAG-3') R (5'-CGAGGAAACTGGAGCTGCTGAT-3')	60
RIPK1	F (5'-AGGTACAGGAGTTTGGTATGGGC-3') R (5'-GGTGGTGCCAAGGAGATGTATG-3')	60
RIPK3	F (5'-TAGTTTATGAAATGCTGGACCGC-3') R (5'-GCCAAGGTGTCAGATGATGTCC-3')	60
NF-κB/P65	F (5'-GACCTGAATGCTGTGCGGC-3') R (5'-ATCTTGAGCTCGGCAGTGTT-3')	58
GPX1	F (5'-GACTACACCCAGATGAACGAGC-3') R (5'-CCCACCAGGAACTTCTCAAAG-3')	58
OGG1	F (5'-GCATCGTACTCTAGCCTCCAC-3') R (5'-AGGACTTTGCTCCCTCCAC-3')	58
TNFα	F (5'-CAGAGGGAAGAGTTCCCCAG-3') R (5'-CCTTGGTCTGGTAGGAGACG-3')	60
GAPDH	F (5'-TCCCTGAGCTGAACGGGAAG-3') R (5'-GGAGGAGTGGGTGTCGCTGT-3')	Specific to gene of interest

CHAPTER 4: RESULTS

4.1 Cytochrome P450 3A4

The cytochrome P450 3A4 (CYP3A4) enzyme activity was assessed to evaluate the rate at which it neutralises or removes small foreign oxidants. This was measured post-treatment with *M. burkeana* crude aqueous extract to detect the metabolism of the plant extract. The CYP3A4 activity in untreated Caco-2 cells (Figure 4.1A) was 273.0±30.60 RLU; *M. burkeana* increased CYP3A4 activity by 4.3-fold to 1169±326.2 RLU in IC_{20}-treated cells and 8.6-fold to 2349±74.49 RLU in IC_{50}-treated cells (p=0.0015). The *M. burkeana* treatment slightly increased CYP3A4 activity in HepG2 cells by 1.1-fold to 5054±123.0 RLU in IC_{20}-treated cells and 1.2-fold to 5650±305.0 RLU in IC_{50} treated cells, compared to 4725±31.19 RLU in untreated cells (Figure 4.1B).

Figure 4.1: The effect of *M. burkeana* leaf extract on CYP3A4 enzyme activity in Caco-2 and HepG2 cells. **(A)** The CYP3A4 enzyme activity increased significantly in Caco-2 cells treated with *M. burkeana* crude aqueous extract for 48 hours. **(B)** Increased CYP3A4 activity induced by *M. burkeana* in HepG2 cells was not significant for IC_{20} and IC_{50} treated cells. [**$p \leq 0.05$ using the unpaired *t*-test with Welch's correction]

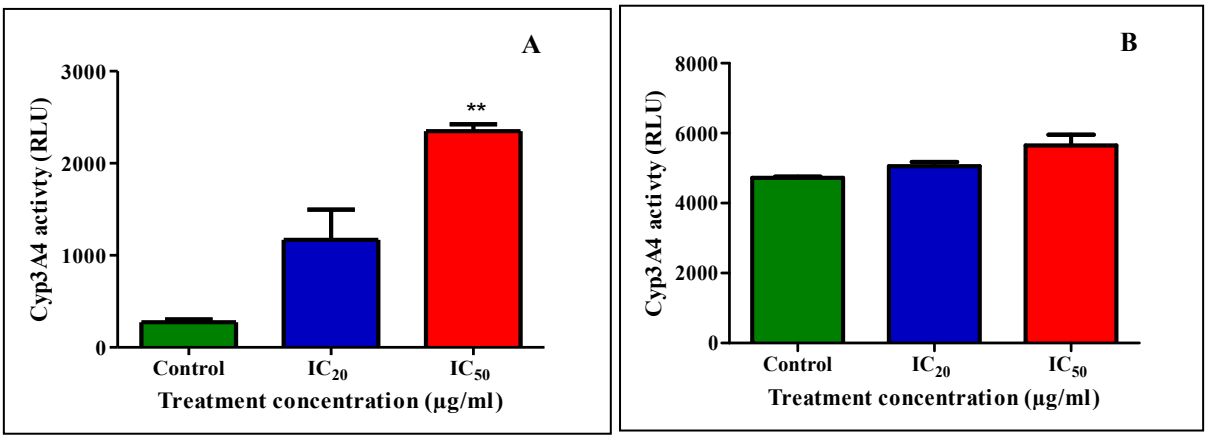

4.2 CYTOTOXIC RESPONSE TO *M. BURKEANA*

4.2.1 Cell Viability (MTT ASSAY)

The MTT assay was used to determine the viability of cells after treatment with varying concentrations (0-5000µg/ml) of *M. burkeana* crude aqueous leaf extract. This assay was conducted to test if *M. burkeana* could inhibit the metabolic activity and respiratory potential of Caco-2 and HepG2 cells at the concentrations utilised. The IC_{50} and IC_{20} were derived from these treatment concentrations and used in the subsequent assays to understand which

pathways contribute to *M. burkeana*'s oxidative stress and apoptosis in colorectal and liver cancer. The linear regression plot showed a dose-dependent decrease in cell viability as the *M. burkeana* treatment concentration increased (Figure 4.2 A, B and C). The dose-response curve for Caco-2 cells (Figure 4.2A) showed the highest cell viability of 110% at 125µg/ml *M. burkeana* treatment. Subsequent increases in *M. burkeana* concentration caused a decrease in cell viability, with the lowest viability of 4.46% at 5000µg/ml. The IC_{50} value, determined from the concentrations used in each M. burkeana plant extract treatment, was found to be 293.8µg/ml, while the IC_{20} value was measured at 169.8 µg/ml. These IC_{50} and IC_{20} values were used for treatments in the subsequent experiments. Cell viability increased to 118% in HepG2 cells treated with 50µg/ml *M. burkeana* plant extract (Figure 4.2B). A decrease in cell viability was noted for subsequent increases in concentration, with the lowest viability of 10.5% at 5000µg/ml. An IC_{50} of 335.4µg/ml and IC_{20} of 154.9µg/ml was calculated for subsequent treatments with *M. burkeana* plant extract. Cell viability in non-cancerous cells was determined using Hek293 cells. At the IC_{50} for Caco-2 and HepG2 cells, the cell viability in the Hek293 cells exceeded 80% and was deemed safe for normal cells. Cell viability of 102% at 125µg/ml *M. burkeana* treatment was obtained from the dose-response curve for Hek293 cells (Figure 4.2C). Subsequent dose increases caused a slower decrease in cell viability than Caco-2 and HepG2 cell lines, with the lowest viability of 8% at 5000µg/ml. The IC_{50} calculated for Hek293 cells was 545.7µg/ml, with an IC_{20} of 208.9 µg/ml of *M. burkeana* plant extract.

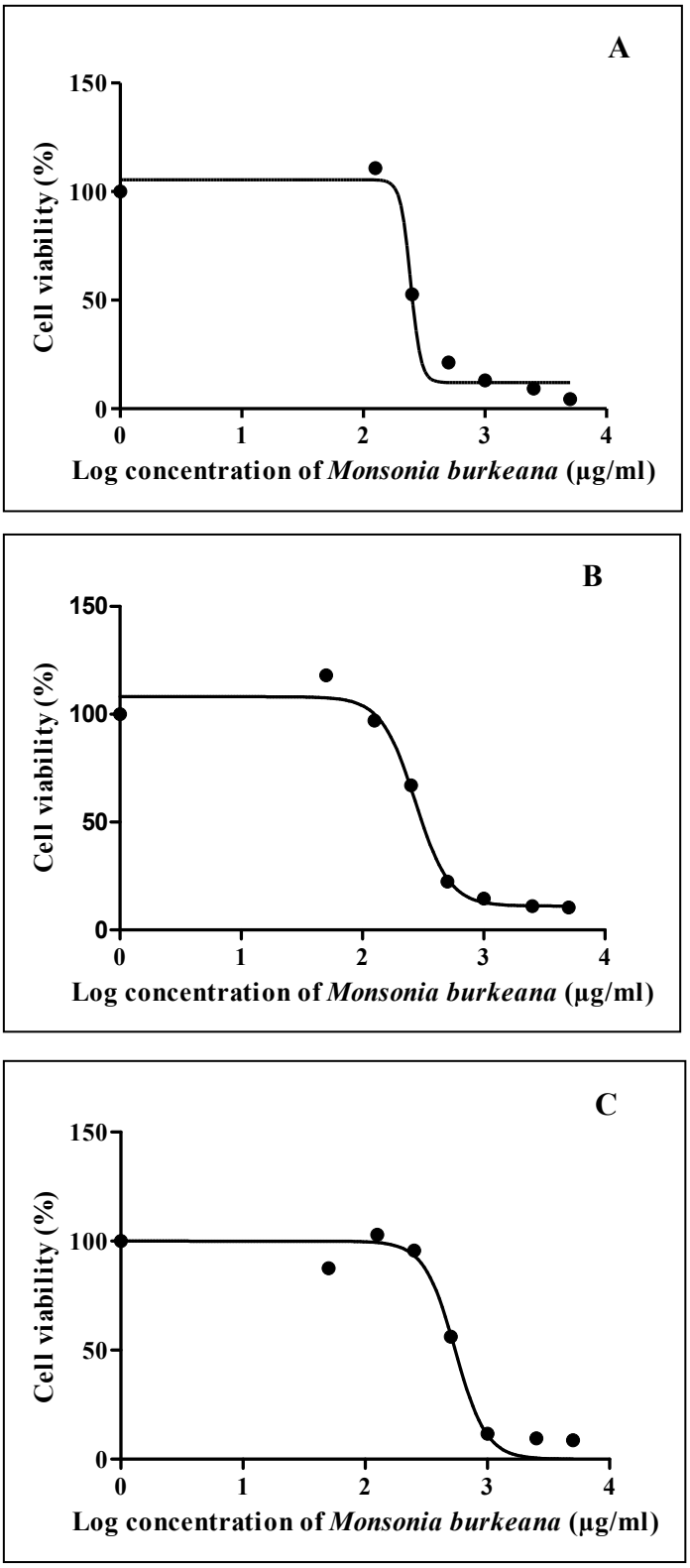

Figure 4.2: The effect of of *M. burkeana* leaf extract on cell viability in Caco-2 and HepG2 cells. **(A)** *M. burkeana* plant aqueous extract decreased cell viability of Caco-2 cells, **(B)** HepG2 cells and **(C)** Hek293 cells in a dose-dependent manner after 48 hour treatment. The data is displayed as a percentage of viable cells relative to an untreated control for each cell line.

4.2.2 Cell membrane damage

LDH externalisation was measured following the treatment with *M. burkeana* crude aqueous extract to determine cellular membrane damage. The LDH concentration in untreated Caco-2 cells (Figure 4.3A) was 0.1827±0.005667 OD. It was similar to the control (0.1703±0.006692 OD) in IC_{20}-treated cells and was increased significantly by *M. burkeana* treatment to 0.2280±0.007371 OD (1.3-fold) in IC_{50}-treated cells (p=0.0165). *M. burkeana* treatment increased extracellular LDH concentration from 0.1643±0.006227 OD in untreated HepG2 cells (Figure 4.3B) to 0.1817±0.01132 OD (1.1-fold) and 0.1830±0.02629 OD (1.1-fold) for IC_{20} and IC_{50} treated cells, respectively.

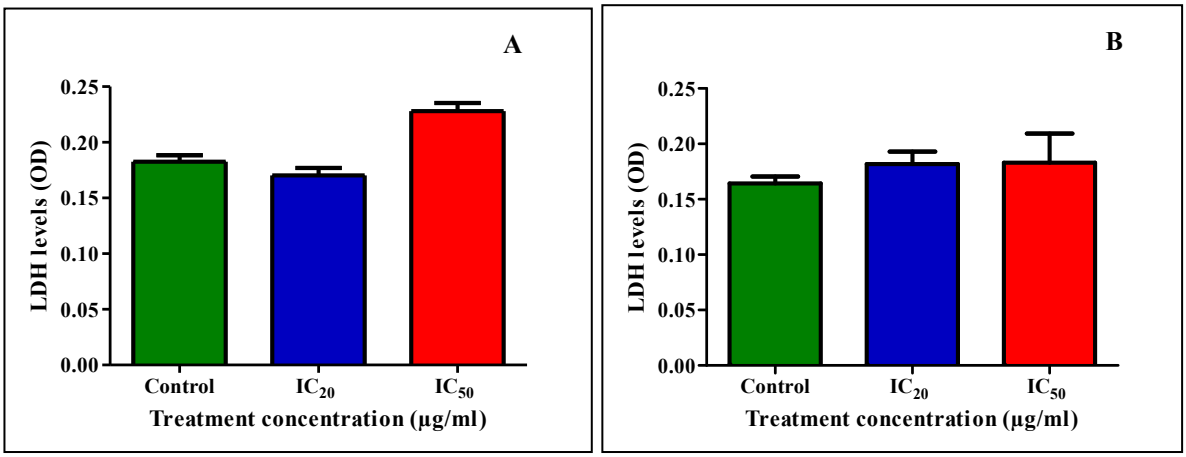

Figure 4.3: The externalisation of LDH using *M. burkeana* crude aqueous extract. **(A)** The IC_{50} concentration of *M. burkeana* increased LDH levels in the IC_{50}-treated Caco-2 cells. **(B)** A non-significant increase in LDH concentration was observed in HepG2 cells for both the IC_{20} and IC_{50} *M. burkeana* treatments. [$p \leq 0.05$ using the unpaired *t*-test with Welch's correction]

4.3 METABOLISM

4.3.1 Adenosine triphosphate (ATP) quantification assay

ATP is the energy source for all living cells. Therefore, this assay quantified ATP as a measure of cell viability. The ATP concentration in Caco-2 cells (Figure 4.4A) treated with *M. burkeana* was decreased by 0.3 fold and 0.1 fold for IC_{20} (5068000±196700 RLU; p<0.0001) and IC_{50} (2053000±96620 RLU; p=0.0003) respectively, in relation to the control (16310000±231300 RLU). In HepG2 cells (Figure 4.4B), *M. burkeana* decreased ATP concentration from 31230000±1011000 RLU in control to 12330000±260300 RLU (0.4-fold;

p=0.0030) for IC_{20}-treated cells and by 0.1-fold for the IC_{50} treatment (4070000±285400 RLU; p=0.0015).

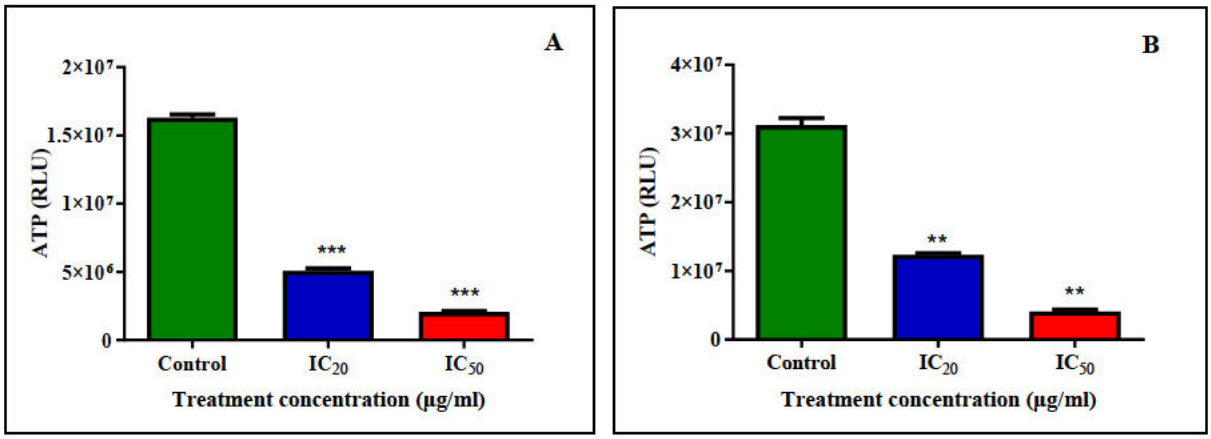

Figure 4.4: The effect of *M. burkeana* leaf extract on ATP activity in Caco-2 and HepG2 cells. **(A)** A significant decrease in ATP concentration was observed in IC_{20} and IC_{50} *M. burkeana*-treated Caco-2 cells. **(B)** A significant decrease in ATP concentration in HepG2 cells treated with IC_{20} and IC_{50} concentrations of *M. burkeana*. [**, ***$p \leq 0.05$ using the unpaired *t*-test with Welch's correction]

4.3.2 Mitochondrial membrane potential (JC-10 assay)

The fluorescent, cationic, lipophilic JC-10 dye was used to assess ΔΨm needed to produce ATP. The ΔΨm in Caco-2 cells (Figure 4.5A) was increased by 1.3-fold and significantly by 1.8-fold for IC_{20} (0.001933±0.0001453) and IC_{50} (0.002633±0.00003333; p<0.0001) *M. burkeana* treatments respectively, in relation to the control (0.001467±0.00003333). The *M. burkeana* treatment did not change ΔΨm significantly from the control (0.002069±0.000481) to the IC_{20}-treated HepG2 cells (0.002021±0.000011, Figure 4.5B), and a slight increase in ΔΨm *(*0.002390 ± 0.000062) was observed for the IC_{50}-treated cells.

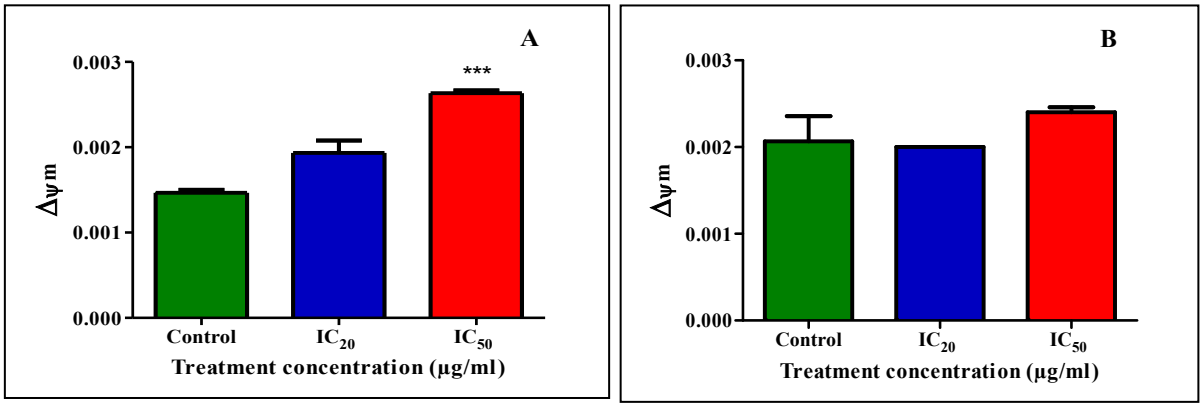

Figure 4.5: The effect of *M. burkeana* leaf extract on mitochondrial membrane potential in Caco-2 and HepG2 cells**. (A)** An increase in ΔΨm in Caco-2 cells treated with IC_{20} and IC_{50} concentrations of *M. burkeana*. **(B)** A non-significant change was observed in the ΔΨm of HepG2 cells treated with *M. burkeana*. [***$p \leq 0.05$ using the unpaired *t*-test with Welch's correction]

4.4 OXIDATIVE STRESS

4.4.1 Peroxidation of cellular macromolecules

The TBARS assay was used to quantify oxidative damage caused by measuring the end product of lipid peroxidation (MDA). The MDA concentration in untreated Caco-2 cells (Figure 4.6A) was 0.1816±0.005653 µM; *M. burkeana* decreased MDA concentration slightly to 0.1774±0.005653 µM in IC_{20}-treated cells and by 0.8-fold in IC_{50}-treated cells (0.1432±0.005653 µM, p=0.0086). The *M. burkeana* treatment decreased MDA concentration by 0.9-fold to 0.1389±0.005653 µM in IC_{20}-treated cells, but MDA remained relatively unchanged in IC_{50}-treated cells (0.1538±0.003701 µM), compared to 0.1560±0.007704 µM in untreated HepG2 cells (Figure 4.6B). Gene expression for *OGG1* was increased by *M. burkeana* to 2.466±0.2640-fold in the IC_{20}-treated Caco-2 cells (p=0.0309), and a non-significant decrease to 0.5502±0.1515-fold was observed in IC_{50}-treated cells (Figure 4.6C). The *OGG1* gene expression decreased to 0.4676±0.2448-fold and 0.6195±0.2558-fold for HepG2 cells treated with IC_{20} and IC_{50} concentrations of *M. burkeana,* respectively (Figure

4.6D).

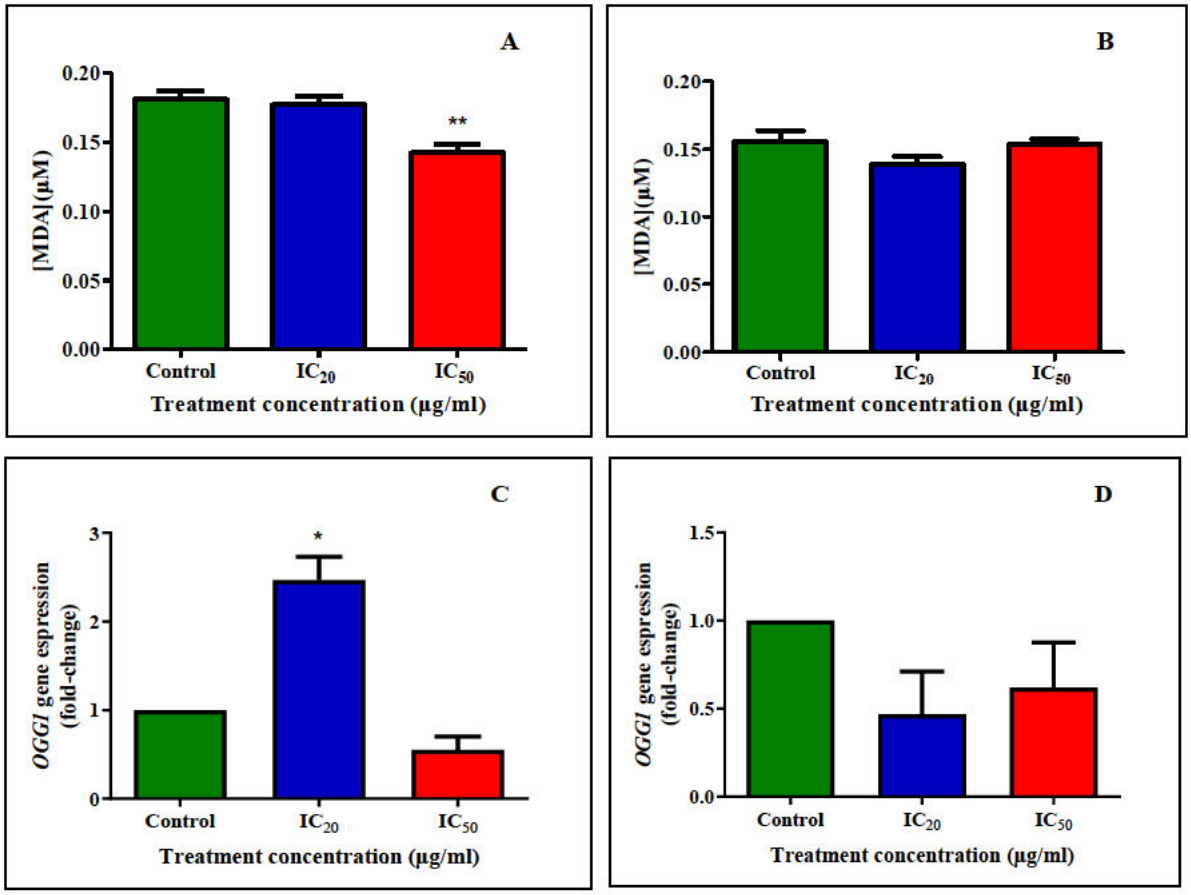

Figure 4.6: The effect of *M. burkeana* leaf extract on oxidative damage in Caco-2 and HepG2 cells. **(A)** A significant decrease in MDA concentration in Caco-2 cells treated with *M. burkeana* IC_{50} compared to the control cells. **(B)** The *M. burkeana* treatment decreased MDA concentration slightly in IC_{20} and IC_{50}-treated HepG2 cells. **(C)** The *OGG1* gene expression in Caco-2 cells increased for IC_{20}-treated cells but decreased for the IC_{50} treatment of *M. burkeana*. **(D)** Gene expression of *OGG1* was decreased for both *M. burkeana* treatments in HepG2 cells. [*, **$p \leq 0.05$ using the unpaired *t*-test with Welch's correction].

4.4.2 Nitric oxide synthase (NOS) assay

The reactive nitrogen species nitric oxide (NO) is produced in a reaction catalysed by NOS and contributes to cell oxidative stress. The nitrite concentration, which indicates NO production decreased from 48.06±0.5590 µM in untreated control Caco-2 cells (Figure 4.7A) to 40.23±0.3552 µM (0.8-fold p=0.0013) for the IC_{20} and 41.94±0.9139 µM (0.9-fold, p=0.0106) for the IC_{50} treatments with *M. burkeana*. Interestingly, the *M. burkeana* treatment

of HepG2 cells increased nitrite concentration significantly by 1.2-fold to 46.67±0.8093 µM (p=0.0065) for the IC_{20} treatment and by 1.3-fold to 48.45±1.657 µM (p=0.0130) for the IC_{50} treatment, compared to 38.45±0.8940 µM in the untreated cells (Figure 4.7B). Western blot was conducted to assess the effects of *M. burkeana* on iNOS protein expression. In Caco-2 cells (Figure 4.7C), the IC_{20} (0.6599±0.02431 RBI, p=0.0419) and IC_{50} (0.5556±0.06101 RBI, p=0.0364) *M. burkeana* treatment concentrations induced a significant 0.8-fold and 0.7-fold decrease in iNOS protein expression respectively, compared to the control (0.8175±0.03915 RBI). The IC_{20} *M. burkeana* concentration caused a non-significant decrease in iNOS protein expression to 0.4041±0.02985 RBI (0.9-fold). At the same time, the IC_{50} treatment induced a 0.7-fold decrease in the iNOS protein expression to 0.3264±0.02318 RBI (p=0.0304) compared to the control (0.4702±0.01106 RBI) in HepG2 cells (Figure 4.7D).

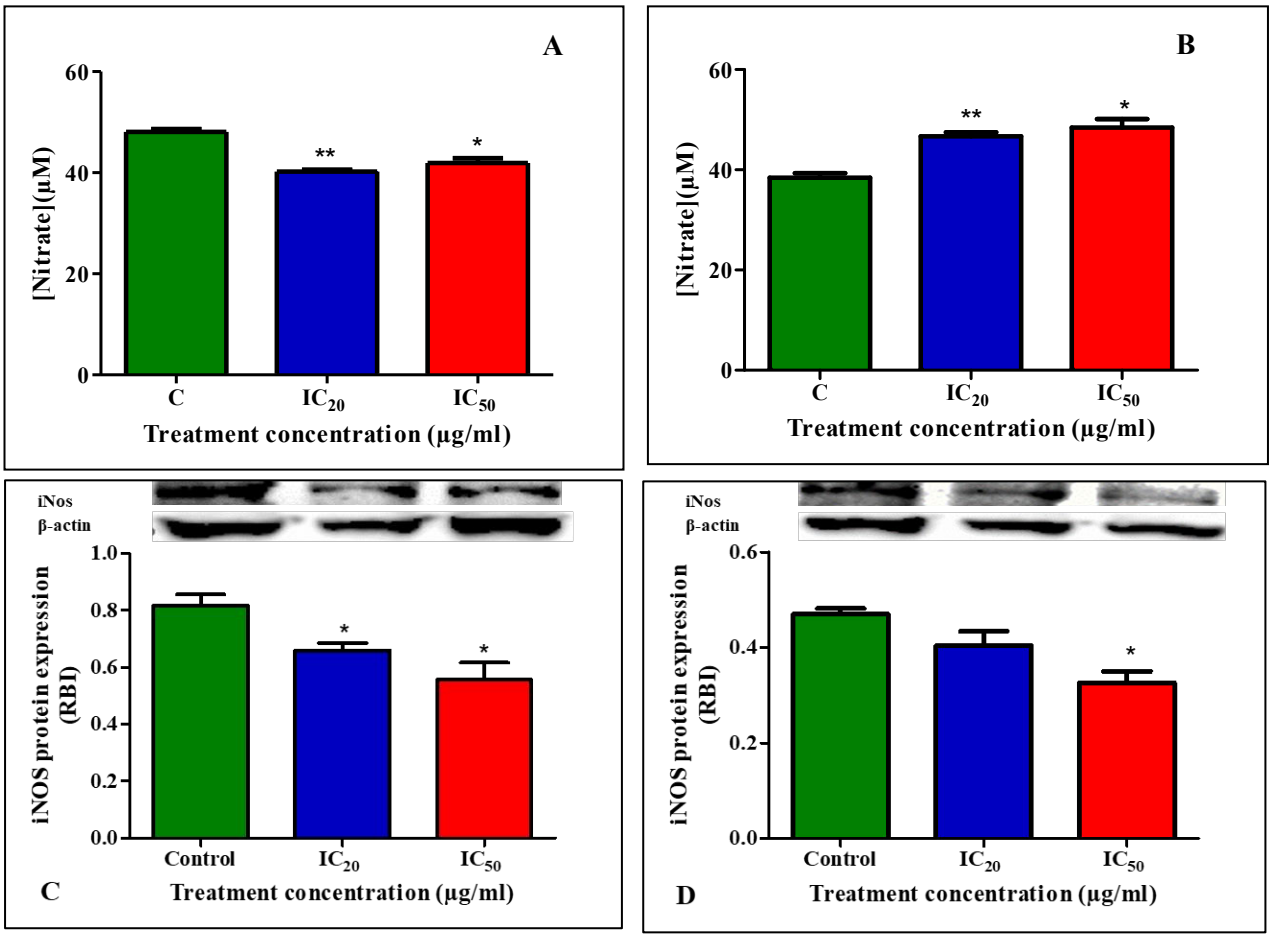

Figure 4.7: The effect of *M. burkeana* leaf extract on the level of reactive nitrogen species in Caco-2 and HepG2 cells. **(A)** A significant decrease in nitrate / nitrite concentration was observed in Caco-2 cells treated with IC_{20} and IC_{50} concentrations of *M. burkeana*. **(B)** Nitrate / nitrite concentration was significantly increased in IC_{20}- and IC_{50} *M. burkeana* treated HepG2 cells. **(C)** The iNOS protein

expression decreased for both *M. burkeana* treatments in Caco-2 cells. **(D)** A significant decrease in iNOS expression was observed for IC_{50} *M. burkeana* treated cells. [*, **$p \leq 0.05$ using the unpaired *t*-test with Welch's correction]

4.5 THE ROLE OF ANTIOXIDANTS

Luminometry, western blot and qPCR assays were conducted to evaluate the role of antioxidants following 48 hours exposure of Caco-2 and HepG2 cells to *M. burkeana* crude aqueous extract. These assays were conducted to establish if *M. burkeana* promotes oxidative stress in both cell lines.

4.5.1 SOD2 protein expression

Evaluating SOD2 protein expression serves as a valuable marker for oxidative stress, as this enzyme is located in mitochondria and plays a crucial role in mitigating cellular damage by converting superoxide radicals into less harmful molecules. For Caco-2 cells (Figure 4,8A), the protein expression of SOD2 was relatively unaltered for the IC_{20} *M. burkeana* treatment (0.2449±0.004568 RBI), but was significantly upregulated by 1.7-fold to 0.4232±0.01651 RBI (p=0.0124) for the IC_{50} treatment compared to the control (0.2569±0.02600 RBI). The *M. burkeana* treatment upregulated SOD2 protein expression in HepG2 cells (Figure 4.8B) from 0.2218±0.03632 RBI in the control by 1.5-fold and 1.2-fold for the IC_{20} (0.3263±0.03464 RBI) and IC_{50} (0.2714±0.01443 RBI) treatments respectively.

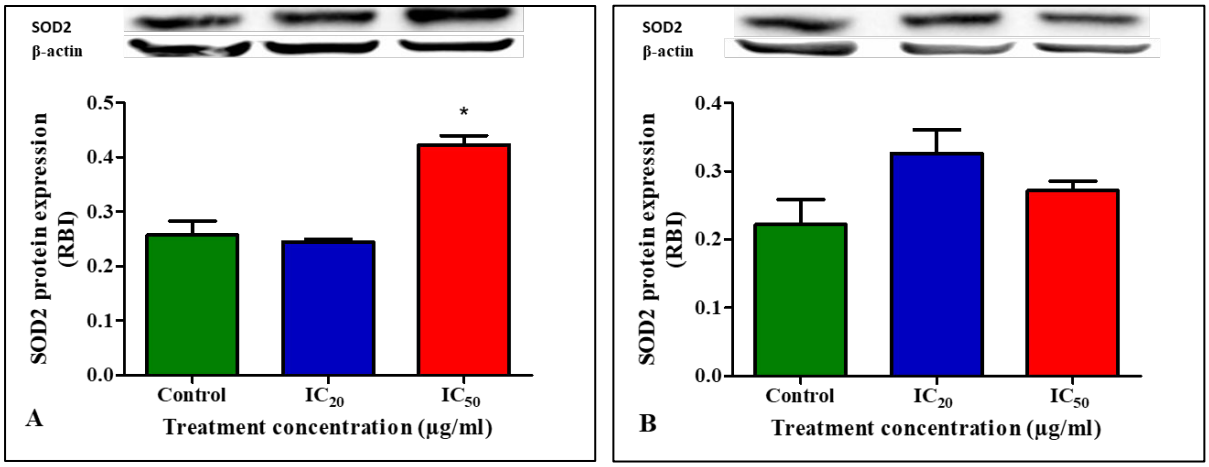

Figure 4.8: The effect of *M. burkeana* leaf extract on the level of SOD2 protein expression in Caco-2 and HepG2 cells. **(A)** SOD2 protein expression for Caco-2 cells increased significantly for the IC_{50} *M. burkeana* treatment. **(B)** A non-significant increase in SOD2 expression was observed in HepG2

cells for both *M. burkeana* treatments. [*$p \leq 0.05$ using the unpaired *t*-test with Welch's correction]

4.5.2 GSH and *Gpx-1* antioxidants

The GSH concentration was evaluated to assess the antioxidant response to the presence of oxidative stress in *M. burkeana* treated cells. In Caco-2 cells (Figure 4.9A), the *M. burkeana* treatment decreased GSH levels by 0.7-fold for the IC_{20} and by 0.6-fold for the IC_{50} treatment to 4030000±155200 RLU (p=0.0124) and 3266000±73470 RLU (p=0.0013) respectively, compared to the control (5433000±29130 RLU). The gene expression of *Gpx-1* (Figure 4.9C) was correspondingly decreased for Caco-2 cells after IC_{20} (0.8568±0.1059 fold-change) and IC_{50} (0.5001±0.07896 fold-change, p=0.0241) *M. burkeana* treatment, compared to the control (1.000±0.0000003191 fold-change). The GSH concentration in HepG2 cells (Figure 4.9B) treated with *M. burkeana* also decreased by 0.6-fold (3782000±162700 RLU) in IC_{20} and 0.5-fold for IC_{50}-treated cells (3587000±198800 RLU (p=0.0462) compared to the control (6723000±669900 RLU). Similarly, *M. burkeana* decreased *Gpx-1* gene expression (Figure 4.9D) significantly for the IC_{20} treatments to 0.9439±0.003777 fold-change (p=0.0045), but was increased for the IC_{50} treatment (1.124±0.1053 fold-change) compared to the control (1.000±0.0000003191 fold-change).

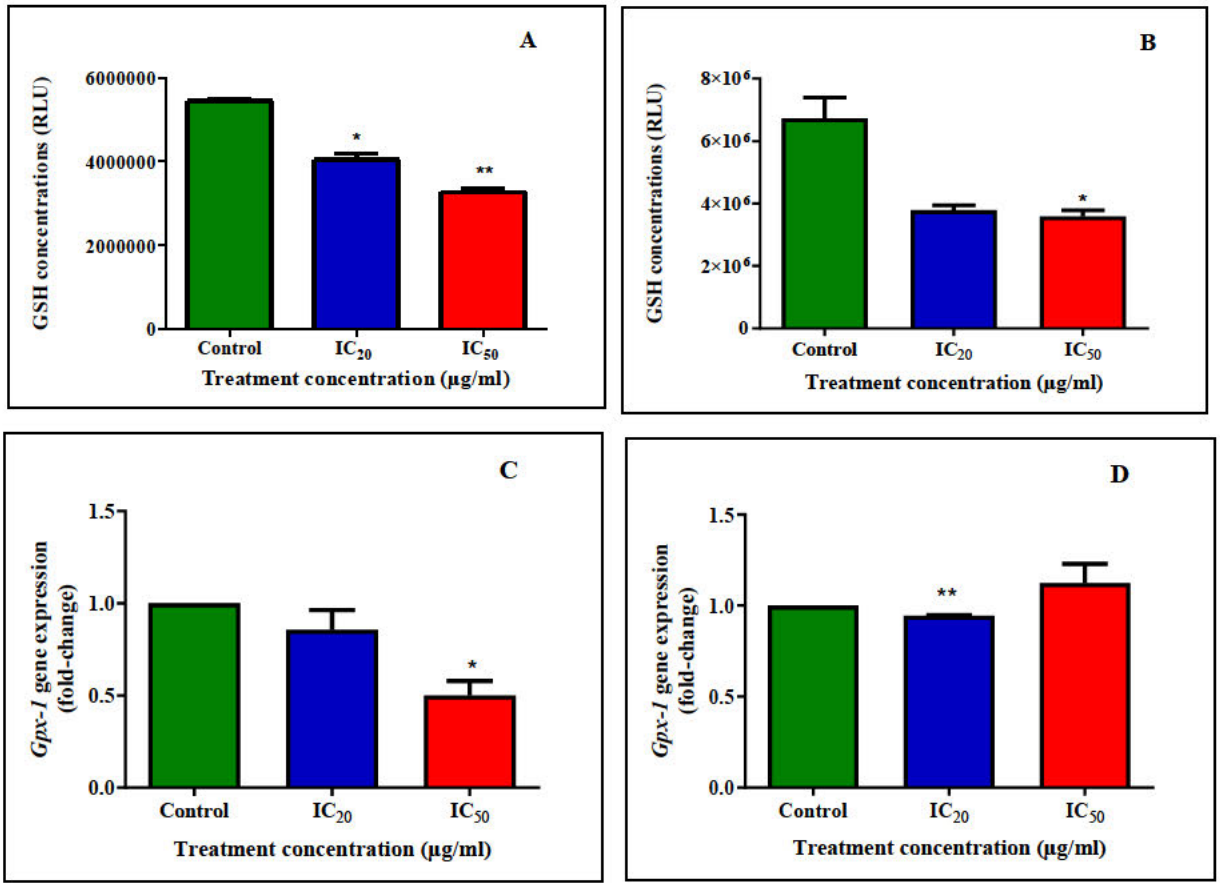

Figure 4.9: The antioxidant level of GSH and Gpx-1 as a result of *M. burkeana* leaf extract in Caco-2 and HepG2 cells. **(A)** The IC_{20} and IC_{50} *M. burkeana* treatments decreased GSH levels in Caco-2 cells. **(B)** A significant decrease in GSH concentration was observed in IC_{20} and IC_{50} *M. burkeana* treated HepG2 cells. **(C)** *M. burkeana* decreased *Gpx-1* gene expression in IC_{20}- and IC_{50}-treated Caco-2 cells. **(D)** There was slightly decreased *Gpx-1* gene expression in IC_{20}-treated HepG2 cells, while increased *Gpx-1* was observed in the IC_{50} *M. burkeana* treatment. [*, **$p \leq 0.05$ using the unpaired *t*-test with Welch's correction]

4.5.3 The NRF2 antioxidant response

The transcription factor NRF2 regulates the expression of antioxidant genes, its expression provides insights into the adaptive mechanisms cells employ to counteract oxidative damage. Protein expression of NRF2 for the Caco-2 cell line (Figure 4.10A) was decreased by *M. burkeana* for the IC_{20} treatment to 0.4385±0.01419 RBD (0.8-fold) and increased slightly by 1.1-fold for the IC_{50} treatment (0.5862±0.09981 RBI) compared to the control (0.5193±0.02536 RBI). For HepG2 cells (Figure 4.10B), *M. burkeana* decreased NRF2 protein expression from 0.5800±0.01942 RBI in the control to 0.5109±0.03760 RBI for the

IC_{20} treatment (0.9-fold) and a slight increase to 0.6271±0.01846 RBI (1.1-fold) for the IC_{50} treatment.

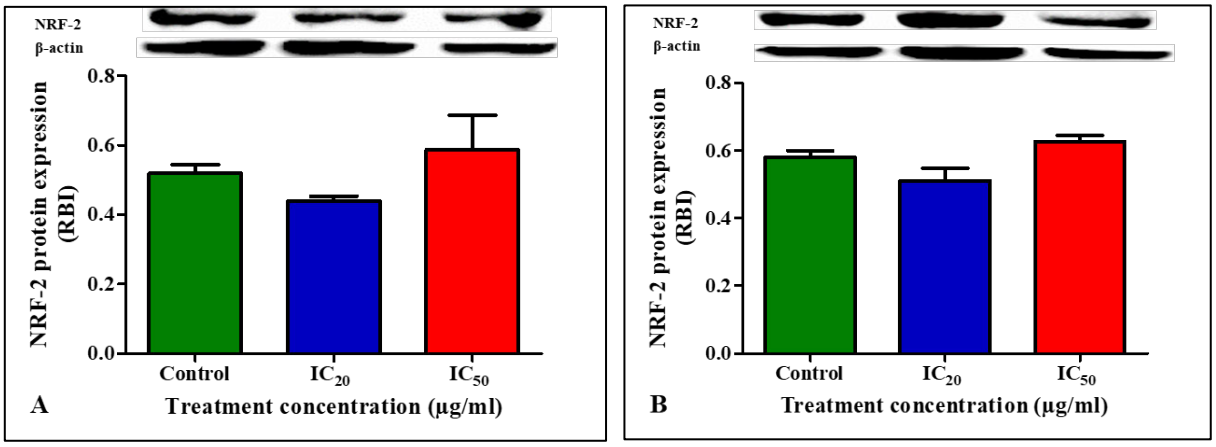

Figure 4.10: The impact of *M. burkeana* leaf extract on NRF2 protein expression in Caco-2 and HepG2 cells. **(A)** Protein expression of NRF-2 decreased for the IC_{20} *M. burkeana* treatment and increased for the IC_{50} treatment in Caco-2 cells. **(B)** In HepG2 cells, there was a non-significant decrease in NRF-2 protein expression for the IC_{20} treatment and a non-significant increase in the IC_{50} treatment with *M. burkeana*.

4.6 CELL DEATH

4.6.1 Initiation of apoptosis

4.6.1.1 Initiator caspases

Caspases are proteases made up of cysteine-aspartate residues that play an important role in apoptosis and inflammation. In this study, initiation of apoptosis by the extrinsic (caspase 8) and intrinsic (caspase 9) pathways were evaluated. The concentration of caspase 8 in Caco-2 cells (Figure 4.11A) was increased significantly by 1.9-fold and 2-fold for IC_{20} (831900±63050 RLU, p=0.0292) and IC_{50} (866600±59140 RLU, p=0.0224) *M. burkeana* treatments respectively, in relation to the control (437100±27950 RLU). The *M. burkeana* treatment decreased caspase 8 concentration in HepG2 (Figure 4.11B) cells for IC_{20} (1855000±99390 RLU, 0.7-fold)) and IC_{50} (1430000±141400 RLU, 0.5-fold) in relation to the control (2656000±341900 RLU). The concentration of caspase 9 in Caco-2 cells (Figure 4.11C) was increased 1.1-fold by *M. burkeana* IC_{20} (2223000±128000 RLU) treatment, and decreased 0.6-fold for IC_{50} (1286000±29050 RLU), in relation to the control

(2019000±393700 RLU). The caspase 9 concentration in HepG2 cells (Figure 4.11D) was slightly decreased by *M. burkeana* for IC_{20} (1604000±69960 RLU) and decreased by 0.4-fold IC_{50} (719900±56010 RLU; p=0.0241) treated cells, in relation to the control (1693000±143200 RLU).

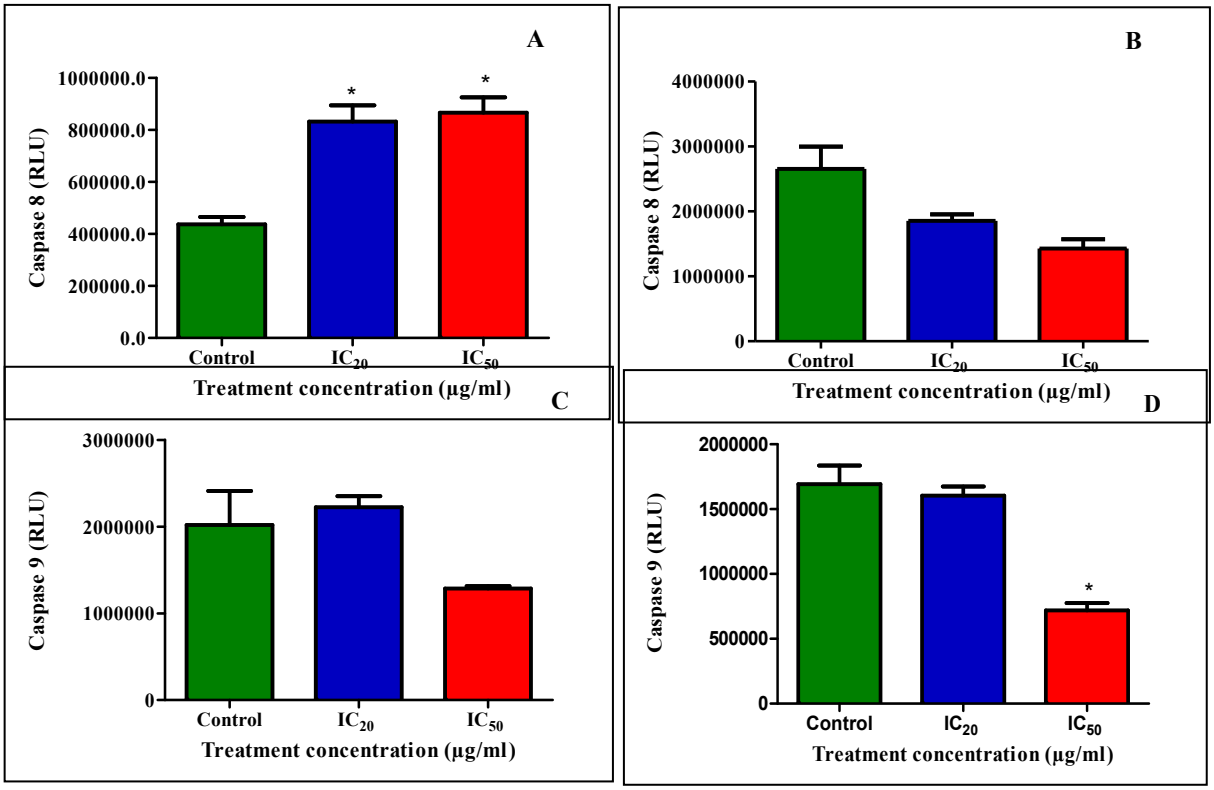

Figure 4.11: The effect of *M. burkeana* leaf extract on caspase activity in Caco-2 and HepG2 cells. **(A)** A significant increase in caspase 8 concentration in Caco-2 cells treated with IC_{20} and IC_{50} concentrations of *M. burkeana*. **(B)** Both treatment concentrations of *M. burkeana* decreased caspase 8 expression in HepG2 cells. **(C)** An increase in caspase 9 activity with IC_{20} and a decrease in IC_{50} *M. burkeana* treated Caco-2 cells. **(D)** *M. burkeana* decreased caspase 9 activity in IC_{20}- and IC_{50}-treated HepG2 cells. [*$p \leq 0.05$ using the unpaired *t*-test with Welch's correction]

4.6.1.2 Proapoptotic proteins: p-53 and p-p53

Calculating the protein expression of proapoptotic p53 and its phosphorylated form, p-p53, is essential for evaluating the initiation of apoptosis. Figure 4.12A shows that the p-p53/p53 ratio was decreased for Caco-2 *M. burkeana* treated cells; a 0.7-fold decrease to 0.6064±0.05473 RBI and a 0.5-fold reduction to 0.4344±0.06981 RBI (p=0.0439) was observed for the IC_{20} and IC_{50} treated cells respectively, compared to the control (0.8683±0.1089 RBI). In HepG2 cells, *M. burkeana* decreased the protein expression ratio slightly by 0.8-fold in IC_{20}-treated cells (0.4472±0.03140 RBI) and increased significantly by 5.4-fold in IC_{50}-treated cells (3.101±0.2352 RBI; p=0.0087) compared to the control (0.5708±0.03268 RBI) (Figure 4.12B).

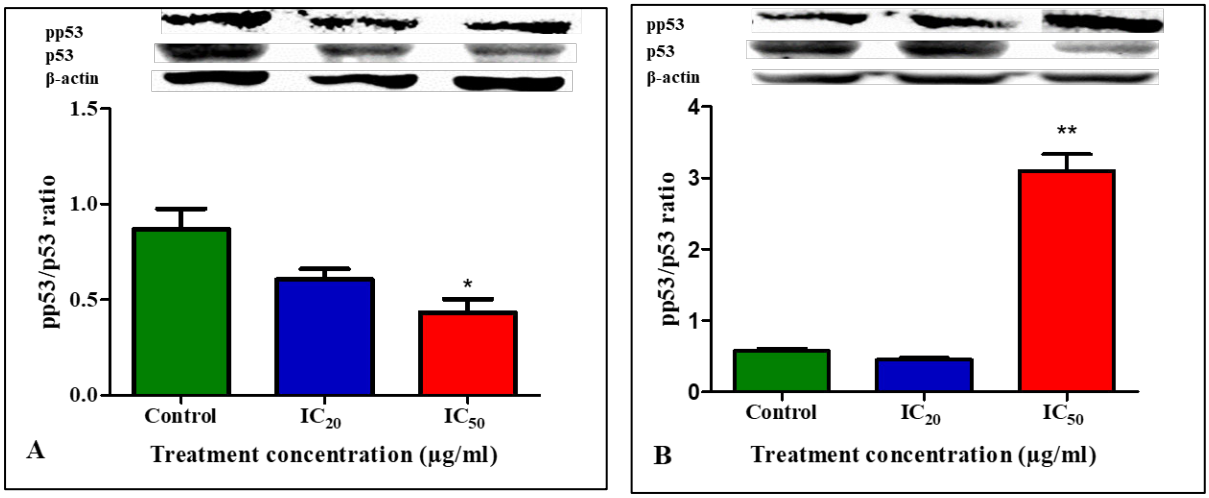

Figure 4.12: The effect of *M. burkeana* leaf extract on the pp53/p53 ratio in Caco-2 and HepG2 cells. **(A)** Decreased protein expression is seen in Caco-2 cells for both *M. burkeana* treatment concentrations. **(B)** In HepG2 IC_{50}-treated cells, a significant increase in protein expression was observed after *M. burkeana* treatment. [*, **p≤0.05 using the unpaired t-test with Welch's correction]

4.6.1.3 Proapoptotic protein: BAX expression

The pro-apoptotic protein BAX promotes cell death by permeabilising the outer mitochondrial membrane. It is a key indicator of the initiation of apoptosis. Protein expression of BAX was downregulated by *M. burkeana* for Caco-2 IC_{20}-treated cells (0.7 fold to 0.4151±0.03702 RBI, p=0.0355) as well as IC_{50}-treated cells (0.6-fold to 0.3730±0.01023 RBI, p=0.0189) compared to the control (0.5836±0.02757 RBI) (Figure 4.13A). A 0.8-fold decrease in BAX protein expression was observed in HepG2 IC_{20}-treated cells (0.7134±0.01031 RBI) but remained

relatively unaltered for the IC_{50} *M. burkeana* treatment concentration (0.9302±0.006356 RBI) compared to the control (0.9154±0.07144 RBI) (Figure 4.13B).

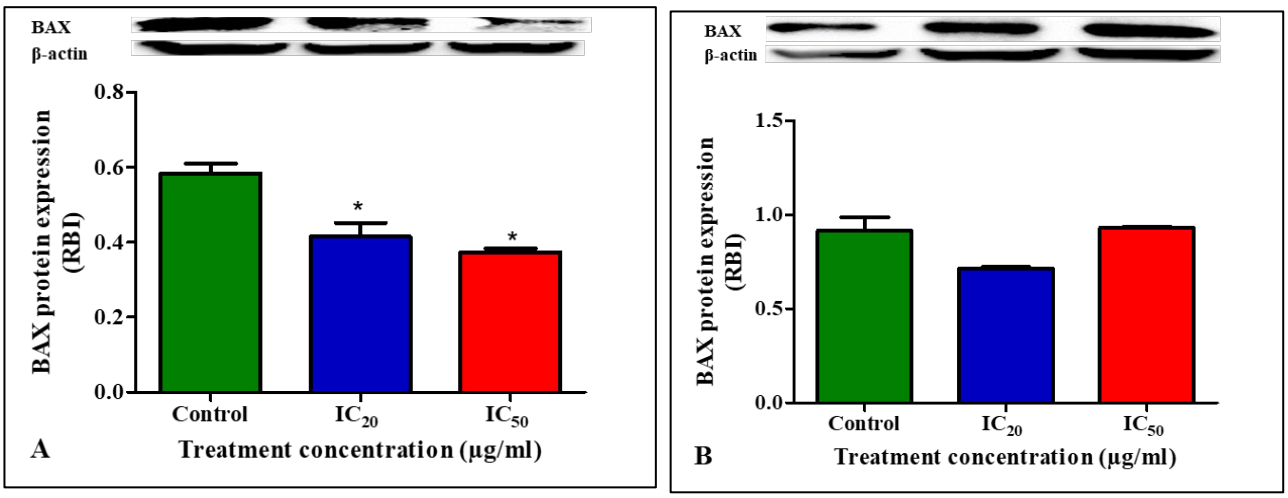

Figure 4.13: The effect of *M. burkeana* leaf extract on BAX protein expression in Caco-2 and HepG2 cells. **(A)** A significant decrease in Caco-2 cells treated with IC_{20} and IC_{50} concentrations of *M. burkeana*. **(B)** A non-significant decrease in BAX protein expression induced by *M. burkeana* IC_{20} treatment concentration in HepG2 cells. [*$p \leq 0.05$ using the unpaired *t*-test with Welch's correction]

4.6.1.4 Anti-apoptotic protein BCL-2

The expression of the anti-apoptotic protein BCL-2 is informative about regulating apoptosis initiation. Elevated BCL-2 levels suggest a potential suppression of apoptosis, as BCL-2 prevents the release of proapoptotic factors from the mitochondria. Protein expression of anti-apoptotic protein BCL-2 after *M. burkeana* treatment was evaluated for Caco-2 and HepG2 cell lines using western blotting. In Caco-2 cells (Figure 4.14A), BCL-2 expression remained unchanged for IC_{20} *M. burkeana* treated cells (1.481±0.1051 RBI) and decreased significantly by 0.6-fold for IC_{50}-treated cells (0.8909±0.06506 RBI; p=0.0083) compared to the control (1.487±0.06996 RBI). In HepG2 cells (Figure 4.14B), BCL-2 expression remained unchanged for the IC_{20}-treated cells (0.8556±0.01821 RBI) and increased significantly by 2.4-fold for IC_{50} *M. burkeana* treated cells (1.922±0.07701 RBI; p=0.0050) compared to the control

(0.8183±0.01248 RBI).

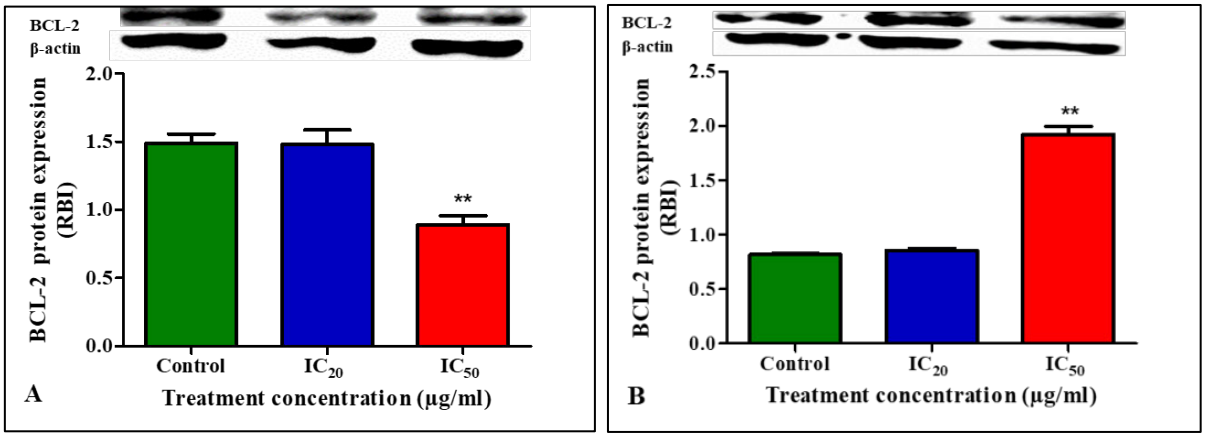

Figure 4.14: The effect of *M. burkeana* leaf extract on BCL-2 protein expression in Caco-2 and HepG2 cells. **(A)** A decrease in BCL-2 protein expression for the Caco-2 cells treated with *M. burkeana* IC_{50} concentration. **(B)** *M. burkeana* increased BCL-2 protein expression in IC_{50}-treated HepG2 cells. [**$p \leq 0.05$ using the unpaired *t*-test with Welch's correction]

4.6.2 Execution of apoptosis

4.6.2.1 Caspase 3/7 activity

Caspase 3/7 are effector caspases that play a central role in the dismantling of cellular components during apoptosis. The detection of cleaved caspase 3, a specific marker for caspase activation, signifies the initiation of the enzymatic cascade responsible for cell death. The *M. burkeana* treatment increased caspase 3/7 activity in Caco-2 cells (Figure 4.15A) by 2.0-fold and 1.9-fold for IC_{20} (1492000±15470 RLU; p=0.0030) and IC_{50} (1442000±25500 RLU; p=0.0006) respectively, in relation to the control (753100±37120 RLU). Caspase 3/7 concentration was also increased significantly by *M. burkeana* in HepG2 (Figure 4.15B) cells by 5.4-fold and 3.7-fold for IC_{20} (1282000±47150 RLU; p=0.0003) and IC_{50} (884300±111100 RLU; p=0.0299) treated cells respectively, in relation to the control (239700±25720 RLU). Protein expression for cleaved caspase 3 in Caco-2 cells remained relatively unchanged for the IC_{20} *M. burkeana* treatment concentration (0.1128±0.005978 RBI) and increased by 1.1-fold in IC_{50}-treated cells (0.1336±0.01614 RBI) compared to the control (0.1206±0.006100 RBI). A significant increase in cleaved caspase 3 protein expression was observed in *M. burkeana* treated HepG2 cells by 1.5-fold in IC_{20} (0.1334±0.04684 RBI) and 1.4-fold in the IC_{50} (0.1272±0.006780 RBI; p=0.0337) treated cells, compared to the control

(0.09077±0.007026 RBI).

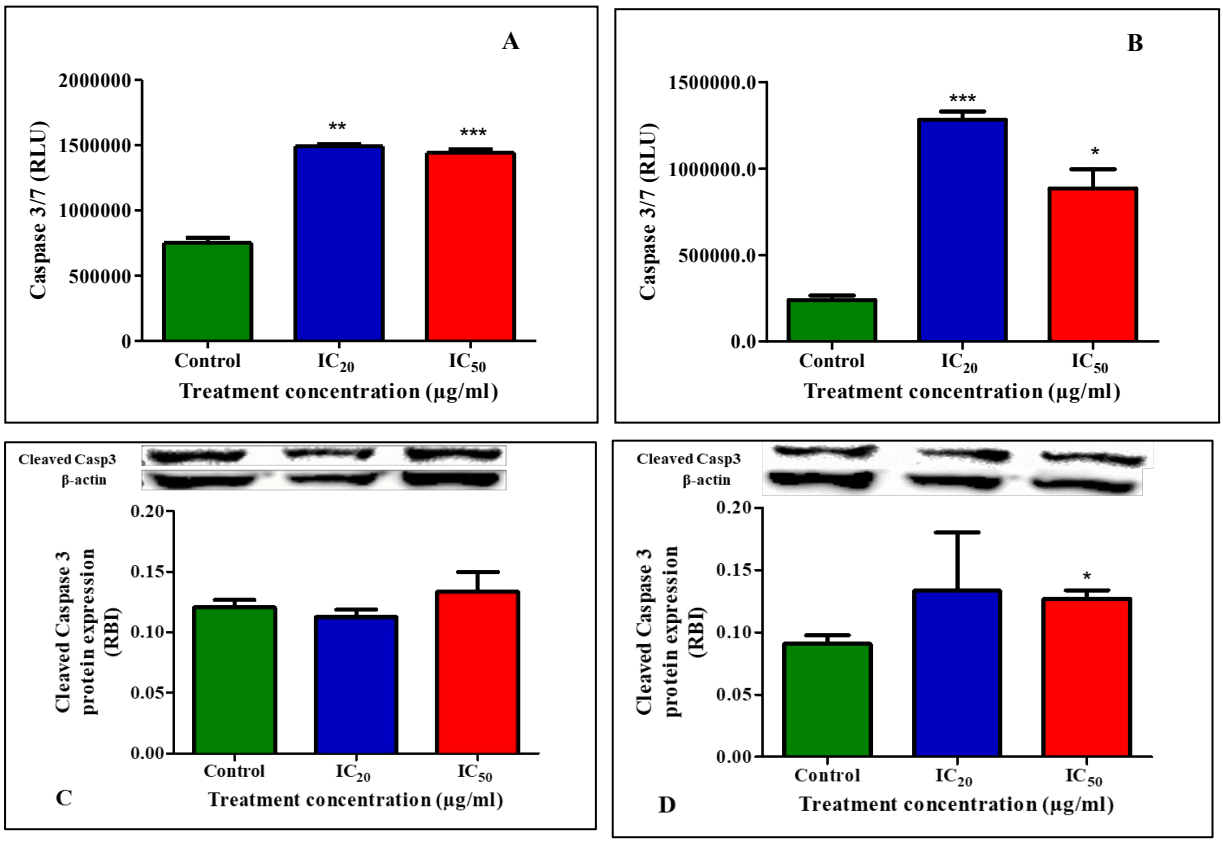

Figure 4.15: The effect of *M. burkeana* leaf extract on caspase 3 activity in Caco-2 and HepG2 cells. **(A)** Caspase 3/7 activity increased in Caco-2 cells treated with both concentrations of *M. burkeana*. **(B)** *M. burkeana* increased caspase 3/7 activity in HepG2 cells in IC_{20} and IC_{50} treated cells. **(C)** In Caco-2 cells, *M. burkeana* induced an increase in cleaved caspase 3 expression in IC_{50} treated cells. **(D)** An increase in cleaved caspase 3 protein expression was observed in the IC_{20} and IC_{50} *M. burkeana* treated HepG2 cells. [*, **, ***$p \leq 0.05$ using the unpaired *t*-test with Welch's correction]

4.6.2.2 Externalisation of phosphatidylserine (PS)

The Annexin V assay distinguishes between apoptotic and necrotic cells. Annexin V luciferase fusion proteins bind to PS during apoptosis, which is detected using a luminescence protocol. A fluorescence protocol detected necrosis when DNA-binding dye enters damaged cells. There was an increase in the number of apoptotic Caco-2 cells (Figure 4.16A) for IC_{20} (4.6-fold, 1538000±315300 RLU) and IC_{50} (4.0-fold, 1335000±78470 RLU, p=0.0065) *M. burkeana* treated cells respectively, in relation to the control (332500±20410 RLU). The number of apoptotic HepG2 cells treated with *M. burkeana* (Figure 4.16B) was increased by

9.3-fold and significantly by 9.8-fold for IC_{20} (1125000±537800 RLU) and IC_{50} (1180000±207500 RLU; p=0.0363) respectively, in relation to the control (120600±5576 RLU).

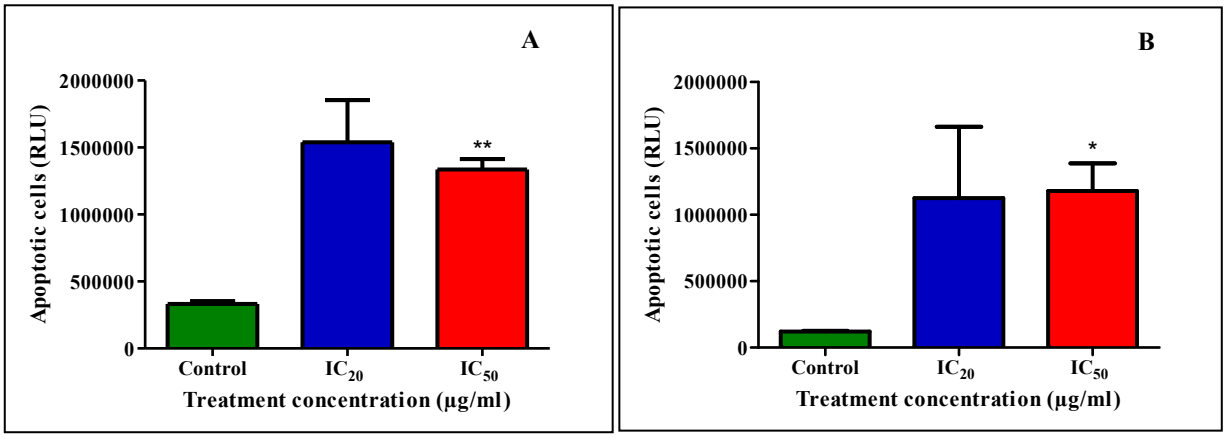

Figure 4.16: The effect of *M. burkeana* leaf extract on apoptotic cells in Caco-2 and HepG2 cells. **(A)** An increase in apoptotic Caco-2 cells treated with IC_{20} and IC_{50} concentrations of *M. burkeana*. **(B)** *M. burkeana* induced an increase in apoptotic HepG2 cells for both treatment concentrations. [*, **p≤0.05 using the unpaired t-test with Welch's correction]

4.6.3 Necrosis and necroptosis

4.6.3.1 Marker of necrosis

The Annexin-V assay was conducted to identify necrotic cells from apoptotic cells when cell membrane integrity is compromised. DNA binding dye thus enters and produces a fluorescent signal. The number of necrotic Caco-2 cells (Figure 4.17A) was increased by 2.6-fold and 2-fold for IC_{20} (264900±67580 RLU) and IC_{50} (205700±27950 RLU) *M. burkeana* treated cells, respectively, in relation to the control (102700±7738 RLU). The number of necrotic HepG2 cells (Figure 4.17B) was increased non-significantly by *M. burkeana*; 1.9-fold for IC_{20} (90900±17080 RLU) and 1.7-fold for IC_{50} (78580±10390 RLU) in relation to the control

(46890±1933 RLU).

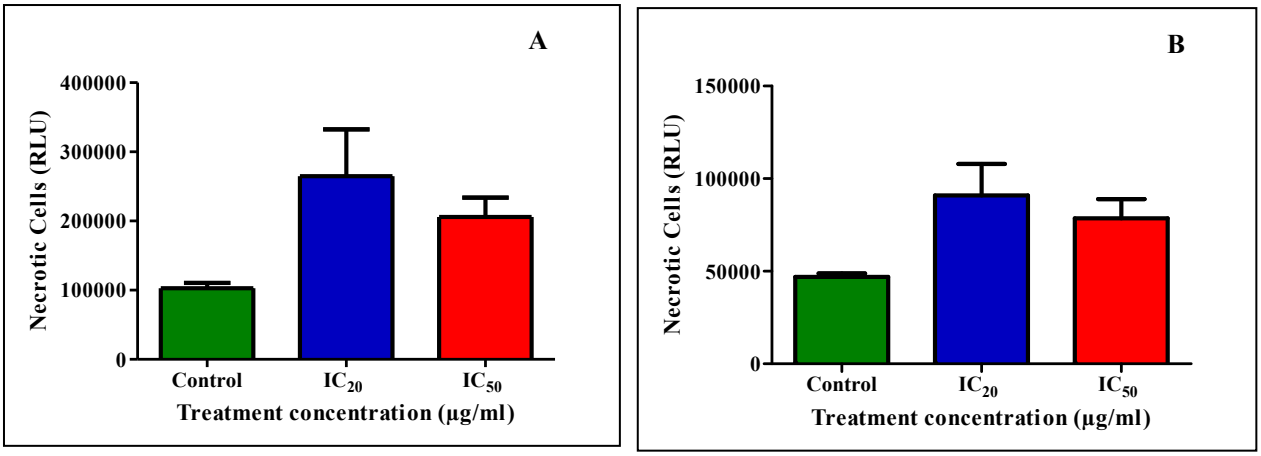

Figure 4.17: The effect of *M. burkeana* leaf extract on necrotic cells in Caco-2 and HepG2 cells. A non-significant increase in necrotic Caco-2 **(A)** and HepG2 **(B)** cells treated with IC_{20} and IC_{50} concentrations of *M. burkeana*.

4.6.3.2 Activation of Complex 1

Monitoring *TNFα* gene expression provides a molecular indicator of necrotic activity, aiding in the assessment of cell damage and inflammatory responses. *M. burkeana* decreased gene expression of *TNFα* for Caco-2 IC_{20}-treated cells (0.7318±0.1884 fold-change), and there was a significant decrease in gene expression for IC_{50}-treated cells (0.4777±0.1101 fold-change, p=0.0417) compared to the control (Figure 4.18A). Gene expression of *TNFα* was decreased by *M. burkeana* in HepG2 cells for IC_{20} treated cells (0.6659±0.07864 fold-change) and IC_{50} treated cells (0.4075±0.08211 fold-change, p=0.0187), compared to the control (Figure 4.18B).

Cellular death pathways, including necrosis, are regulated by RIPK1. The mRNA expression of *RIPK1* in Caco-2 cells decreased significantly for *M. burkeana* IC_{20}-treated cells (0.1663±0.07927 fold-change, p=0.0089) and IC_{50}-treated cells (0.4106±0.1074 fold-change, p=0.0317) compared to the control (Figure 4.18C). In HepG2 cells, *M. burkeana* upregulated gene expression of *RIPK1* for IC_{20}-treated cells (4.509±1.404 fold-change) and IC_{50}-treated cells (1.511±0.07539 fold-change, p=0.0211) compared to the control (Figure 4.18D).

Monitoring cIAP2 protein expression helps evaluate the anti-apoptotic potential within cells and provides insights into the regulation of necrotic events. *M. burkeana* upregulated the protein expression of cIAP2 in Caco-2 cells from 0.1861±0.006152 RLU in control (Figure 4.18E) to 0.3089±0.01384 RBI (1.7-fold, p=0.0149) for IC_{20}-treated cells and 0.3913±0.01862 RBI (2.1-fold, p=0.0090) for IC_{50}-treated cells. In HepG2 cells, there was a significant decrease in cIAP2 protein expression by 0.4-fold in IC_{20}-treated cells (0.1617±0.02948 RBI) and a reduction by 0.2-fold in IC_{50} *M. burkeana* treated cells (0.08194±0.001357 RBI, p=0.0259), compared to the control (0.4502±0.06046 RBI) (Figure 4.18F).

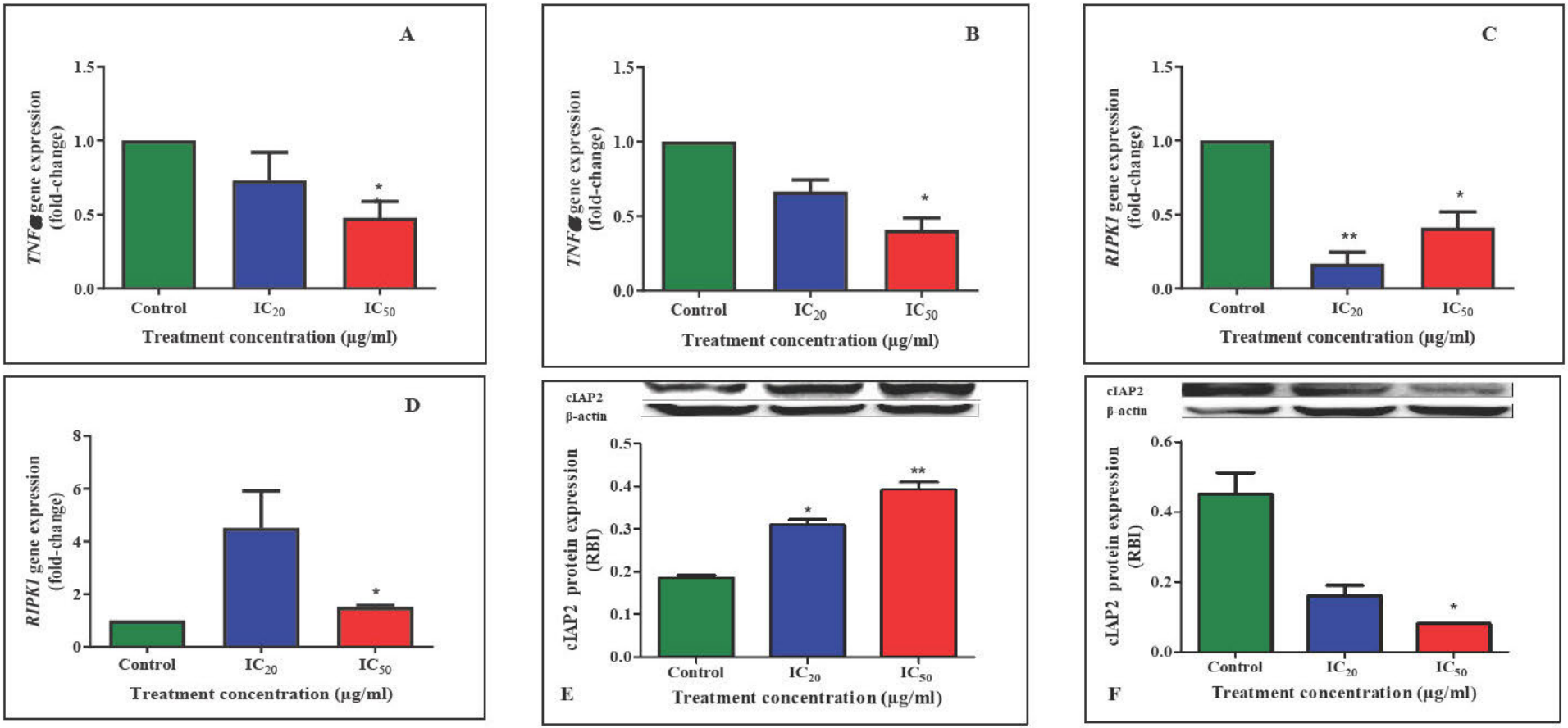

Figure 4.18: (A) *M. burkeana* decreased *TNFα* gene expression for Caco-2 IC_{50}-treated cells. **(B)** Gene expression of *TNFα* was decreased significantly by *M. burkeana* in IC_{50}-treated HepG2 cells. **(C)** Treatment with *M. burkeana* IC_{20} and IC_{50} concentrations induced a significant decrease *RIPK1* gene expression for Caco-2 cells. **(D)** A significant decrease in *RIPK1* gene expression for HepG2 cells treated with *M. burkeana* IC_{50} concentration. **(E)** A significant increase in cIAP2 protein expression for Caco-2 cells treated with *M. burkeana* IC_{20} and IC_{50} concentrations. **(F)** Decreased cIAP2 protein expression by *M. burkeana* was observed in HepG2 IC_{50}-treated cells. [*, **$p \leq 0.05$ using the unpaired *t*-test with Welch's correction]

4.6.3.3 Activation of complex 2a and b

The activation of RIPK3 is a key step in promoting necroptosis, and its kinase activity is essential for executing the cell death process. The mRNA expression of *RIPK3* in Caco-2 cells was decreased significantly by *M. burkeana in* IC_{20}-treated cells (0.4839±0.1042 fold-change, p=0.0384) and IC_{50}-treated cells (0.5806±0.009291 fold-change, p=0.0005), compared to the control (Figure 4.19A). In HepG2 cells, *M. burkeana* induced a significant increase in gene expression for IC_{20}-treated cells (1.832±0.1421 fold-change, p =0.0280) and no substantial change in IC_{50}-treated cells (0.9205±0.4162 fold-change), compared to the control (Figure 4.19B).

The *M. burkeana* treatment decreased *MLKL* gene expression in Caco-2 cells significantly for both IC_{20} and IC_{50} treatments compared to the control (0.2417±0.01302 fold-change, p=0.0003 and 0.1607±0.01932 fold-change, p=0.0005 respectively) (Figure 4.19C). In HepG2 cells, *M. burkeana* induced an increase in gene expression of *MLKL* for IC_{20}-treated cells (1.184±0.09180 fold-change) and IC_{50}-treated cells (1.860±0.02233 fold-change, p=0.0007), compared to the control (1.000±0.0000003191 fold-change) (Figure 4.19D).

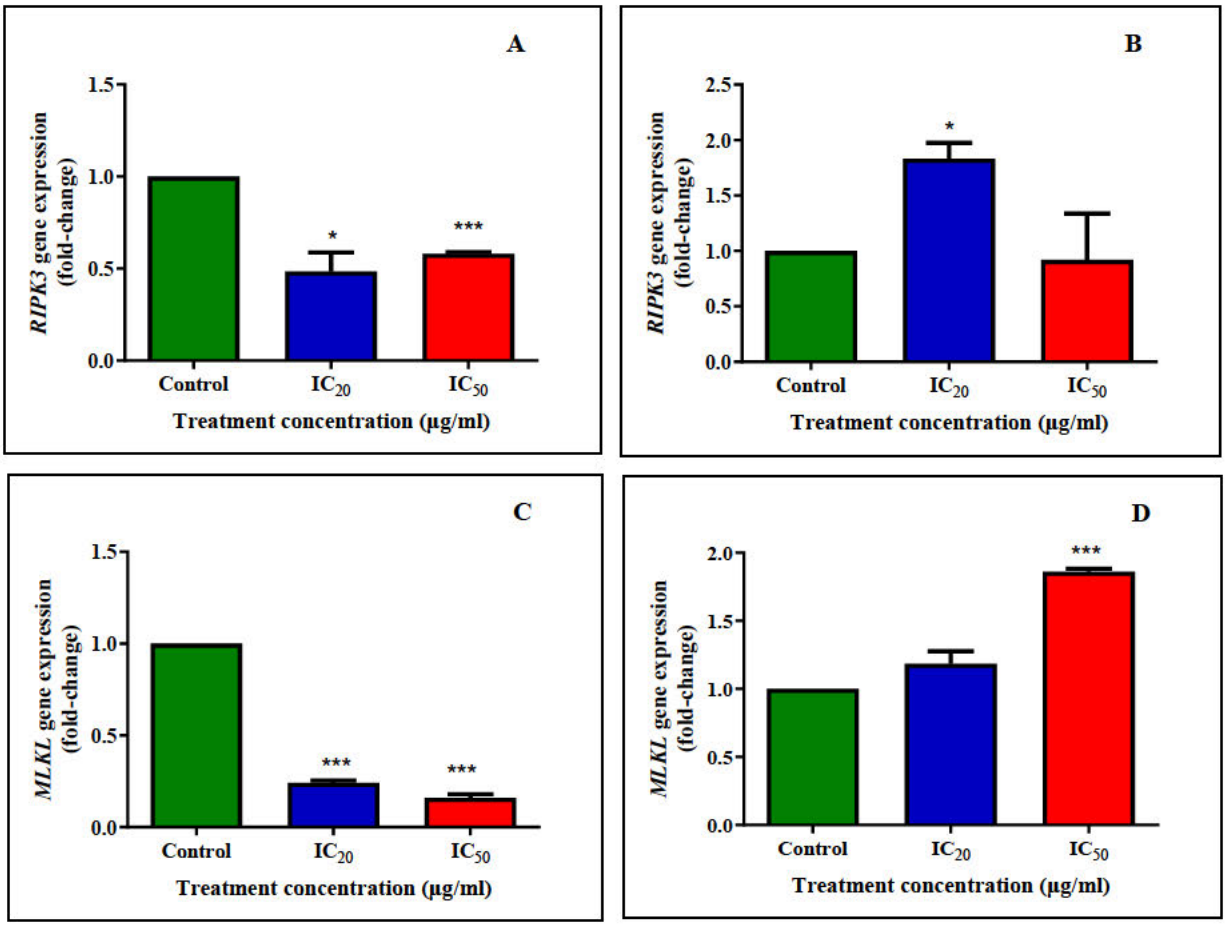

Figure 4.19: The effect of *M. burkeana* leaf extract on *RIP3* and *MLKL* gene expression in Caco-2 and HepG2 cells. **(A)** The mRNA expression of *RIPK3* in Caco-2 cells decreased for both IC_{20} and IC_{50} *M. burkeana* treatment concentrations. (**B)** Gene expression of *RIPK3* increased in HepG2 cells treated with the IC_{20} concentration of *M. burkeana*. **(C)** *M. burkeana* decreased the mRNA expression of *MLKL* in Caco-2 cells for both IC_{20} and IC_{50} treatment concentrations. **(D)** The *MLKL* gene expression increased in the *M. burkeana* IC_{20} treatment concentration for HepG2 cells. [*, ***$p \leq 0.05$ using the unpaired *t*-test with Welch's correction]

4.6.3.4 NFκB

Necrosis is a type of cell death that occurs as a result of cellular injury or inflammation, hence NFκB expression was assessed using qPCR and western blotting to understand its role in necroptosis. It is a key regulator of inflammation and controls gene expression involved in the inflammatory response, cell survival, the immune response and apoptosis (Verzella *et al.*, 2020). Gene expression of *NF-κB* remained relatively unaffected for Caco-2 IC_{20}-treated cells (0.9736±0.1583 fold-change), but decreased for *M. burkeana* IC_{50}-treated cells (0.7666±0.05061 fold-change, p=0.0440) (Figure 4.20A). *M. burkeana* increased *NF-κB* gene

expression in IC_{20}-treated HepG2 cells (1.115±0.1355 fold-change), and no significant change was observed in IC_{50}-treated cells compared to the control (Figure 4.20B). Protein expression of NF-κB was decreased by *M. burkeana* to 0.7-fold for IC_{20}-treated (0.6342±0.05401 RBI) and 0.6-fold in IC_{50}-treated cells (0.4699±0.03236 RBI, p=0.0099) compared to the control (0.6947±0.02052 RBI) (Figure 4.20C). Similarly, in HepG2 cells *M. burkeana* decreased protein expression of NF-κB for both IC_{20} (0.9887±0.006408 RBI) and IC_{50}-treated cells (0.7670±0.03927 RBI, p=0.0085), compared to the untreated control (1.239±0.06548 RBI) (Figure 4.20D).

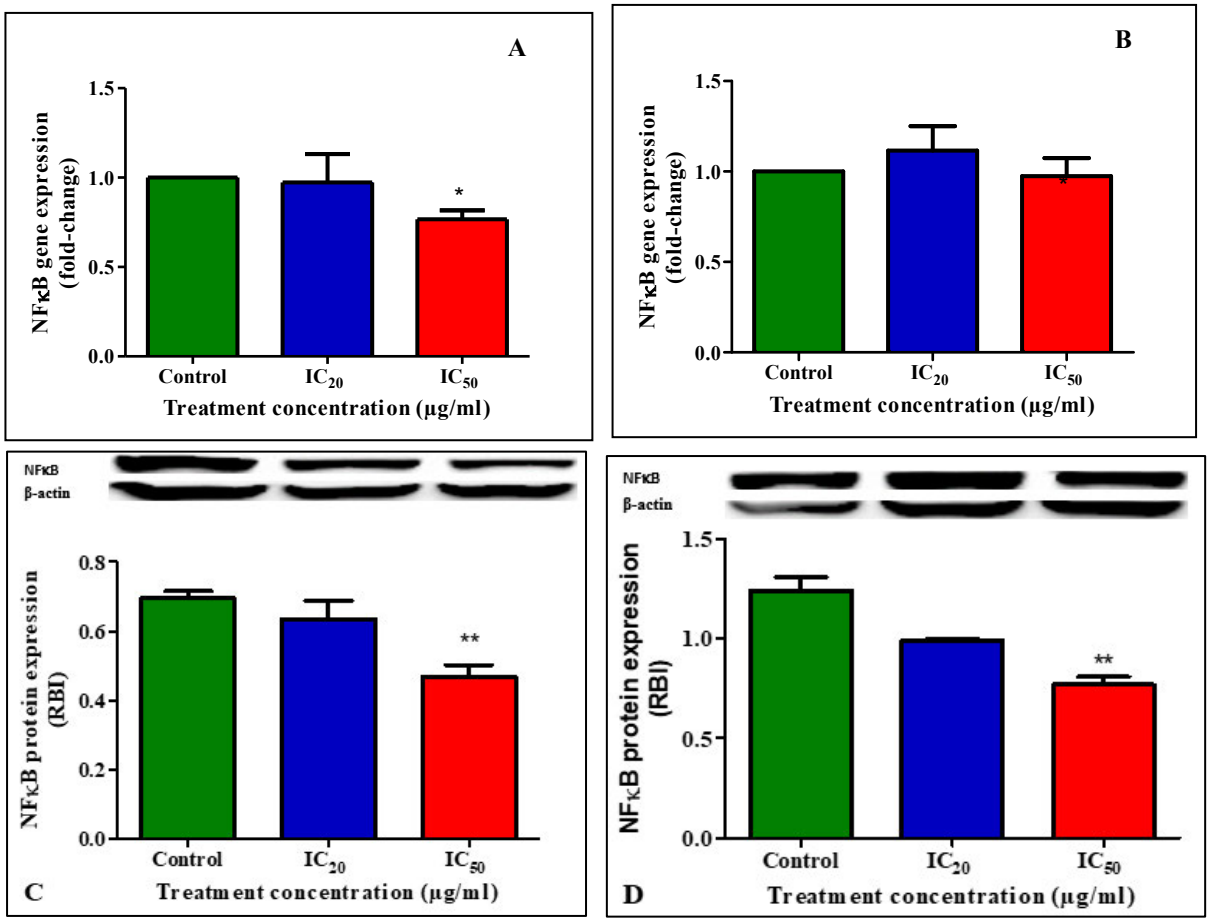

Figure 4.20: The effect of *M. burkeana* leaf extract on *NF-κB* protein expression in Caco-2 and HepG2 cells. **(A)** *M. burkeana* decreased the gene expression of *NF-κB* in IC_{50}-treated Caco-2 cells. **(B)** A slight increase in gene expression of *NF-κB* was induced by *M. burkeana* in IC_{20}-treated HepG2 cells. **(C) & (D)** Decreased protein expression of NF-κB was observed in both cell lines after treatment with *M. burkeana.* [*, **p≤0.05 using the unpaired t-test with Welch's correction]

CHAPTER 5: DISCUSSION

Colorectal and liver cancer rank second and third, respectively, for cancer-related deaths (Sung *et al.*, 2021). In addition, these cancers have low 5-year survival rates (Nikbakht *et al.*, 2020, Calderon-Martinez *et al.*, 2023). An individual's five-year survival rate after diagnosis is higher the earlier colorectal cancer (CRC) is detected. According to the National Cancer Institute's Surveillance, Epidemiology and End Results (SEER) Program database, colorectal cancer's five-year relative survival rate from 2013-2019 was 65% (National Cancer Institute, 2023). The 5-year close survival rate for early diagnosis of HCC is linked to over 70%, but advanced stages may have fewer than 20% survival rates (Calderon-Martinez *et al.*, 2023). Clinically, the main treatment strategies used for cancer treatment are surgery, radiotherapy and chemotherapy (Debela *et al.*, 2021). However, chemotherapy has several shortcomings, such as toxicity, poor response rates, innate and acquired resistance, and decreased tumour-specific selectivity (Mustapha *et al.*, 2022). Consequently, this sparked interest in searching for novel approaches to replace or supplement conventional CRC and HCC chemotherapy. *Monsonia burkeana* is a highly beneficial medicinal plant found in South Africa. Due to its various health benefits, communities widely consume decoctions of this "special tea" (Mamphiswana *et al.*, 2010a). Research shows that *M. burkeana* is abundant in phenolic compounds; the highest phenolic content were found in *M. burkeana* leaves and fruits, followed by the stem and roots (Nnzeru *et al.*, 2016). Phenolics have potential therapeutic value due to antioxidant, anti-inflammatory and anticancer properties, but also show significant promise as cytotoxic anti-cancer drugs that target angiogenesis, growth and differentiation, and metastasis, while also encouraging apoptosis and lowering proliferation (Abotaleb *et al.*, 2020). This study investigated the antioxidant and antiproliferative mechanisms *of M. burkeana* crude aqueous leaf extract in Caco-2 and HepG2 cells.

Cytochromes P450 (CYPs) are a family of inducible haem enzymes that oxidise endogenous or exogenous substances such as drugs, chemicals, pollutants, steroids, bile and fatty acids, vitamin D, other natural products, and xenobiotics, either rendering the product water soluble for excretion or bioactivation it to increase cytotoxicity (Groves, 2015). The CYP3A4 isoform is mainly expressed in the liver and gastrointestinal tract and accounts for approximately 30%

of CYP content in the liver; it is also the most abundant CYP in the small intestine (Zhao *et al.*, 2021). This isoform metabolises compounds varying in structure and size (Sevrioukova and Poulos, 2013). In this study, IC_{20} and IC_{50} treatment with *M. burkeana* induced CYP3A4 activity in Caco-2 and HepG2 cells (Figure 4.1). Research has shown that dietary phenolics interact with CYP3A4 to alter expression and activity (Basheer and Kerem, 2015). Induction of CYP3A4 may alter the bioavailability of active compounds and render co-administered drugs inactive; in the case of plant polyphenols, the introduction of a hydroxyl group primes the intermediate for phase II enzymes that increase water solubility and excretion. On the other hand, increased toxicity by this interaction is also an undesirable effect. Various classes of polyphenols present conflicting reports on the influence on CYP activity. For example, consumption of St. John's wort extract-induced CYP activity is associated with high flavanone levels, specifically quercetin, increasing CYP3A4 mRNA expression (Basheer and Kerem, 2015). Isoflavones from soy inhibit CYP3A4, while Genstein facilitated CYP3A4 metabolism. The data suggests that the metabolism of the *M. burkeana* phytochemicals in this study enhanced the cytotoxicity as observed in the cell viability assay (Figure 4.2).

Cell viability is an essential marker in assessing the overall health of cells and the efficacy of an administered treatment. In this study, the MTT assay was conducted to measure the metabolic activity of cells that were exposed to *M. burkeana* crude aqueous extract. A dose-dependent decrease in cell viability was observed for Caco-2, HepG2 and Hek293 cell lines (Figure 4.2). This indicates the cytotoxicity of the *M. burkeana* crude aqueous leaf extract on all three cell lines. At both the IC_{20} and IC_{50} concentrations of Caco-2 and HepG2 cells, the Hek293 cell viability was not adversely affected, confirming the selective toxicity of *M. burkeana* to Caco-2 and HepG2 cancer cells. Research shows that phenolic compounds known to be present in *M. burkeana* may be responsible for inhibiting cell proliferation and reducing cell viability in primary rat hepatocytes, human liver and colon cancer cells (Huang *et al.*, 2009, Samodien *et al.*, 2020). Samodien *et al*. (2020) reported IC_{50} values of 0.14±0.01 mg/ml for HepG2 cells treated with green rooibos and 0.45±0.01 mg/ml for the green tea extract (Samodien *et al.*, 2020). Therefore, this study's IC_{50} of 293.8 µg/ml and 335.4 µg/ml for Caco-2 and HepG2 cells suggests that the *M. burkeana* plant extract inhibits cell proliferation at comparable levels. Furthermore, the decreased cell viability in this study

corresponds to cytotoxicity induced by the water extract of 'special tea' in Vero cells and the methanolic *M. burkeana* extract in HeLa cells (Mathivha *et al.*, 2019, Malongane *et al.*, 2022).

Cells that are viable and have active metabolism convert the MTT salt into a purple formazan product with an absorbance maximum near 570nm. Dead cells cannot convert the MTT salt to formazan products; therefore, the colour change observed indicates only viable cells (Riss *et al.*, 2016). The reduction of MTT salt by succinate dehydrogenase (SDH) was decreased for both cell lines. Succinate dehydrogenase (SDH) is an enzyme complex that is part of the citric acid cycle and the electron transport chain (Moreno *et al.*, 2020). In the citric acid cycle, the SDH complex catalyses the oxidation of succinate to fumarate and transfers electrons into complex III of the respiratory chain so that oxygen can be reduced to form water. This causes an electrochemical gradient to develop across the inner membrane of the mitochondria, enabling the generation of ATP. In this study, the depletion of ATP for both Caco-2 and HepG2 cell lines (Figure 4.4) indicates cell death observed, as seen in the MTT assay results (Figure 4.2). These findings also imply that mitochondrial toxicity was induced by *M. burkeana* (Figure 4.4). Indeed, ΔΨm increased for both cell lines (Figure 4.4) as the *M. burkeana* treatment concentrations increased, which directly impacted ATP and possibly ROS production. *Monsonia burkeana* contains phytochemicals such as gallic acid, chlorogenic acid, quercetin, catechins (EGCG) and polyphenols, which can cause cell death through different pathways (Mathivha *et al.*, 2019, Nnzeru *et al.*, 2016). A study conducted by Khiewkamrop *et al*. (2018) found that EGCG and EC decreased HepG2 cell viability by increasing apoptosis and causing cell cycle arrest (Khiewkamrop *et al.*, 2018). Apoptosis was associated with increased ΔΨm) and increased ROS, indicating an oxidative stress-induced mechanism in causing apoptosis in HepG2 cells.

Electrons may also be redirected to the ubiquinone pool (UQ) to provide reducing equivalents needed to reduce superoxide anions ($O_2^{\bullet-}$) produced from the respiratory chain or exogenous sources (Rustin *et al.*, 2002). The lack of SDH function will decrease electron flow to both complex III of the respiratory chain and the UQ. Although mitochondria are the main source of ROS such as $O_2^{\bullet-}$, ROS may also be produced by cellular respiration during arachidonic acid

metabolism by lipooxygenases and cyclooxygenases and by endothelial and inflammatory cells (Wang *et al.*, 2021). Although cells can scavenge ROS, it may not be sufficient to remove elevated ROS produced by the mitochondria (Pizzino *et al.*, 2017). Free radicals can attack polyunsaturated fatty acids' carbon-carbon double bonds, causing lipid peroxidation (Ayala *et al.*, 2014). In this study, there were decreased MDA levels, reducing lipid peroxidation for both cell lines (Figure 4.6). In addition, increased OGG1 for the Caco-2 IC_{20} treatment (Figure 4.6) suggests DNA oxidation for this treatment only. Macromolecule disruption may also be attributed to RNS, which causes nitrosation and alters integrity (Zarkovic, 2020). In Caco-2 cells, nitrite levels decreased for both treatments compared to the control but were increased for both treatments in HepG2 cells (Figure 4.7). There was also a decrease in iNOS protein expression for both cell lines at the IC_{20} and IC_{50} treatment concentrations.

Interestingly, increased LDH (Figure 4.3) implied membrane disruption was unrelated to lipid peroxidation by ROS or RNS in Caco-2 cells. Still, RNS-induced membrane disruption may be associated with increased LDH in HepG2 cells (Figure 4.3). Reactive nitrogen species have a longer mean half-life and react with other molecules three times faster than $O_2^{\bullet-}$. They permanently damage cell membranes, resulting in necrosis and cell death (Perez-Torres *et al.*, 2020). A recent study by Moghtaderi *et al*. (2018) showed that a combination of gallic acid and curcumin (present in *M. burkeana*) increased ROS and nitrite production and decreased GSH (Moghtaderi *et al.*, 2018). This hints that gallic acid could be one of the major components that increase nitrite levels in HepG2 cells, leading to nitrosative stress in the current study.

Decreased lipid peroxidation does not necessarily imply reduced ROS production. Indeed, an antioxidant defence system consisting of mainly enzymatic components is used by cells as protection from ROS-induced damage (Jena *et al.*, 2023). Superoxide produced by the dysregulation of mitochondrial function (Figure 4.4) was detoxified by SOD2, as indicated by its upregulated expression (Figure 4.8B), particularly in HepG2 cells. The upregulated protein expression of SOD2 facilitates the conversion of $O_2^{\bullet-}$ to H_2O_2. The increased H_2O_2 due to the upregulation of SOD2 may be harmful to cells if directed to the formation of $^{\bullet}OH$ via the Fenton reaction (Rosa *et al.*, 2021). However, the significant decrease in GSH levels for IC_{20} and IC_{50} treatments in both cell lines (Figure 4.9) suggests its utilisation to reduce H_2O_2 to water. A depletion of GSH is associated with oxidative stress (Yoo *et al.*, 2019), and supports the notion

of increased free radical production. Since GSH is a co-factor for Gpx-1, so GSH levels may influence its expression (Kim *et al.*, 2022). Most cancer types have abnormally increased expression of Gpx-1, which acts as a tumour promoter by controlling their proliferation, migration, invasion, apoptosis, and drug sensitivity (Zhao *et al.*, 2022). In this study, the mRNA expression of *Gpx-1* decreased for Caco-2 cells and the IC_{20} treatment in HepG2 cells (Figure 4.9) and may be attributed to the role of *Gpx-1* in detoxifying antioxidants. However, mRNA expression of *Gpx-1* for HepG2 cells (Figure 4.9) increased for the IC_{50} treatment concentration. There was also an increase in NRF-2 protein expression for both cell lines at the IC_{50} treatment concentrations (Figure 4.10), as there was a need to regulate antioxidant proteins to reduce oxidative damage in cells (Ngo and Duennwald, 2022).

Despite the antioxidant response mediated at the transcriptional level by increased NRF-2 (Figure 4.10) and *Gpx-1* (Figure 4.9), as well as increased SOD2 (Figure 4.8), oxidative and nitrosative stress was induced by *M. burkeana* in Caco-2 and HepG2 cells, respectively. The increased ROS and macromolecule damage associated with oxidative and nitrosative stress collectively lead to loss of function and may activate pathways that lead to cell death (Salim, 2017). Several cell death pathways may be activated, including apoptosis and necrosis (Obeng, 2021). In this study, initiator caspase 8 activity increased at IC_{20} and IC_{50} treatment concentrations in Caco-2 cells but was decreased in HepG2 cells, and caspase 9 increased for IC_{20}-treated Caco-2 cells (Figure 4.11). For HepG2 cells, caspase 9 activity decreased for both treatment concentrations (Figure 4.11). Caspase 8 plays a pivotal role in the extrinsic pathway of apoptosis, and its upregulation by *M. burkeana* in Caco-2 cells implies that the extrinsic pathway triggered apoptosis. In addition, the data suggests that intrinsic apoptosis was initiated in the IC_{20}-treated Caco-2 cells only. Interestingly, neither extrinsic nor intrinsic apoptosis was initiated by *M. burkeana* in HepG2 cells (Figure 4.11).

Intrinsic apoptosis is mediated by p53-control of the BCL-2 family of proteins (Aubrey *et al.*, 2018). However, the protein expression of p-p53/p53 decreased for both treatments in Caco-2 cells (Figure 4.12). Thus, p53 did not mediate the transcription of pro-apoptotic BCL-2 family genes such as PUMA and NOXA, and BAX decreased (Figure 4.13) (Hao *et al.*, 2023).

Interestingly, anti-apoptotic BCL-2 was also decreased in Caco-2 cells. Thus, the increased caspase 9 in the IC_{20}-treated Caco-2 cells was not mediated by the BCL-2 family and suggested that ROS-mediated mitochondrial membrane permeabilisation; MDA levels were less controlled in the IC_{20}-treated Caco-2 cells (Figure 4.6). In HepG2 cells, the protein expression of p-p53/p53 increased for IC_{50}-treated cells (Figure 4.12), but the BAX and BCL-2 protein expression (Figure 4.13, 4.14) effectively prevented MOMP and induction of the intrinsic pathway (Kalkavan and Green, 2018). This study shows that *M. burkeana* facilitated the execution of apoptosis in both cell lines, as caspase 3/7 was increased (Figure 4.15). Caspase 3/7 directs the ordered cell demolition by cleaving structural proteins and is responsible for externalising phosphatidylserine, an early marker of apoptosis (Calianese and Birge, 2020). The data shows phosphatidylserine was externalised in both cell lines (Figure 4.16). However, necrosis was also increased (Figure 4.17). Since both apoptosis and necrosis are modes of cell death induced by *M. burkeana* in the Caco-2 cells, it may be suggested that programmed necrosis or necroptosis is occurring. Necroptosis is activated when TNFα binding causes the formation of complex-1 via the recruitment of RIPK1, a cellular inhibitor of apoptosis proteins 1/2 (cIAP1/2), TNFR1-associated death domain (TRADD), and TNF receptor-associated factor 2/5 (TRAF2/5) (Kang *et al.*, 2022). Thereafter, RIPK1 ubiquitination by cIAP1/2, linear ubiquitin chain assembly complex (LUBAC) and TRAF2/5 causes initiation of the MAPK and NF-κB pathways (Zhao *et al.*, 2015). In this study, necroptosis was excluded as the mode of cell death in Caco-2 cells. Despite downregulation of TNFα (Figure 4.18), decreased *RIPK1*, *RIPK3* and *MLKL* corresponded with increased cIAP2 (Figure 4.18, 4.19). Furthermore, increased cIAP2, a potent inhibitor of apoptotic cell death (Biswas *et al.*, 2022), suggests that the extrinsic pathway initiated by *M. burkeana* in Caco-2 cells was via Fas-induced DISC formation. The necrosis in the Caco-2 cells may be attributed to secondary necrosis, which occurs in cells that have gone through the apoptotic program (Sachet *et al.*, 2017). The downregulation of initiator caspase 8 (Figure 4.11), with increased executor caspase 3/7 (Figure 4.15), phosphatidylserine externalisation (Figure 4.16) and necrosis (Figure 4.17), suggests that the possible mode of cell death observed in HepG2 cells is necroptosis. In HepG2 cells, there is an increase in *RIPK1* gene expression for both the IC_{20} and IC_{50} treatment concentrations (Figure 4.18). The concomitant decrease in $cIAP_2$ protein expression (Figure 4.18 for both treatments suggests the formation of complex 1. After the deubiquination of RIPK1 in complex 1, complex 2a or 2b forms. Complex 2a results in

the activation of caspase 8 and results in apoptosis, which was not evident in HepG2 cells. However, when caspase 8 is inhibited (Figure 4.11), complex 2b is formed, and a necroptotic pathway is activated. Thus, *RIPK1* recruits *RIPK3* (Figure 4.19) and induces the auto and transphosphorylation with oligomerisation of phosphorylated *RIPK3* to form the necrosome (McQuade *et al.*, 2013). RIPK3 recruits and phosphorylates MLKL (Figure 4.19), which is associated with cell membrane rupture (Samson *et al.*, 2020). Indeed, increased extracellular LDH in this study implied a loss of plasma membrane integrity (Figure 4.3).

CHAPTER 6: CONCLUSION

Monsonia burkeana, the traditional Southern African plant widely consumed as herbal tea to treat various ailments, including erectile dysfunction and blood cleansing, has also shown promise as a potential anticancer agent due to its antioxidant capabilities. The antioxidant and antiproliferative mechanisms have not been explored on Caco-2 and HepG2 cells; thus, this study investigated these pathways induced by *Monsonia burkeana* crude aqueous leaf extract.

The overall proposed mechanism of action of *M. burkeana* in Caco-2 and HepG2 cells is illustrated in Figure 6.1. Increased CYP3A4 activity in both cell lines leads to a dose-dependent decrease in cell viability. A reduction in ATP concentration and an increase in $\Delta\Psi m$ in both treatments confirmed reduced metabolic activity in Caco-2 and HepG2 cells. Lipid peroxidation occurred for both cell lines as indicated by the decreased MDA levels and DNA oxidation was suggested by increased OGG1 gene expression in Caco-2 IC_{20}-treated cells only. Nitrite levels decreased in Caco-2 cells but increased in HepG2 cells, with a reduction in iNOS protein expression in both cell lines. Membrane disruption was confirmed by elevated LDH levels in both cell lines, with RNS-induced membrane damage specifically noted in HepG2 cells. Oxidative stress was evident from decreased GSH concentrations and increased SOD2 protein expression at both treatment concentrations in Caco-2 and HepG2 cells. However, *Gpx-1* levels decreased in Caco-2 cells and HepG2 cells treated with IC_{20}. An associated upregulation of NRF-2 protein expression was observed at IC_{50} treatment concentrations in both cell lines, aiding in regulating antioxidant proteins. In Caco-2 cells, initiator caspase 8 activity increased at both treatment concentrations, indicating apoptosis via the extrinsic pathway. Intrinsic apoptosis was also suggested in IC_{20}-treated Caco-2 cells by increased caspase 9 activity. In contrast, caspase 8 and 9 activity decreased in HepG2 cells at both treatment concentrations. The p-p53/p53 ratio decreased in Caco-2 cells for both treatments, indicating that p53 did not mediate the transcription of pro-apoptotic BCL-2 family genes, resulting in decreased BAX and anti-apoptotic BCL-2. In HepG2 cells, the p-p53/p53 ratio of protein expression remained relatively unchanged in IC_{20}-treated cells and increased in IC_{50}-treated cells, with decreased BAX for IC_{20}-treated cells and increased BCL-2 protein expression for the IC_{50}-treatment concentration. Apoptosis was triggered by *M.*

burkeana in both cell lines, indicated by heightened caspase 3/7 activity and phosphatidyl serine externalisation, along with necrosis. In Caco-2 cells, *TNFα* was downregulated, while *RIPK1, RIPK3* and *MLKL* levels decreased in both treatment concentrations, corresponding with an increase in cIAP2. In HepG2 cells, *RIPK1* gene expression increased at both IC_{20} and IC_{50} treatment concentrations, cIAP2 protein expression decreased, and *RIPK3* and *MLKL* gene expression increased.

This study provides evidence supporting the role of *M. burkeana* in causing caspase-dependent apoptosis in Caco-2 cells for both treatment concentrations. Still, the intrinsic apoptotic pathway was only stimulated for the IC_{20} treatment. Nitrosative stress-induced necroptosis was the mechanism by which *M. burkeana* exerted its cytotoxic effect in HepG2 cells. The results showed promise of *M. burkeana* potentially being used as an anticancer treatment for colorectal and hepatocellular carcinomas. Additional studies should be conducted to determine the specific phytochemicals responsible for the different cytotoxic effects exerted by *M. burkeana.*

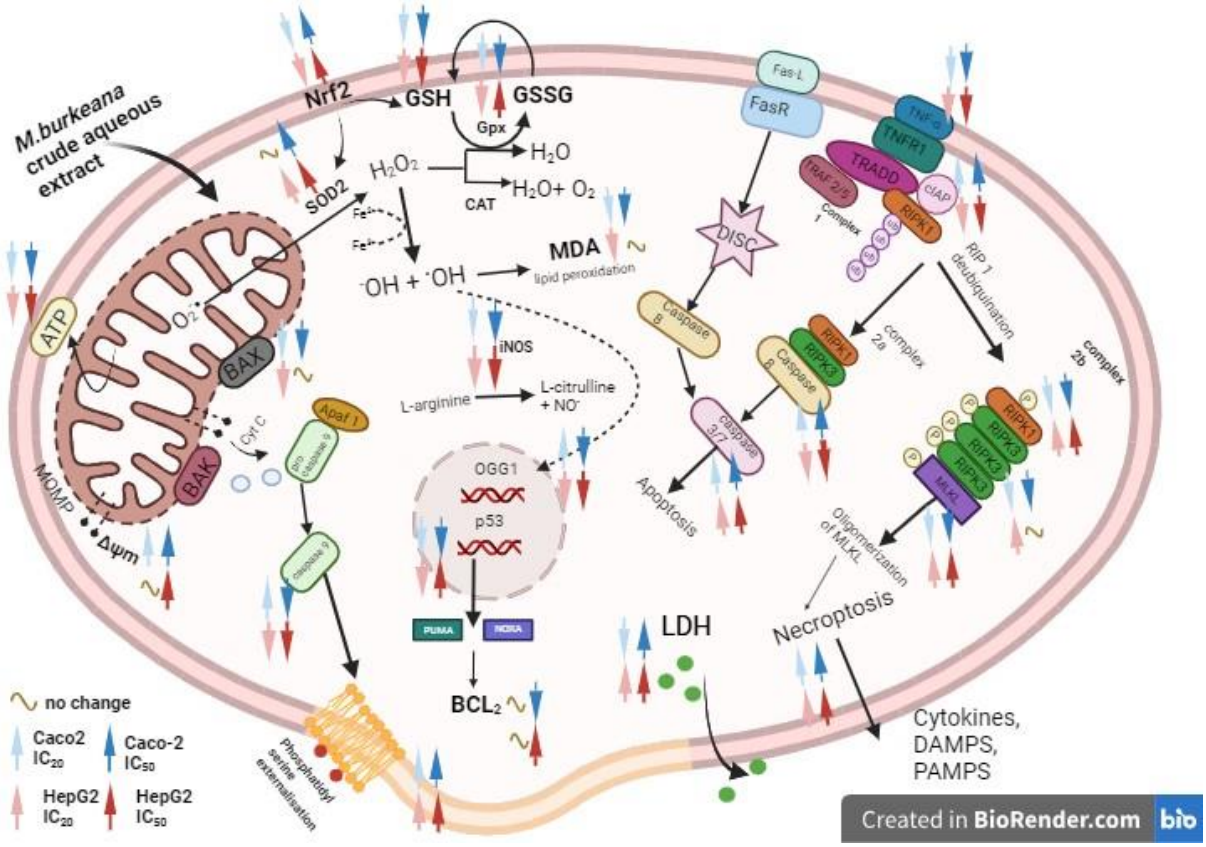

Figure 6.1: Summary of the effects mediated by *M. burkeana* in Caco-2 and HepG2 cells. In Caco-2 cells, *M. burkeana* induces caspase-dependent apoptosis at both treatment concentrations and stimulates the intrinsic apoptotic pathway at the IC_{20} treatment level. In HepG2 cells, *M.burkeana* exerts its cytotoxic effect through nitrosative stress-induced necroptosis.

REFERENCES

AARONS, C. B., SHANMUGAN, S. & BLEIER, J. I. 2014. Management of malignant colon polyps: current status and controversies. *World J Gastroenterol,* 20**,** 16178-83.

ABAANDOU, L., QUAN, D. & SHILOACH, J. 2021. Affecting HEK293 Cell Growth and Production Performance by Modifying the Expression of Specific Genes. *Cells,* 10.

ABE, C., MIYAZAWA, T. & MIYAZAWA, T. 2022. Current Use of Fenton Reaction in Drugs and Food. *Molecules,* 27.

ABOTALEB, M., LISKOVA, A., KUBATKA, P. & BUSSELBERG, D. 2020. Therapeutic Potential of Plant Phenolic Acids in the Treatment of Cancer. *Biomolecules,* 10.

AGUILAR DIAZ DE LEON, J. & BORGES, C. R. 2020. Evaluation of Oxidative Stress in Biological Samples Using the Thiobarbituric Acid Reactive Substances Assay. *J Vis Exp*.

AHMED, R., SINGH, J. K., WUNNAVA, A., AL-OBEED, O., ABDULLA, M. & SRIVASTAVA, S. K. 2021. Emerging trends in colorectal cancer: Dysregulated signaling pathways (Review). *International Journal of Molecular Medicine* 47.3.

AKBARI, M. E., GHELICHI-GHOJOGH, M., NIKEGHBALIAN, Z., KARAMI, M., AKBARI, A., HASHEMI, M., NOORAEI, S., GHIASI, M., FARAROUEI, M. & MORADIAN, F. 2022. Neoadjuvant VS adjuvant chemotherapy in patients with locally advanced breast cancer; a retrospective cohort study. *Ann Med Surg (Lond),* 84**,** 104921.

AMERICAN CANCER SOCIETY. 2020. *Surgery for Colon Cancer* [Online]. Available: https://www.cancer.org/cancer/colon-rectal-cancer/treating/colon-surgery.html#:~:text=A%20colectomy%20is%20surgery%20to,normal%20colon%20on%20either%20side. [Accessed].

AMERICAN CANCER SOCIETY. 2022. *Colorectal Cancer* [Online]. [Accessed].

ANAND, U., DEY, A., CHANDEL, A. K. S., SANYAL, R., MISHRA, A., PANDEY, D. K., DE FALCO, V., UPADHYAY, A., KANDIMALLA, R., CHAUDHARY, A., DHANJAL, J. K., DEWANJEE, S., VALLAMKONDU, J. & PEREZ DE LA LASTRA, J. M. 2023. Cancer chemotherapy and beyond: Current status, drug candidates, associated risks and progress in targeted therapeutics. *Genes Dis,* 10**,** 1367-1401.

ANDREW, A. S., PARKER, S., ANDERSON, J. C., REES, J. R., ROBINSON, C., RIDDLE, B. & BUTTERLY, L. F. 2018. Risk Factors for Diagnosis of Colorectal Cancer at a Late Stage: a Population-Based Study. *J Gen Intern Med,* 33**,** 2100-2105.

ANNIBALDI, A. & WALCZAK, H. 2020. Death Receptors and Their Ligands in Inflammatory Disease and Cancer. *Cold Spring Harb Perspect Biol,* 12.

ARZUMANIAN, V. A., KISELEVA, O. I. & POVERENNAYA, E. V. 2021. The Curious Case of the HepG2 Cell Line: 40 Years of Expertise. *Int J Mol Sci,* 22.

AUBREY, B. J., KELLY, G. L., JANIC, A., HEROLD, M. J. & STRASSER, A. 2018. How does p53 induce apoptosis and how does this relate to p53-mediated tumour suppression? *Cell Death Differ,* 25**,** 104-113.

AYALA, A., MUNOZ, M. F. & ARGUELLES, S. 2014. Lipid peroxidation: production, metabolism, and signaling mechanisms of malondialdehyde and 4-hydroxy-2-nonenal. *Oxid Med Cell Longev,* 2014**,** 360438.

BANSAL, S., SYAN, N., MATHUR, P. & CHOUDHARY, S. 2011. Pharmacological profile of green tea and its polyphenols: a review. *Medicinal Chemistry Research,* 21**,** 3347-3360.

BASHEER, L. & KEREM, Z. 2015. Interactions between CYP3A4 and Dietary Polyphenols. *Oxid Med Cell Longev,* 2015**,** 854015.

BASKAR, R., LEE, K. A., YEO, R. & YEOH, K. W. 2012. Cancer and radiation therapy: current advances and future directions. *Int J Med Sci,* 9**,** 193-9.

BATTISTELLI, M. & FALCIERI, E. 2020. Apoptotic Bodies: Particular Extracellular Vesicles Involved in Intercellular Communication. *Biology (Basel),* 9.

BENITEZ-GUZMAN, A., ARRIAGA-PIZANO, L., MORAN, J. & GUTIERREZ-PABELLO, J. A. 2018. Endonuclease G takes part in AIF-mediated caspase-independent apoptosis in Mycobacterium bovis-infected bovine macrophages. *Vet Res,* 49**,** 69.

BERTHELOOT, D., LATZ, E. & FRANKLIN, B. S. 2021. Necroptosis, pyroptosis and apoptosis: an intricate game of cell death. *Cell Mol Immunol,* 18**,** 1106-1121.

BISWAS, D. D., MARTIN, R. K., BROWN, L. N., MOCKENHAUPT, K., GUPTA, A. S., SURACE, M. J., THARAKAN, A., YESTER, J. W., BHARDWAJ, R., CONRAD, D. H. & KORDULA, T. 2022. Cellular inhibitor of apoptosis 2 (cIAP2) restricts neuroinflammation during experimental autoimmune encephalomyelitis. *J Neuroinflammation,* 19**,** 158.

BONNARDEL, J., T'JONCK, W., GAUBLOMME, D., BROWAEYS, R., SCOTT, C. L., MARTENS, L., VANNESTE, B., DE PRIJCK, S., NEDOSPASOV, S. A., KREMER, A., VAN HAMME, E., BORGHGRAEF, P., TOUSSAINT, W., DE BLESER, P., MANNAERTS, I., BESCHIN, A., VAN GRUNSVEN, L. A., LAMBRECHT, B. N., TAGHON, T., LIPPENS, S., ELEWAUT, D., SAEYS, Y. & GUILLIAMS, M. 2019. Stellate Cells, Hepatocytes, and Endothelial Cells Imprint the Kupffer Cell Identity on Monocytes Colonizing the Liver Macrophage Niche. *Immunity,* 51**,** 638-654.e9.

BONORA, M., PATERGNANI, S., RIMESSI, A., DE MARCHI, E., SUSKI, J. M., BONONI, A., GIORGI, C., MARCHI, S., MISSIROLI, S., POLETTI, F., WIECKOWSKI, M. R. & PINTON, P. 2012. ATP synthesis and storage. *Purinergic Signal,* 8**,** 343-57.

BRAR, G., GRETEN, T. F., GRAUBARD, B. I., MCNEEL, T. S., PETRICK, J. L., MCGLYNN, K. A. & ALTEKRUSE, S. F. 2020. Hepatocellular Carcinoma Survival by Etiology: A SEER-Medicare Database Analysis. *Hepatol Commun,* 4**,** 1541-1551.

BRATTON, S. B. & SALVESEN, G. S. 2010. Regulation of the Apaf-1-caspase-9 apoptosome. *J Cell Sci,* 123**,** 3209-14.

BRAY, F., FERLAY, J., SOERJOMATARAM, I., SIEGEL, R. L., TORRE, L. A. & JEMAL, A. 2018. Global cancer statistics 2018: GLOBOCAN estimates of incidence and mortality worldwide for 36 cancers in 185 countries. *CA Cancer J Clin,* 68**,** 394-424.

BREITZIG, M., BHIMINENI, C., LOCKEY, R. & KOLLIPUTI, N. 2016. 4-Hydroxy-2-nonenal: a critical target in oxidative stress? *Am J Physiol Cell Physiol,* 311**,** C537-C543.

BRYAN, N. S. & GRISHAM, M. B. 2007. Methods to detect nitric oxide and its metabolites in biological samples. *Free Radic Biol Med,* 43**,** 645-57.

CALDERON-MARTINEZ, E., LANDAZURI-NAVAS, S., VILCHEZ, E., CANTU-HERNANDEZ, R., MOSQUERA-MOSCOSO, J., ENCALADA, S., AL LAMI, Z., ZEVALLOS-DELGADO, C. & CINICOLA, J. 2023. Prognostic Scores and Survival Rates by Etiology of Hepatocellular Carcinoma: A Review. *Journal of Clinical Medicine Research,* 15**,** 200-207.

CALIANESE, D. C. & BIRGE, R. B. 2020. Biology of phosphatidylserine (PS): basic physiology and implications in immunology, infectious disease, and cancer. *Cell Commun Signal,* 18**,** 41.

CARREÑO, E. A., ALBERTO, A. V. P., DE SOUZA, C. A. M., DE MELLO, H. L., HENRIQUES-PONS, A. & ANASTACIO ALVES, L. 2021. Considerations and Technical Pitfalls in the Employment of the MTT Assay to Evaluate Photosensitizers for Photodynamic Therapy. *Applied Sciences,* 11.

CESUR-ERGUN, B. & DEMIR-DORA, D. 2023. Gene therapy in cancer. *J Gene Med,* 25**,** e3550.

CHAKRABARTI, S., PETERSON, C. Y., SRIRAM, D. & MAHIPAL, A. 2020. Early stage colon cancer: Current treatment standards, evolving paradigms, and future directions. *World J Gastrointest Oncol,* 12**,** 808-832.

CHARTAMPILAS, E., RAFAILIDIS, V., GEORGOPOULOU, V., KALARAKIS, G., HATZIDAKIS, A. & PRASSOPOULOS, P. 2022. Current Imaging Diagnosis of Hepatocellular Carcinoma. *Cancers (Basel),* 14.

CHAUDHARY, P., JANMEDA, P., DOCEA, A. O., YESKALIYEVA, B., ABDULL RAZIS, A. F., MODU, B., CALINA, D. & SHARIFI-RAD, J. 2023. Oxidative stress, free radicals and antioxidants: potential crosstalk in the pathophysiology of human diseases. *Front Chem,* 11**,** 1158198.

CHIDAMBARANATHAN-REGHUPATY, S., FISHER, P. B. & SARKAR, D. 2021. Hepatocellular carcinoma (HCC): Epidemiology, etiology and molecular classification. *Adv Cancer Res,* 149**,** 1-61.

CHOUDHARI, A. S., MANDAVE, P. C., DESHPANDE, M., RANJEKAR, P. & PRAKASH, O. 2019. Phytochemicals in Cancer Treatment: From Preclinical Studies to Clinical Practice. *Front Pharmacol,* 10**,** 1614.

CRUZ, R. A., RAGUPATHI, M., PEDRAZA, R., PICKRON, T. B., LE, A. T. & HAAS, E. M. 2011. Minimally invasive approaches for the management of "difficult" colonic polyps. *Diagn Ther Endosc,* 2011**,** 682793.

D'ARCY, M. S. 2019. Cell death: a review of the major forms of apoptosis, necrosis and autophagy. *Cell Biol Int,* 43**,** 582-592.

D'ARCHIVIO, M., SANTANGELO, C., SCAZZOCCHIO, B., VARÌ, R., FILESI, C., MASELLA, R. & GIOVANNINI, C. 2008. Modulatory Effects of Polyphenols on Apoptosis Induction: Relevance for Cancer Prevention *International Journal of molecular sciences*.

DASGUPTA., AMITAVA., KLEIN. & KIMBERLY. 2014. Methods for Measuring Oxidative Stress in the Laboratory. *Antioxidants in Food, Vitamins and Supplements.*

DE' ANGELIS, G. L., BOTTARELLI, L., AZZONI, C., DE' ANGELIS, N., LEANDRO, G., DI MARIO, F., GAIANI, F. & NEGRI, F. 2018. Microsatellite instability in colorectal cancer. *Acta Biomed,* 89**,** 97-101.

DEBELA, D. T., MUZAZU, S. G., HERARO, K. D., NDALAMA, M. T., MESELE, B. W., HAILE, D. C., KITUI, S.

K. & MANYAZEWAL, T. 2021. New approaches and procedures for cancer treatment: Current perspectives. *SAGE Open Med,* 9**,** 20503121211034366.

DHANASEKARAN, R., BANDOH, S. & ROBERTS, L. R. 2016. Molecular pathogenesis of hepatocellular carcinoma and impact of therapeutic advances. *F1000Res,* 5.

DI-IACOVO, N., PIERONI, S., PIOBBICO, D., CASTELLI, M., SCOPETTI, D., FERRACCHIATO, S., DELLA-FAZIA, M. A. & SERVILLO, G. 2023. Liver Regeneration and Immunity: A Tale to Tell. *Int J Mol Sci,* 24.

DONATO, M. T., TOLOSA, L. & GOMEZ-LECHON, M. J. 2015. Culture and Functional Characterization of Human Hepatoma HepG2 Cells. *Methods Mol Biol,* 1250**,** 77-93.

DOUAIHER, J., RAVIPATI, A., GRAMS, B., CHOWDHURY, S., ALATISE, O. & ARE, C. 2017. Colorectal cancer-global burden, trends, and geographical variations. *J Surg Oncol,* 115**,** 619-630.

EL ORFI, N., BOUTAYEB, S., HADDOU RAHOU, B. & ERRIHANI, H. 2022. Use of Medicinal Plants by Cancer Patients Under Chemotherapy in the Northwest of Morocco (Rabat Area) : Cross-Sectional Study. *J Evid Based Integr Med,* 27**,** 2515690X221128036.

FERLAY, J., ERVIK, M., LAM, F., COLOMBET, M., MERY, L., PIÑEROS, M., ZNAOR, A., SOERJOMATARAM, I. & BRAY, F. 2020. Colorectal cancer. *In:* TODAY, G. C. O. C. (ed.).

G-BIOSCIENCES. 2021. *JC-10 Mitochondrial Membrane Potential Assay* [Online]. Available: https://www.gbiosciences.com/Bioassays/Cell_Health_Assay/Apoptosis-Assays-Accessories/JC-10_Mitochondrial_Membrane_Potential_Assay [Accessed].

GHAFOURIFAR, P., PARIHAR, M. S., NAZAREWICZ, R., ZENEBE, W. J. & PARIHAR, A. 2008. Detection Assays for Determination of Mitochondrial Nitric Oxide Synthase Activity; Advantages and Limitations. *Nitric Oxide, Part F.*

GHAREGHOMI, S., HABIBI-REZAEI, M., ARESE, M., SASO, L. & MOOSAVI-MOVAHEDI, A. A. 2022. Nrf2 Modulation in Breast Cancer. *Biomedicines,* 10.

GHASEMI, M., TURNBULL, T., SEBASTIAN, S. & KEMPSON, I. 2021. The MTT Assay: Utility, Limitations, Pitfalls, and Interpretation in Bulk and Single-Cell Analysis. *Int J Mol Sci,* 22.

GILL, J., G., PISKOUNOVA, E. & MORRISON, S., J. 2016. Cancer, Oxidative Stress, and Metastasis.

GOLFIERI, R., BARGELLINI, I., SPREAFICO, C. & TREVISANI, F. 2019. Patients with Barcelona Clinic Liver Cancer Stages B and C Hepatocellular Carcinoma: Time for a Subclassification. *Liver Cancer,* 8**,** 78-91.

GONG, Y., FAN, Z., LUO, G., YANG, C., HUANG, Q., FAN, K., CHENG, H., JIN, K., NI, Q., YU, X. & LIU, C. 2019. The role of necroptosis in cancer biology and therapy. *Mol Cancer,* 18**,** 100.

GREEN, M. R. & SAMBROOK, J. 2019. Polymerase Chain Reaction. *Cold Spring Harb Protoc,* 2019.

GREEN., DOUGLAS, R., GOLDSTEIN., JOSHUA, C., WATERHOUSE., J., N., JUIN., PHILLIPE., EVAN. & GERARD, I. 2000. The coordinate release of cytochrome c during apoptosis is rapid, complete and kinetically invariant. *Nature Cell Biology,* 2**,** 156-162.

GRIESS, J. P. 1879. Ber. Deutsch Chem. *Deutsch Chem,* 12.

GROVES, J. T. 2015. Cytochrome P450 enzymes: understanding the biochemical hieroglyphs.

F1000Research, 4.

HALLIWELL, B. & GUTTERIDGE, J., M. 2015. Free radicals in biology and medicine. *Oxford university press*.

HAO, Q., CHEN, J., LU, H. & ZHOU, X. 2023. The ARTS of p53-dependent mitochondrial apoptosis. *J Mol Cell Biol,* 14.

HASSAN, M., WATARI, H., ABUALMAATY, A., OHBA, Y. & SAKURAGI, N. 2014. Apoptosis and molecular targeting therapy in cancer. *Biomed Res Int,* 2014**,** 150845.

HATOK, J. & RACAY, P. 2016. Bcl-2 family proteins: master regulators of cell survival. *Biomol Concepts,* 7**,** 259-70.

HAYES, J. D., DINKOVA-KOSTOVA, A. T. & TEW, K. D. 2020. Oxidative Stress in Cancer. *Cancer Cell,* 38**,** 167-197.

HE, F., RU, X. & WEN, T. 2020. NRF2, a Transcription Factor for Stress Response and Beyond. *Int J Mol Sci,* 21.

HERBST, M. 2015. *Fact Sheet on Colorectal Cancer*.

HOSSAIN, M. S., KARUNIAWATI, H., JAIROUN, A. A., URBI, Z., OOI, J., JOHN, A., LIM, Y. C., KIBRIA, K. M. K., MOHIUDDIN, A. K. M., MING, L. C., GOH, K. W. & HADI, M. A. 2022. Colorectal Cancer: A Review of Carcinogenesis, Global Epidemiology, Current Challenges, Risk Factors, Preventive and Treatment Strategies. *Cancers (Basel),* 14.

HUANG, S. H., KAO, Y. H., MULLER, C. J. F., JOUBERT, E. & CHUU, C. P. 2020. Aspalathin-rich green Aspalathus linearis extract suppresses migration and invasion of human castration-resistant prostate cancer cells via inhibition of YAP signaling. *Phytomedicine,* 69**,** 153210.

HUANG, W.-Y., CAI, Y.-Z. & ZHANG, Y. 2009. Natural phenolic compounds from medicinal herbs and dietary plants: potential use for cancer prevention. *Nutrition and cancer,* 62**,** 1-20.

HUCK, M. B. & BOHL, J. L. 2016. Colonic Polyps: Diagnosis and Surveillance. *Clin Colon Rectal Surg,* 29**,** 296-305.

HYDE, M., A. , WURSTEN, B., T. , BALLINGS, P. & COATES, P., M. 2022. *Flora of Zimbabwe: Species information: Monsonia burkeana.* [Online]. Available: https://www.zimbabweflora.co.zw/speciesdata/species.php?species_id=132710 [Accessed].

IOVINE, N. M., PURSNANI, S., VOLDMAN, A., WASSERMAN, G., BLASER, M. J. & WEINRAUCH, Y. 2008. Reactive nitrogen species contribute to innate host defense against Campylobacter jejuni. *Infect Immun,* 76**,** 986-93.

JAN, R. & CHAUDHRY, G. E. 2019. Understanding Apoptosis and Apoptotic Pathways Targeted Cancer Therapeutics. *Adv Pharm Bull,* 9**,** 205-218.

JEMAL, A., WARD, E. M., JOHNSON, C. J., CRONIN, K. A., MA, J., RYERSON, B., MARIOTTO, A., LAKE, A. J., WILSON, R., SHERMAN, R. L., ANDERSON, R. N., HENLEY, S. J., KOHLER, B. A., PENBERTHY, L., FEUER, E. J. & WEIR, H. K. 2017. Annual Report to the Nation on the Status of Cancer, 1975-2014, Featuring Survival. *J Natl Cancer Inst,* 109.

JENA, A. B., SAMAL, R. R., BHOL, N. K. & DUTTAROY, A. K. 2023. Cellular Red-Ox system in health and disease: The latest update. *Biomed Pharmacother,* 162**,** 114606.

JIE, Z., LIU, J., SHU, M., YING, Y. & YANG, H. 2023. Detection strategies for superoxide anion: A review. *Talanta*.

JOMOVA, K., RAPTOVA, R., ALOMAR, S. Y., ALWASEL, S. H., NEPOVIMOVA, E., KUCA, K. & VALKO, M. 2023. Reactive oxygen species, toxicity, oxidative stress, and antioxidants: chronic diseases and aging. *Arch Toxicol,* 97**,** 2499-2574.

JUAN, C. A., PEREZ DE LA LASTRA, J. M., PLOU, F. J. & PEREZ-LEBENA, E. 2021. The Chemistry of Reactive Oxygen Species (ROS) Revisited: Outlining Their Role in Biological Macromolecules (DNA, Lipids and Proteins) and Induced Pathologies. *Int J Mol Sci,* 22.

KALKAVAN, H. & GREEN, D. R. 2018. MOMP, cell suicide as a BCL-2 family business. *Cell Death Differ,* 25**,** 46-55.

KALRA, A., YETISKUL, E., WEHRLE, C., J. & TUMA, F. 2022. *Physiology, Liver,* Treasure Island (FL), StatPearls Publishing.

KAMILOGLU, S., SARI, G., OZDAL, T. & CAPANOGLU, E. 2020. Guidelines for cell viability assays. *Food Frontiers,* 1**,** 332-349.

KANG, K., PARK, C. & CHAN, F. K.-M. 2022. Necroptosis at a glance. *Journal of Cell Science,* 135.

KASHYAP, D., GARG, V. K. & GOEL, N. 2021. Intrinsic and extrinsic pathways of apoptosis: Role in cancer development and prognosis. *Adv Protein Chem Struct Biol,* 125**,** 73-120.

KAUR, G. & DUFOUR, J. M. 2012. Cell lines: Valuable tools or useless artifacts. *Spermatogenesis,* 2**,** 1-5.

KERR, J. F., WYLLIE, A. H. & CURRIE, A. R. 1972. Apoptosis: a basic biological phenomenon with wide-ranging implications in tissue kinetics. *Br J Cancer,* 26**,** 239–257.

KHIEWKAMROP, P., PHUNSOMBOON, P., RICHERT, L., PEKTHONG, D. & SRISAWANG, P. 2018. Epistructured catechins, EGCG and EC facilitate apoptosis induction through targeting de novo lipogenesis pathway in HepG2 cells. *Cancer Cell Int,* 18**,** 46.

KIM, J. E., LEE, D. S., KIM, T. H. & KANG, T. C. 2022. Glutathione Regulates GPx1 Expression during CA1 Neuronal Death and Clasmatodendrosis in the Rat Hippocampus following Status Epilepticus. *Antioxidants (Basel),* 11.

KıRAN, T. R., OTLU, O. & KARABULUT, A. B. 2023. Oxidative stress and antioxidants in health and disease. *Journal of Laboratory Medicine,* 47**,** 1-11.

KOLAPPAN, S., SHEN, D. L., MOSI, R., SUN, J., MCEACHERN, E. J., VOCADLO, D. J. & CRAIG, L. 2015. Structures of lactate dehydrogenase A (LDHA) in apo, ternary and inhibitor-bound forms. *Acta Crystallogr D Biol Crystallogr,* 71**,** 185-95.

KRALIK, P. & RICCHI, M. 2017. A Basic Guide to Real Time PCR in Microbial Diagnostics: Definitions, Parameters, and Everything. *Front Microbiol,* 8**,** 108.

KUMAR, S., DOBOS, G. J. & RAMPP, T. 2017. The Significance of Ayurvedic Medicinal Plants. *J Evid Based Complementary Altern Med,* 22**,** 494-501.

KUMAR, S., FAIRMICHAEL, C., LONGLEY, D. B. & TURKINGTON, R. C. 2020. The Multiple Roles of the IAP Super-family in cancer. *Pharmacol Ther,* 214**,** 107610.

LEA, T. 2015. *The Impact of Food Bioactives on Health: in vitro and ex vivo models*, Springer.

LEROTHOLI, L., CHAUDHARY, S. K., COMBRINCK, S. & VILJOEN, A. 2017. Bush tea (Athrixia phylicoides): A review of the traditional uses, bioactivity and phytochemistry. *South African Journal of Botany,* 110**,** 4-17.

LEWANDOWSKA, A., RUDZKI, G., LEWANDOWSKI, T., STRYJKOWSKA-GORA, A. & RUDZKI, S. 2022. Risk Factors for the Diagnosis of Colorectal Cancer. *Cancer Control,* 29**,** 10732748211056692.

LIU, X., MILLER, M. J. S., JOSHI, M. S., SADOWSKA-KROWICKA, H., CLARK, D. A. & LANCASTER, J. R. 1998. Diffusion-limited Reaction of Free Nitric Oxide with Erythrocytes. *Journal of Biological Chemistry,* 273**,** 18709–18713. .

LIU, Y., SHI, Y., HAN, R., LIU, C., QIN, X., LI, P. & GU, R. 2023. Signaling pathways of oxidative stress response: the potential therapeutic targets in gastric cancer. *Front Immunol,* 14**,** 1139589.

LIVAK, K. J. & SCHMITTGEN, T. D. J. M. 2001. Analysis of relative gene expression data using real-time quantitative PCR and the 2− ΔΔCT method. 25**,** 402-408.

LOTFOLLAHZADEH, S., RECIO-BOILES, A. & CAGIR, B. 2023. *Colon Cancer,* Treasure Island (FL), StatPearls Publishing.

MA, Q. 2013. Role of nrf2 in oxidative stress and toxicity. *Annu Rev Pharmacol Toxicol,* 53**,** 401-26.

MAHMOOD, T. & YANG, P. C. 2012. Western blot: technique, theory, and trouble shooting. *N Am J Med Sci,* 4**,** 429-34.

MAIDA, M., ORLANDO, E., CAMMÀ, C. & CABIBBO, G. 2014. Staging systems of hepatocellular carcinoma: A review of literature. *World J Gastroenterol,* 20**,** 4141-50.

MALIK, D., MAHENDIRATTA, S., KAUR, H. & MEDHI, B. 2021. Futuristic approach to cancer treatment. *Gene,* 805**,** 145906.

MALONGANE, F., MCGAW, L. J., OLAOKUN, O. O. & MUDAU, F. N. 2022. Anti-Inflammatory, Anti-Diabetic, Anti-Oxidant and Cytotoxicity Assays of South African Herbal Teas and Bush Tea Blends. *Foods,* 11.

MAMPHISWANA, N., MASHELA, P. W. & MDEE, L. 2010a. Accuulative capabilities of essential nutrient elements in organs of Monsonia burkeana. *African Journal of Biotechnology,* 10.

MAMPHISWANA, N. D., MASHELA, P. W. & MDEE, L. K. 2010b. Distribution of total phenolics and antioxidant activity in fruit, leaf, stem and root of Monsonia burkeana. *African Journal of Agricultural Research,* 5**,** 2570-2575.

MANDAL, M., SARKAR, M., KHAN, A., BISWAS, M., MASI, A., RAKWAL, R., AGRAWAL, G. K., SRIVASTAVA, A. & SARKAR, A. 2022. Reactive Oxygen Species (ROS) and Reactive Nitrogen Species (RNS) in plants– maintenance of structural individuality and functional blend. *Advances in Redox Research,* 5.

MARMIROLI, N. & MAESTRI, E. 2007. Polymerase chain reaction (PCR). *Food Toxicants Analysis.*

MARTINEZ-OSORIO, V., ABDELWAHAB, Y. & ROS, U. 2023. The Many Faces of MLKL, the Executor of

Necroptosis. *Int J Mol Sci,* 24.

MATHIVHA, L. P., THIBANE, V. S. & MUDAU, F. N. 2019. Anti-diabetic and anti-proliferative activities of herbal teas, Athrixia phylicoides DC and Monsonia burkeana Planch. ex Harv, indigenous to South Africa. *British Food Journal,* 121**,** 964-974.

MATSUURA, K., CANFIELD, K., FENG, W. & KUROKAWA, M. 2016. Metabolic Regulation of Apoptosis in Cancer. *Int Rev Cell Mol Biol,* 327**,** 43-87.

MAYO FOUNDATION FOR MEDICAL EDUCATION AND RESEARCH. 2022. *Colon cancer* [Online]. Available: https://www.mayoclinic.org/diseases-conditions/colon-cancer/diagnosis-treatment/drc-20353674 [Accessed].

MCQUADE, T., CHO, Y. & CHAN, F. K. 2013. Positive and negative phosphorylation regulates RIP1- and RIP3-induced programmed necrosis. *Biochem J,* 456**,** 409-15.

MEFTAHI, G. H., BAHARI, Z., ZAREI MAHMOUDABADI, A., IMAN, M. & JANGRAVI, Z. 2021. Applications of western blot technique: From bench to bedside. *Biochem Mol Biol Educ,* 49**,** 509-517.

MILLS, S., E. 2015. *Sternberg's Diagnostic Surgical Pathology*

MITTAL, S. & EL-SERAG, H., B. 2013. Epidemiology of Hepatocellular Carcinoma. *Journal of Clinical Gastroenterology,* 47.

MOGHTADERI, H., SEPEHRI, H., DELPHI, L. & ATTARI, F. 2018. Gallic acid and curcumin induce cytotoxicity and apoptosis in human breast cancer cell MDA-MB-231. *Bioimpacts,* 8**,** 185-194.

MOLLER, I. M., ROGOWSKA-WRZESINSKA, A. & RAO, R. S. 2011. Protein carbonylation and metal-catalyzed protein oxidation in a cellular perspective. *J Proteomics,* 74**,** 2228-42.

MORENO, C., SANTOS, R. M., BURNS, R. & ZHANG, W. C. 2020. Succinate Dehydrogenase and Ribonucleic Acid Networks in Cancer and Other Diseases. *Cancers (Basel),* 12.

MORGAN, E., ARNOLD, M., GINI, A., LORENZONI, V., CABASAG, C. J., LAVERSANNE, M., VIGNAT, J., FERLAY, J., MURPHY, N. & BRAY, F. 2023. Global burden of colorectal cancer in 2020 and 2040: incidence and mortality estimates from GLOBOCAN. *Gut.,* 72**,** 338-344.

MURPHY, M., P. 2009. How mitochondria produce reactive oxygen species. *Biochem. J.,* 417**,** 1-13.

MURPHY, M. P., BAYIR, H., BELOUSOV, V., CHANG, C. J., DAVIES, K. J. A., DAVIES, M. J., DICK, T. P., FINKEL, T., FORMAN, H. J., JANSSEN-HEININGER, Y., GEMS, D., KAGAN, V. E., KALYANARAMAN, B., LARSSON, N. G., MILNE, G. L., NYSTROM, T., POULSEN, H. E., RADI, R., VAN REMMEN, H., SCHUMACKER, P. T., THORNALLEY, P. J., TOYOKUNI, S., WINTERBOURN, C. C., YIN, H. & HALLIWELL, B. 2022. Guidelines for measuring reactive oxygen species and oxidative damage in cells and in vivo. *Nat Metab,* 4**,** 651-662.

MUSTAPHA, A., ABDULFATAI, I., SHEHU, U. A., OPEYEMI, N. H., PETER, I. & BERINYUY, E. B. 2022. Cancer Chemotherapy: A Review Update of the Mechanisms of Actions, Prospects and Associated Problems. *BIOMED Natural and Applied Science*.

NAEINI, M. B., BIANCONI, V., PIRRO, M. & SAHEBKAR, A. 2020. The role of phosphatidylserine recognition receptors in multiple biological functions. *Cell Mol Biol Lett,* 25**,** 23.

NAGATA, S., SUZUKI, J., SEGAWA, K. & FUJII, T. 2016. Exposure of phosphatidylserine on the cell surface. *Cell Death & Differentiation,* 23**,** 952-961.

NATIONAL CANCER INSTITUTE. 2021. *What is Cancer?* [Online]. Available: https://www.cancer.gov/about-cancer/understanding/what-is-cancer#:~:text=Pittsburgh%20Cancer%20Institute-,The%20Definition%20of%20Cancer,up%20of%20trillions%20of%20cells. [Accessed].

NATIONAL CANCER INSTITUTE. 2022. *Risk Factors for Cancer* [Online]. [Accessed 15/07/22].

NATIONAL CANCER INSTITUTE. 2023. *Cancer Stat Facts: Colorectal Cancer* [Online]. U.S National Cancer Institute, National Institute of Health. Available: https://seer.cancer.gov/statfacts/html/colorect.html [Accessed].

NGO, V. & DUENNWALD, M. L. 2022. Nrf2 and Oxidative Stress: A General Overview of Mechanisms and Implications in Human Disease. *Antioxidants (Basel),* 11.

NGOEPE, N. M., MBITA, Z., MATHIPA, M., MKETO, N., NTSENDWANA, B. & HINTSHO-MBITA, N. C. 2018. Biogenic synthesis of ZnO nanoparticles using Monsonia burkeana for use in photocatalytic, antibacterial and anticancer applications. *Ceramics International,* 44**,** 16999-17006.

NIKBAKHT, H. A., HASSANIPOUR, S., SHOJAIE, L., VALI, M., GHAFFARI-FAM, S., GHELICHI-GHOJOGH, M., MALEKI, Z., ARAB-ZOZANI, M., ABDZADEH, E., DELAM, H., SALEHINIYA, H., SHAFIEE, M. & MOHAMMADI, S. 2020. Survival Rate of Colorectal Cancer in Eastern Mediterranean Region Countries: A Systematic Review and Meta-Analysis. *Cancer Control,* 27**,** 1073274820964146.

NNZERU, L. R. 2019. 1h Nuclear Magnetic Resonance Spectroscopy Reveals Secondary Metabolic Variations of Special Tea (Monsonia Burkeana Planch. Ex Harv) Populations from Three Selected Locations in South Africa. *Applied Ecology and Environmental Research,* 17.

NNZERU, L. R., NTUSHELO, K. & MUDAU, F. N. 2016. Physical appraisal and attributed of Monsonia Burkeana (Special Tea):The perspective of tea users.

NURGALI, K., JAGOE, R. T. & ABALO, R. 2018. Editorial: Adverse Effects of Cancer Chemotherapy: Anything New to Improve Tolerance and Reduce Sequelae? *Front Pharmacol,* 9**,** 245.

OBENG, E. 2021. Apoptosis (programmed cell death) and its signals - A review. *Braz J Biol,* 81**,** 1133-1143.

OBRADOVIC, J., JURISIC, V., TOSIC, N., MRDJANOVIC, J., PERIN, B., PAVLOVIC, S. & DJORDJEVIC, N. 2013. Optimization of PCR conditions for amplification of GC-Rich EGFR promoter sequence. *J Clin Lab Anal,* 27**,** 487-93.

PAI, R. K., BETTINGTON, M., SRIVASTAVA, A. & ROSTY, C. 2019. An update on the morphology and molecular pathology of serrated colorectal polyps and associated carcinomas. *Mod Pathol,* 32**,** 1390-1415.

PARK, W., WEI, S., KIM, B. S., KIM, B., BAE, S. J., CHAE, Y. C., RYU, D. & HA, K. T. 2023. Diversity and complexity of cell death: a historical review. *Exp Mol Med,* 55**,** 1573-1594.

PEREZ-TORRES, I., MANZANO-PECH, L., RUBIO-RUIZ, M. E., SOTO, M. E. & GUARNER-LANS, V. 2020. Nitrosative Stress and Its Association with Cardiometabolic Disorders. *Molecules,* 25.

PFEFFER, C. M. & SINGH, A. T. K. 2018. Apoptosis: A Target for Anticancer Therapy. *Int J Mol Sci,* 19.

PIZZINO, G., IRRERA, N., CUCINOTTA, M., PALLIO, G., MANNINO, F., ARCORACI, V., SQUADRITO, F., ALTAVILLA, D. & BITTO, A. 2017. Oxidative Stress: Harms and Benefits for Human Health. *Oxid Med Cell Longev,* 2017**,** 8416763.

PROMEGA CORPORATION. 2016. *P450-Glo™ Assays* [Online]. Available: https://worldwide.promega.com/-/media/files/resources/protocols/technicalbulletins/101/p450-glo-assays-protocol.pdf?rev=66707cade2d248bcad7a4b79be4b329b&sc_lang=en [Accessed 16/08/22].

PROMEGA CORPORATION. 2022a. *ATP Assays* [Online]. Available: https://www.promega.com/resources/guides/cell-biology/atp-assays/#:~:text=Higher%20ATP%20concentration%20indicates%20higher,as%20colorimetric%2C%20fluorescent%20and%20bioluminescent. [Accessed].

PROMEGA CORPORATION. 2022b. *GSH-Glo™ Glutathione Assay* [Online]. Available: https://worldwide.promega.com/products/cell-health-assays/oxidative-stress-assays/gsh_glo-glutathione-assay/?catNum=V6911 [Accessed].

PROMEGA CORPORATION. 2022c. *RealTime-Glo™ Annexin V Apoptosis and Necrosis Assay* [Online]. Available: https://worldwide.promega.com/products/cellhealthassays/apoptosisassays/realtime-gloannexin-vapoptosisassay/catNum=JA1011 [Accessed].

PROMEGA CORPORATION. 2023. *Caspase-Glo® 3/7 Assay* [Online]. Available: https://www.promega.com/-/media/files/resources/protocols/technical-bulletins/101/caspase-glo-3-7-assay-protocol.pdf [Accessed].

QASIM, M., ABIDEEN, Z., ADNAN, M. Y., GULZAR, S., GUL, B., RASHEED, M. & KHAN, M. A. 2017. Antioxidant properties, phenolic composition, bioactive compounds and nutritive value of medicinal halophytes commonly used as herbal teas. *South African Journal of Botany,* 110**,** 240-250.

QUE, X., HUNG, M. Y., YEANG, C., GONEN, A., PROHASKA, T. A., SUN, X., DIEHL, C., MAATTA, A., GADDIS, D. E., BOWDEN, K., PATTISON, J., MACDONALD, J. G., YLA-HERTTUALA, S., MELLON, P. L., HEDRICK, C. C., LEY, K., MILLER, Y. I., GLASS, C. K., PETERSON, K. L., BINDER, C. J., TSIMIKAS, S. & WITZTUM, J. L. 2018. Oxidized phospholipids are proinflammatory and proatherogenic in hypercholesterolaemic mice. *Nature,* 558**,** 301-306.

RAWLA, P., SUNKARA, T. & BARSOUK, A. 2019. Epidemiology of colorectal cancer: incidence, mortality, survival, and risk factors. *Prz Gastroenterol,* 14**,** 89-103.

RILEY, R. S., JUNE, C. H., LANGER, R. & MITCHELL, M. J. 2019. Delivery technologies for cancer immunotherapy. *Nat Rev Drug Discov,* 18**,** 175-196.

RISS, T. L., MORAVEC, R. A. & NILES, A. L. 2016. *Cell Viability Assays*.

ROSA, A. C., CORSI, D., CAVI, N., BRUNI, N. & DOSIO, F. 2021. Superoxide Dismutase Administration: A Review of Proposed Human Uses. *Molecules,* 26.

ROUFAYEL, R., YOUNES, K., AL-SABI, A. & MURSHID, N. 2022. BH3-Only Proteins Noxa and Puma Are

Key Regulators of Induced Apoptosis. *Life (Basel),* 12.

ROY, A., KHAN, A., AHMAD, I., ALGHAMDI, S., RAJAB, B. S., BABALGHITH, A. O., ALSHAHRANI, M. Y., ISLAM, S. & ISLAM, M. R. 2022. Flavonoids a Bioactive Compound from Medicinal Plants and Its Therapeutic Applications. *Biomed Res Int,* 2022**,** 5445291.

RUSTIN, P., MUNNICH, A. & ROTIG, A. 2002. Succinate dehydrogenase and human diseases: new insights into a well-known enzyme. *Eur J Hum Genet,* 10**,** 289-91.

SACHET, M., LIANG, Y. Y. & OEHLER, R. 2017. The immune response to secondary necrotic cells. *Apoptosis,* 22**,** 1189-1204.

SALIM, S. 2017. Oxidative Stress and the Central Nervous System. *J Pharmacol Exp Ther,* 360**,** 201-205.

SAMODIEN, S., KOCK, M. D., JOUBERT, E., SWANEVELDER, S. & GELDERBLOM, W. C. 2020. Differential cytotoxicity of rooibos and green tea extracts against primary rat hepatocytes and human liver and colon cancer cells–causal role of major flavonoids. *Nutrition and Cancer***,** 1-15.

SAMSON, A. L., ZHANG, Y., GEOGHEGAN, N. D., GAVIN, X. J., DAVIES, K. A., MLODZIANOSKI, M. J., WHITEHEAD, L. W., FRANK, D., GARNISH, S. E., FITZGIBBON, C., HEMPEL, A., YOUNG, S. N., JACOBSEN, A. V., CAWTHORNE, W., PETRIE, E. J., FAUX, M. C., SHIELD-ARTIN, K., LALAOUI, N., HILDEBRAND, J. M., SILKE, J., ROGERS, K. L., LESSENE, G., HAWKINS, E. D. & MURPHY, J. M. 2020. MLKL trafficking and accumulation at the plasma membrane control the kinetics and threshold for necroptosis. *Nat Commun,* 11**,** 3151.

SAWICKI, T., RUSZKOWSKA, M., DANIELEWICZ, A., NIEDZWIEDZKA, E., ARLUKOWICZ, T. & PRZYBYLOWICZ, K. E. 2021. A Review of Colorectal Cancer in Terms of Epidemiology, Risk Factors, Development, Symptoms and Diagnosis. *Cancers (Basel),* 13.

SEO, J., NAM, Y. W., KIM, S., OH, D. B. & SONG, J. 2021. Necroptosis molecular mechanisms: Recent findings regarding novel necroptosis regulators. *Exp Mol Med,* 53**,** 1007-1017.

SEVER, R. & BRUGGE, J. S. 2015. Signal transduction in cancer. *Cold Spring Harb Perspect Med,* 5.

SEVRIOUKOVA, I. F. & POULOS, T. L. 2013. Understanding the mechanism of cytochrome P450 3A4: recent advances and remaining problems. *Dalton Trans,* 42**,** 3116-26.

SHARMA, R., AASHIMA, NANDA, M., FRONTERRE, C., SEWAGUDDE, P., SSENTONGO, A. E., YENNEY, K., ARHIN, N. D., OH, J., AMPONSAH-MANU, F. & SSENTONGO, P. 2022. Mapping Cancer in Africa: A Comprehensive and Comparable Characterization of 34 Cancer Types Using Estimates From GLOBOCAN 2020. *Front Public Health,* 10**,** 839835.

SHENG, Y., ABREU, I. A., CABELLI, D. E., MARONEY, M. J., MILLER, A. F., TEIXEIRA, M. & VALENTINE, J. S. 2014. Superoxide dismutases and superoxide reductases. *Chem Rev,* 114**,** 3854-918.

SIES, H. 2020. Oxidative Stress: Concept and Some Practical Aspects. *Antioxidants (Basel),* 9.

SILVA, A., C. , HARA, A., K. , LEIGHTON, J., A. & HEPPELL, J., P. 2005. Ct Colonography with Intravenous Contrast Material: Varied Appearances of Colorectal Carcinoma. *Radiographics,* 25**,** 1321-34.

SINGH, A., KUKRETI, R., SASO, L. & KUKRETI, S. 2019. Oxidative Stress: Role and Response of Short Guanine Tracts at Genomic Locations. *Int J Mol Sci,* 20.

SINGH, V., KHURANA, A., NAVIK, U., ALLAWADHI, P., BHARANI, K. K. & WEISKIRCHEN, R. 2022. Apoptosis and Pharmacological Therapies for Targeting Thereof for Cancer Therapeutics. *Sci,* 4.

SIVANDZADE, F., BHALERAO, A. & CUCULLO, L. 2019. Analysis of the Mitochondrial Membrane Potential Using the Cationic JC-1 Dye as a Sensitive Fluorescent Probe. *Bio Protoc,* 9.

SMILEY, S. T., REERS, M., MOTTOLA-HARTSHORN, C., LIN, M., CHEN, A., SMITH, T. W., STEELE, G. D. & CHEN, L. B. 1991. Intracellular heterogeneity in mitochondrial membrane potentials revealed by a J-aggregate-forming lipophilic cation JC-1. *Proceedings of the National Academy of Sciences,* 88**,** 3671–3675.

STANFORD HEALTHCARE. 2022. *Types of Colorectal Cancer* [Online]. [Accessed].

STATISTICS SOUTH AFRICA 2023. Cancer in South Africa (2008 – 2019) Pretoria.

STEPANENKO, A. A. & DMITRENKO, V. V. 2015. Pitfalls of the MTT assay: Direct and off-target effects of inhibitors can result in over/underestimation of cell viability. *Gene,* 574**,** 193-203.

SUNG, H., FERLAY, J., SIEGEL, R., L. , LAVERSANNE, M., SOERJOMATARAM, I., JEMAL, A. & BRAY, F. 2021. Global Cancer Statistics 2020: GLOBOCAN Estimates of Incidence and Mortality Worldwide for 36 Cancers in 185 Countries. *CA CANCER J CLIN,* 71**,** 209-249.

TANG, D., KANG, R., BERGHE, T. V., VANDENABEELE, P. & KROEMER, G. 2019. The molecular machinery of regulated cell death. *Cell Res,* 29**,** 347-364.

THERMO FISCHER SCIENTIFIC 2014. Pierce LDH Cytotoxicity Assay Kit.

THERMO FISCHER SCIENTIFIC 2022. CyQUANT™ LDH Cytotoxicity Assay.

THERMOFISHER SCIENTIFIC. 2023. The Basics: RNA Isolation. Available: https://www.thermofisher.com/za/en/home/references/ambion-tech-support/rna-isolation/general-articles/the-basics-rna-isolation.html.

TONNUS, W., MEYER, C., PALIEGE, A., BELAVGENI, A., VON MASSENHAUSEN, A., BORNSTEIN, S. R., HUGO, C., BECKER, J. U. & LINKERMANN, A. 2019. The pathological features of regulated necrosis. *J Pathol,* 247**,** 697-707.

TRAN, Q., LEE, H., KIM, C., KONG, G., GONG, N., KWON, S. H., PARK, J., KIM, S. H. & PARK, J. 2020. Revisiting the Warburg Effect: Diet-Based Strategies for Cancer Prevention. *Biomed Res Int,* 2020**,** 8105735.

TREFTS, E., GANNON, M. & WASSERMAN, D. H. 2017. The liver. *Curr Biol,* 27**,** R1147-R1151.

TRISHA, A. T., SHAKIL, M. H., TALUKDAR, S., ROVINA, K., HUDA, N. & ZZAMAN, W. 2022. Tea Polyphenols and Their Preventive Measures against Cancer: Current Trends and Directions. *Foods,* 11.

TSHIVHANDEKANO, I., NTUSHELO, K., NGEZIMANA, W., TSHIKALANGE, T. E. & MUDAU, F. N. 2014. Chemical compositions and antimicrobial activities of Athrixia phylicoides DC. (bush tea), Monsonia burkeana (special tea) and synergistic effects of both combined herbal teas. *Asian Pac J Trop Med,* 7S1**,** S448-53.

TUMEN, D., HEUMANN, P., GULOW, K., DEMIRCI, C. N., COSMA, L. S., MULLER, M. & KANDULSKI, A.

2022. Pathogenesis and Current Treatment Strategies of Hepatocellular Carcinoma. *Biomedicines,* 10.

TUMMERS, B. & GREEN, D. R. 2017. Caspase-8: regulating life and death. *Immunol Rev,* 277**,** 76-89.

TUNGMUNNITHUM, D., THONGBOONYOU, A., PHOLBOON, A. & YANGSABAI, A. 2018. Flavonoids and Other Phenolic Compounds from Medicinal Plants for Pharmaceutical and Medical Aspects: An Overview. *Medicines (Basel),* 5.

TZANI, M. A., GIOFTSIDOU, D. K., KALLITSAKIS, M. G., PLIATSIOS, N. V., KALOGIOURI, N. P., ANGARIDIS, P. A., LYKAKIS, I. N. & TERZIDIS, M. A. 2021. Direct and Indirect Chemiluminescence: Reactions, Mechanisms and Challenges. *Molecules,* 26.

VARGAS-MENDOZA, N., MORALES-GONZALEZ, A., MADRIGAL-SANTILLAN, E. O., MADRIGAL-BUJAIDAR, E., ALVAREZ-GONZALEZ, I., GARCIA-MELO, L. F., ANGUIANO-ROBLEDO, L., FREGOSO-AGUILAR, T. & MORALES-GONZALEZ, J. A. 2019. Antioxidant and Adaptative Response Mediated by Nrf2 during Physical Exercise. *Antioxidants (Basel),* 8.

VERZELLA, D., PESCATORE, A., CAPECE, D., VECCHIOTTI, D., URSINI, M. V., FRANZOSO, G., ALESSE, E. & ZAZZERONI, F. 2020. Life, death, and autophagy in cancer: NF-kappaB turns up everywhere. *Cell Death Dis,* 11**,** 210.

VILLARS, A., MATAMORO-VIDAL, A., LEVILLAYER, F. & LEVAYER, R. 2022. Microtubule disassembly by caspases is an important rate-limiting step of cell extrusion. *Nat Commun,* 13**,** 3632.

WANG, B., WU, L., CHEN, J., DONG, L., CHEN, C., WEN, Z., HU, J., FLEMING, I. & WANG, D. W. 2021. Metabolism pathways of arachidonic acids: mechanisms and potential therapeutic targets. *Signal Transduction and Targeted Therapy,* 6.

WANG, H., SUN, L., SU, L., RIZO, J., LIU, L., WANG, L. F., WANG, F. S. & WANG, X. 2014. Mixed lineage kinase domain-like protein MLKL causes necrotic membrane disruption upon phosphorylation by RIP3. *Mol Cell,* 54**,** 133-146.

WATABE, M., HISHIKAWA, K., TAKAYANAGI, A., SHIMIZU, N. & NAKAKI, T. 1999. Caffeic acid phenethyl ester induces apoptosis by inhibition of NFkappaB and activation of Fas in human breast cancer MCF-7 cells. *Biol Chem* 279**,** 6017-26.

WELLS, M., J. , BALSINHAS, V., M., JOFFE, H., ENGELBRECHT, V., M., HARDING, G. & STIRTON, C., H. 1986. A Catalogue of Problem Plants in Southern Africa, Incorporating the National Weed List of South Africa. *Memoirs of the Botanical Survey of South Africa,* 53.

WILLEMS, E., LEYNS, L. & VANDESOMPELE, J. 2008. Standardization of real-time PCR gene expression data from independent biological replicates. *Anal Biochem,* 379**,** 127-9.

WINIKOFF, S. E. 2005. Measuring Immunity:Cytolytic Assays. 343–349.

WINTERBOURN, C. C. 2020. Biological chemistry of superoxide radicals. *ChemTexts,* 6.

WORLD HEALTH ORGANISATION. 2020. *Cancer* [Online]. Available: https://www.who.int/news-room/fact-sheets/detail/cancer#:~:text=Cancer%20is%20a%20leading%20cause,and%20rectum%20and%20prostate%20cancers. [Accessed 2023].

WORLD HEALTH ORGANISATION INTERNATIONAL AGENCY FOR RESEARCH ON CANCER (IARC). 2021.

Colorectal Cancer Awareness Month 2021 [Online]. Available: https://www.iarc.who.int/featured-news/ccam2021/#:~:text=IARC%20estimates%20that%20in%202020,causing%20almost%201%20million%20deaths. [Accessed].

WOZNIAK, P., KONTEK, B., SKALSKI, B., KROL, A., ROZANSKI, W. & OLAS, B. 2019. Oxidative Stress and Hemostatic Parameters in Patients With Nephrolithiasis Before and After Ureteroscopic Lithotripsy. *Front Physiol,* 10**,** 799.

XIE, Y. H., CHEN, Y. X. & FANG, J. Y. 2020. Comprehensive review of targeted therapy for colorectal cancer. *Signal Transduct Target Ther,* 5**,** 22.

YE, K., CHEN, Z. & XU, Y. 2023. The double-edged functions of necroptosis. *Cell Death & Disease,* 14.

YIN, C., EVASON, K. J., ASAHINA, K. & STAINIER, D. Y. 2013. Hepatic stellate cells in liver development, regeneration, and cancer. *J Clin Invest,* 123**,** 1902-10.

YOO, D., JUNG, E., NOH, J., HYUN, H., SEON, S., HONG, S., KIM, D. & LEE, D. 2019. Glutathione-Depleting Pro-Oxidant as a Selective Anticancer Therapeutic Agent. *ACS Omega,* 4**,** 10070-10077.

ZAMAN, S., WANG, R. & GANDHI, V. 2014. Targeting the apoptosis pathway in hematologic malignancies. *Leuk Lymphoma,* 55**,** 1980-92.

ZARKOVIC, N. 2020. Roles and Functions of ROS and RNS in Cellular Physiology and Pathology. *Cells,* 9.

ZHAO, H., JAFFER, T., EGUCHI, S., WANG, Z., LINKERMANN, A. & MA, D. 2015. Role of necroptosis in the pathogenesis of solid organ injury. *Cell Death Dis,* 6**,** e1975.

ZHAO, M., MA, J., LI, M., ZHANG, Y., JIANG, B., ZHAO, X., HUAI, C., SHEN, L., ZHANG, N., HE, L. & QIN, S. 2021. Cytochrome P450 Enzymes and Drug Metabolism in Humans. *Int J Mol Sci,* 22.

ZHAO, Y., WANG, H., ZHOU, J. & SHAO, Q. 2022. Glutathione Peroxidase GPX1 and Its Dichotomous Roles in Cancer. *Cancers (Basel),* 14.

ZINATIZADEH, M. R., SCHOCK, B., CHALBATANI, G. M., ZARANDI, P. K., JALALI, S. A. & MIRI, S. R. 2021. The Nuclear Factor Kappa B (NF-kB) signaling in cancer development and immune diseases. *Genes Dis,* 8**,** 287-297.

ZOROVA, L. D., POPKOV, V. A., PLOTNIKOV, E. Y., SILACHEV, D. N., PEVZNER, I. B., JANKAUSKAS, S. S., BABENKO, V. A., ZOROV, S. D., BALAKIREVA, A. V., JUHASZOVA, M., SOLLOTT, S. J. & ZOROV, D. B. 2018. Mitochondrial membrane potential. *Anal Biochem,* 552**,** 50-59.

APPENDICES

APPENDIX 1: MTT TREATMENTS AND ANALYSIS

Caco-2, HepG2, and Hek-293 cells were treated with MB crude aqueous leaf extract with concentrations ranging from 0 – 5000 µg/ml for 48 hours. A dose-dependent decrease in cell viability with increased treatment concentration was observed for all cell lines. The IC_{20} and IC_{50} values were determined as: 169.8 and 293.8 µg/ml for Caco-2, 154.9 and 335.4 µg/ml for HepG2, and 208.93 and 545.7 µg/ml for Hek-293, respectively.

Table 1A: Changes in cell viability over the treatment range for Caco-2 cells determined by the MTT assay.

Treatment concentration (µg/ml)	**Log MB concentration**	**Average absorbance**	**Viability (%)**
0		2,227	100
50	1,699	1,497	67,220
125	2,097	2,469	110,867
250	2,398	1,173	52,687
500	2,699	0,474	21,284
1000	3,000	0,291	13,082
2500	3,398	0,209	9,362
5000	3,699	0,099	4,460

Table 1B: Changes in cell viability over the treatment range for HepG2 cells determined by the MTT assay.

Treatment concentration (µg/ml)	**Log MB concentration**	**Average absorbance**	**Viability (%)**
0		1,442	100,000
50	1,699	1,702	118,031
125	2,097	1,399	97,041
250	2,398	0,967	67,025
500	2,699	0,323	22,423
1000	3,000	0,210	14,563
2500	3,398	0,159	11,003
5000	3,699	0,151	10,448

Table 1C: Changes in cell viability over the treatment range for Hek293 cells determined by the MTT assay.

Treatment concentration (µg/ml)	**Log MB concentration**	**Average absorbance**	**Viability (%)**
0		1,407	100,000
50	1,699	1,232	87,562
125	2,097	1,448	102,878
250	2,398	1,347	95,736
500	2,699	0,790	56,148
1000	3,000	0,164	11,680
2500	3,398	0,135	9,595
5000	3,699	0,122	8,671

APPENDIX 2: QUANTIFICATION OF NITRITES

Table 2: Reactive nitrite quantification using the NOS assay.

Std nitrite [] (µM)	OD1	OD2	OD3	Ave abs	Ave abs-bla
0	0,199	0,221	0,226	0,215333	0
12,5	0,284	0,286	0,274	0,281333	0,066
25	0,32	0,338	0,321	0,326333	0,111
50	0,435	0,44	0,448	0,441	0,225667
75	0,541	0,577	0,569	0,562333	0,347
100	0,669	0,647	0,625	0,647	0,431667
150	0,823	0,923	0,872	0,872667	0,657333
200	1,017	1,07	1,123	1,07	0,854667

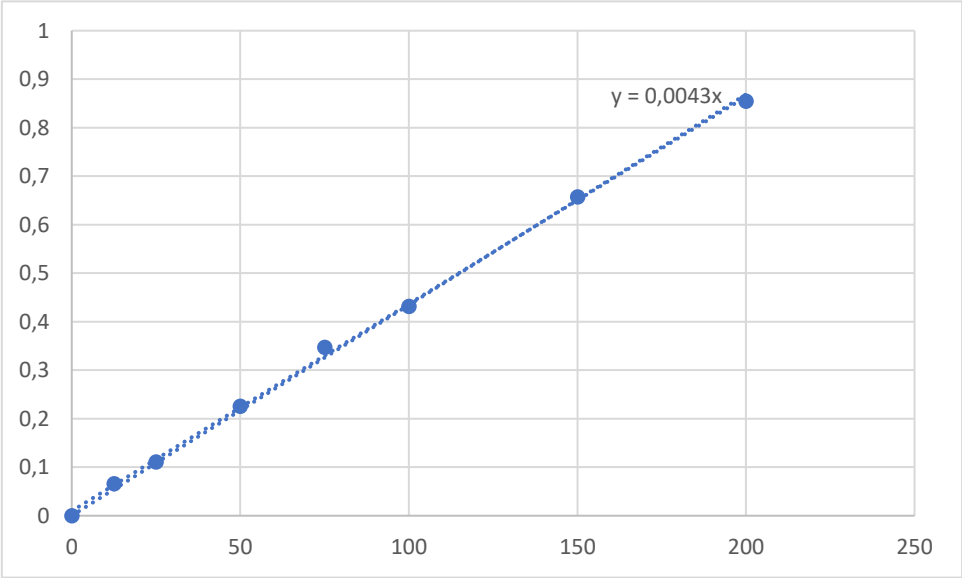

Figure 1: Standard curve showing nitrite concentration.

APPENDIX 3: PLATE LAYOUT FOR LUMINOMETRIC ASSAYS

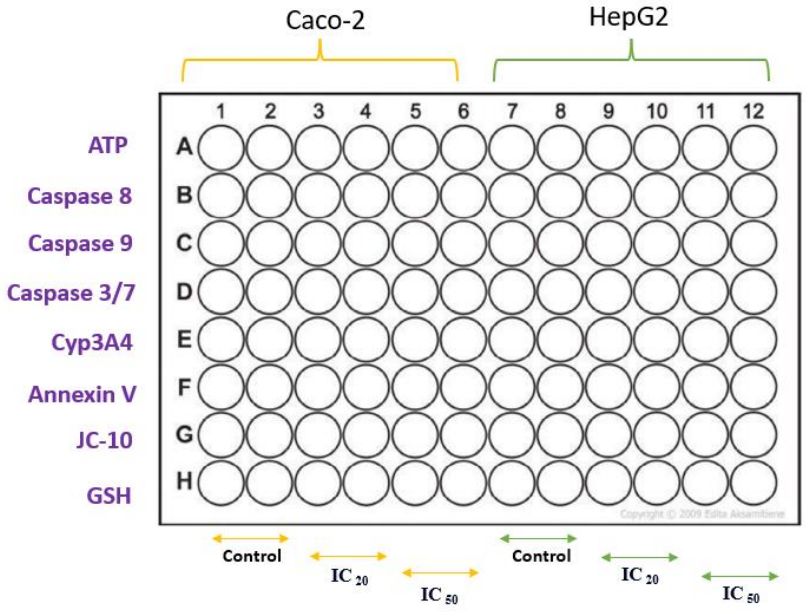

Figure 2: Plate layout depicting the order of luminometric assays conducted at various treatment concentrations for Caco-2 and HepG2 cell lines.

APPENDIX 4 : PROTEIN STANDARDISATION

Table 3: Quantification and standardisation of proteins using BSA (Bovine Serum Albumin) method.

BSA (mg/ml)	Abs 1	Abs 2	Average	Average - Blank
0	0,105	0,103	0,104	0
0,2	0,373	0,324	0,3485	0,2445
0,4	0,48	0,498	0,489	0,385
0,6	0,606	0,617	0,6115	0,5075
0,8	0,805	0,874	0,8395	0,7355
1	0,941	1,034	0,9875	0,8835

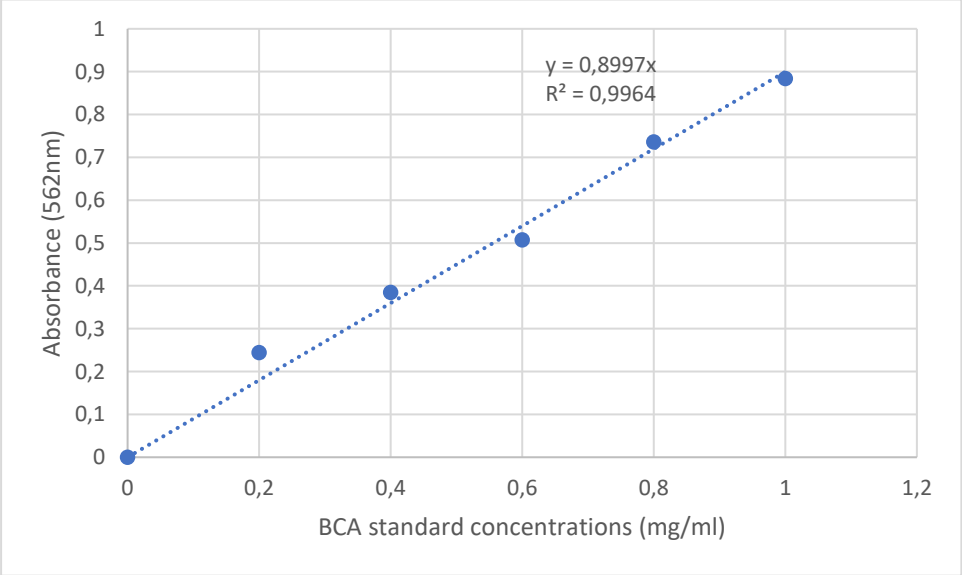

Figure 3: Standard curve created using BSA standards to determine protein concentrations.

APPENDIX 5: MELT CURVES FOR qPCR

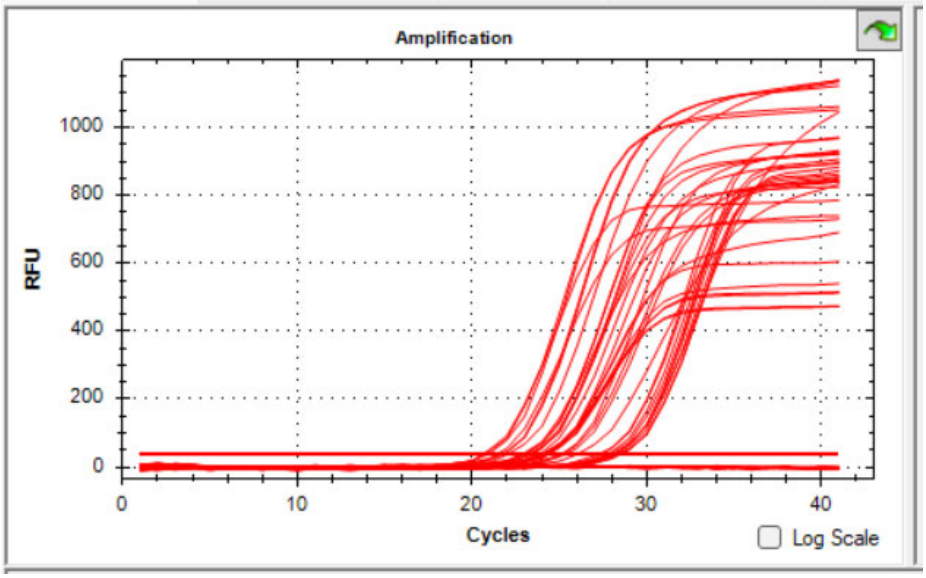

Figure 4: Melt curve depicting MLKL gene expression.

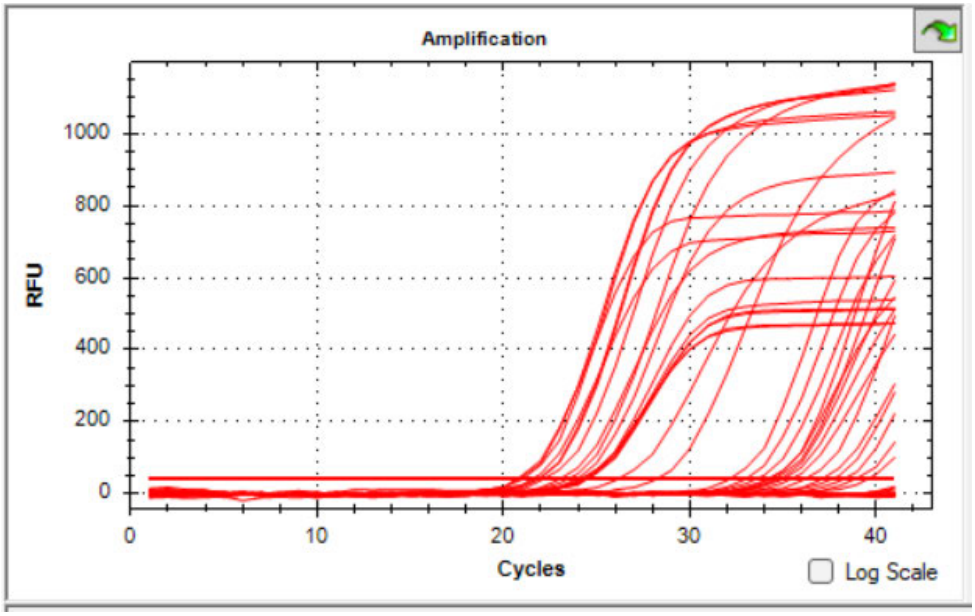

Figure 5: Melt curve depicting *RIPK1* gene expression.

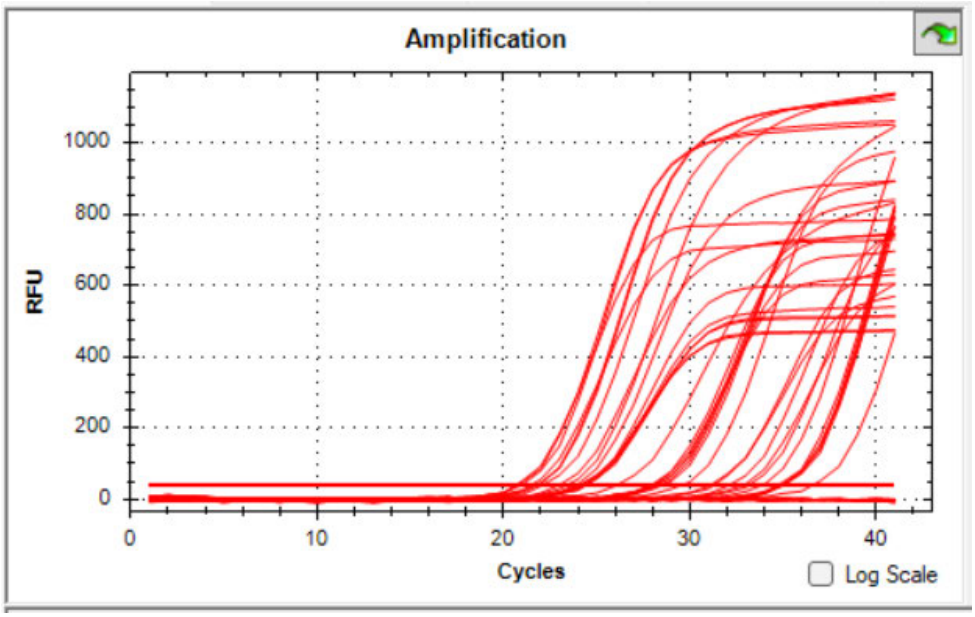

Figure 6: Melt curve depicting *RIPK3* gene expression.

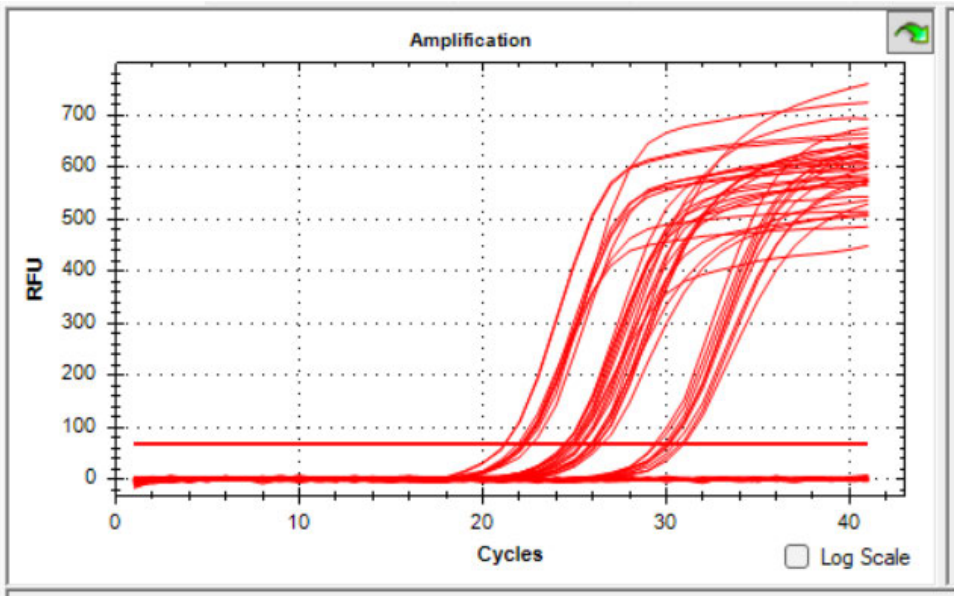

Figure 7: Melt curve depicting *NF-κB* gene expression.

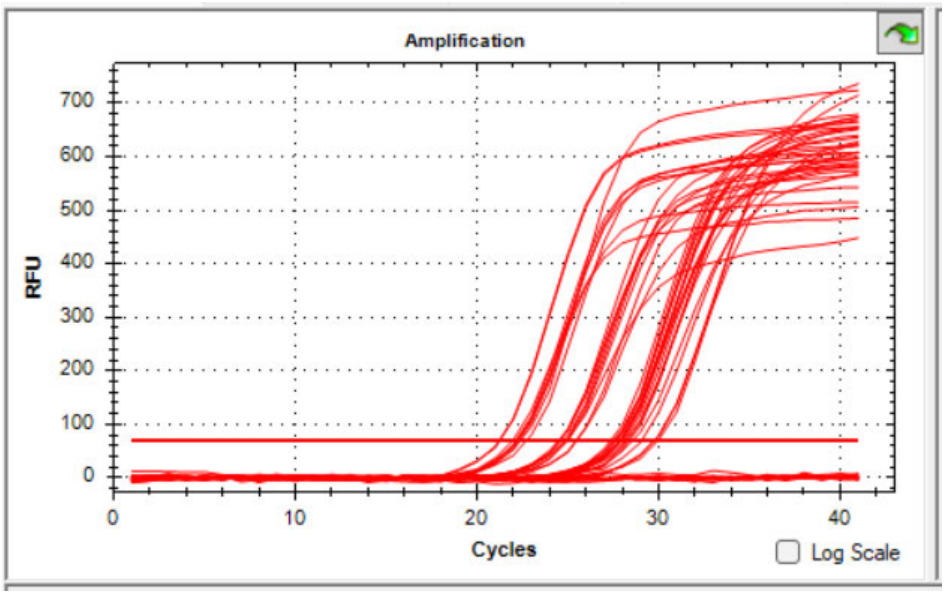

Figure 8: Melt curve depicting *Gpx* gene expression.

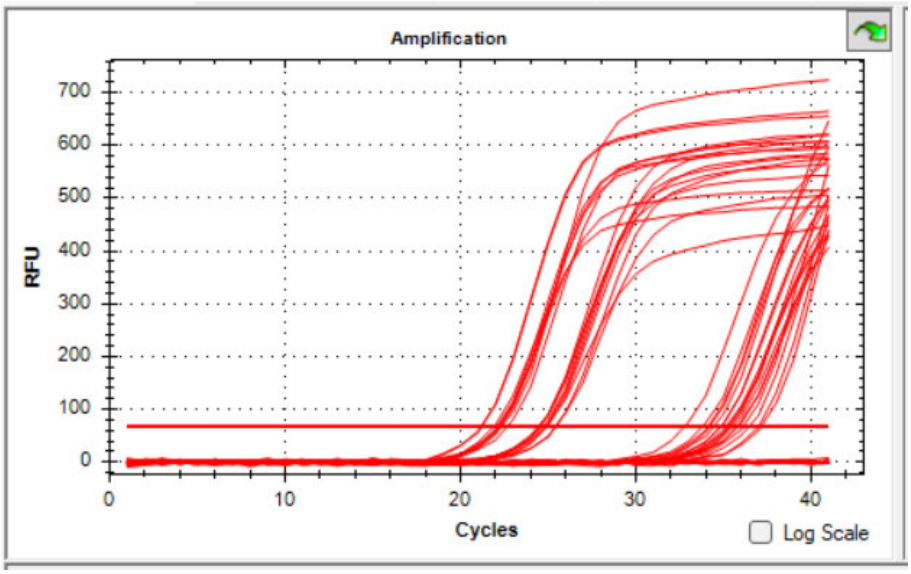

Figure 9: Melt curve depicting *OGG1* gene expression.

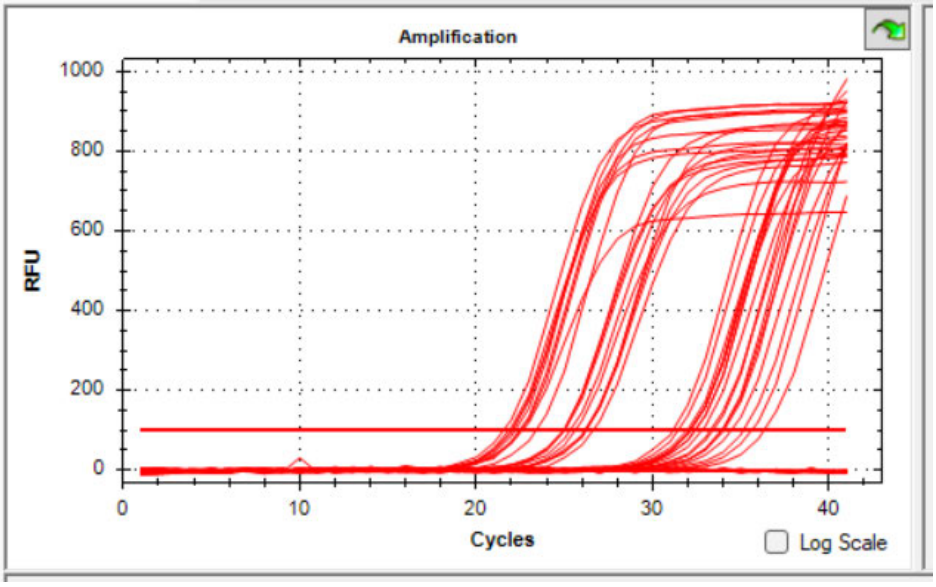

Figure 10: Melt curve depicting TNFα gene expression.

APPENDIX 6 : ETHICS SUPPORT

UNIVERSITY OF KWAZULU-NATAL
INYUVESI YAKWAZULU-NATALI

22 November 2023

Miss Mayanka Naicker (215025490)
School of Laboratory Medicine & Medical Science
Howard College

Dear Miss Naicker,

Protocol reference number: BREC/00005020/2022
Project title: Anticancer effects of Monsonia Burkeana in Liver and Colorectal Cancer cells.
Degree: MMedSci

RECERTIFICATION APPLICATION APPROVAL NOTICE

Approved:	21 December 2023
Expiration of Ethical Approval:	21 December 2024

I wish to advise you that your application for recertification for the above study has been noted and approved by a subcommittee of the Biomedical Research Ethics Committee (BREC). The start and end dates of this period are indicated above.

If any modifications or adverse events occur in the project before your next scheduled review, you must submit them to BREC for review. Except in emergency situations, no change to the protocol may be implemented until you have received written BREC approval for the change.

The committee will be notified of the above approval at its next meeting to be held on 12 December 2023.

Yours sincerely

[redacted]

.....
Ms A Marimuthu
(for) Prof D Wassenaar
Chair: Biomedical Research Ethics Committee

Biomedical Research Ethics Committee
Chair: Professor D R Wassenaar
UKZN Research Ethics Office Westville Campus, Govan Mbeki Building
Postal Address: Private Bag X54001, Durban 4000
Email: BREC@ukzn.ac.za
Website: http://research.ukzn.ac.za/Research-Ethics/Biomedical-Research-Ethics.aspx

APPENDIX 7 : TURNITIN REPORT

Mayanka Naicker (215025490)

ORIGINALITY REPORT

7%	6%	9%	0%
SIMILARITY INDEX	INTERNET SOURCES	PUBLICATIONS	STUDENT PAPERS

PRIMARY SOURCES

1	researchspace.ukzn.ac.za Internet Source	1%
2	Systems Biology of Free Radicals and Antioxidants, 2014. Publication	1%
3	docplayer.net Internet Source	1%
4	"Encyclopedia of Cancer", Springer Science and Business Media LLC, 2017 Publication	1%
5	www.mdpi.com Internet Source	1%
6	search.oecd.org Internet Source	1%
7	edoc.ub.uni-muenchen.de Internet Source	1%
8	www.biorxiv.org Internet Source	1%
9	doi.org	

Internet Source 1%